Hot Accretion Flows Around Black Holes

Hot Accretion Flows Around Black Holes

Feng Yuan

Shanghai Astronomical Observatory, Chinese Academy of Sciences, 80 Nandan Road, Shanghai 200030, China; email: fyuan@shao.ac.cn

Ramesh Narayan

Harvard-Smithsonian Center for Astrophysics, 60 Garden Street, Cambridge, MA 02138, USA; email: rnarayan@cfa.harvard.edu

KEYWORDS: accretion disks, active galactic nuclei, active galactic feedback, black holes, black hole X-ray binaries, jet, outflow

ABSTRACT: Black hole accretion flows can be divided into two broad classes: cold and hot. Cold accretion flows, which consist of cool optically thick gas, are found at relatively high mass accretion rates. Prominent examples are the standard thin disk, which occurs at a fraction of the Eddington mass accretion rate, and the slim disk at super-Eddington rates. These accretion flows are responsible for luminous systems such as active galactic nuclei radiating at or close to the Eddington luminosity and black hole X-ray binaries in the soft state. Hot accretion flows, the topic of this review, are virially hot and optically thin. They occur at lower mass accretion rates, and are described by models such as the advection-dominated accretion flow and luminous hot accretion flow. Because of energy advection, the radiative efficiency of these flows is in general lower than that of a standard thin accretion disk. Moreover, the efficiency decreases with decreasing mass accretion rate. Detailed modeling of hot accretion flows is hampered by theoretical uncertainties on the heating of electrons, equilibration of electron and ion temperatures, and relative roles of thermal and non-thermal particles. Observations show that hot accretion flows are associated with jets. In addition, theoretical arguments suggest that hot flows should produce strong winds. This link between the hot mode of accretion and outflows of various kinds is currently being explored via hydrodynamic and magnetohydrodynamic computer simulations. Hot accretion flows are believed to be present in low-luminosity active galactic nuclei and in black hole X-ray binaries in the hard and quiescent states. The prototype is Sgr A*, the ultra-low-luminosity supermassive black hole at our Galactic center. The jet, wind and radiation from a supermassive black hole with a hot accretion flow can interact with the external interstellar medium and modify the evolution of the host galaxy. Details of this "maintenance-mode feedback" could, in principle, be worked out through theoretical studies and numerical simulations of hot accretion flows.

CONTENTS

1 Introduction

Black hole accretion is a fundamental physical process in the universe, and is the primary power source behind active galactic nuclei (AGNs), black hole X-ray binaries (BHBs) and possibly gamma-ray bursts. The first genuine model of an accretion disk — by which we mean a rotating flow with viscous transport of angular momentum — is the celebrated thin disk model developed in the early 1970s (Shakura & Sunyaev 1973, Novikov & Thorne 1973, Lynden-Bell & Pringle 1974; see reviews by Pringle 1981, Frank et al. 2002, Kato et al. 2008, Abramowicz & Fragile 2013, Blaes 2013). Depending on the mass of the central black hole, the gas temperature in this model lies in the range $10^4 - 10^7\,\mathrm{K}$, which is quite cold relative to the virial temperature. The disk is geometrically thin, while the gas is optically thick and radiates thermal blackbody-like radiation. Many accreting black hole sources have been successfully modeled as thin disks, e.g., luminous AGNs (see reviews above; but also Koratkar & Blaes 1999) and BHBs in the thermal state (Remillard & McClintock 2006, McClintock et al. 2013).

The thin disk model applies whenever the disk luminosity L is somewhat below the Eddington luminosity $L_{\rm Edd}$, or equivalently, when the mass accretion rate $\dot{M}$ is below the Eddington rate,[1] $\dot{M}_{\rm Edd} \equiv 10L_{\rm Edd}/c^2 = 1.39\times10^{18}(M/M_\odot)\,\mathrm{g\,s^{-1}}$, where M is the mass of the black hole. When $\dot{M}$ approaches or exceeds $\dot{M}_{\rm Edd}$, the accreting gas becomes optically too thick to radiate all the dissipated energy locally (a key requirement of the thin disk model). Radiation is then trapped and advected inward with the accretion flow. Consequently, the radiative efficiency becomes lower, and L becomes progressively smaller than $0.1\dot{M}c^2$. The disk solution that describes such a system is called the slim disk, or equivalently,

[1]While everyone agrees on the definition of the Eddington luminosity, viz., $L_{\rm Edd} = 4\pi GMc/\kappa_{\rm es}$, where $\kappa_{\rm es}$ is the electron scattering opacity, usually taken to be $0.4\,\mathrm{cm^2 g^{-1}}$, many definitions are used for $\dot{M}_{\rm Edd}$. In this article we use a definition which assumes that the accretion disk has a nominal radiative efficiency of 10%, hence $L_{\rm Edd} = 0.1\dot{M}_{\rm Edd}c^2$. Some authors use $L_{\rm Edd} = \dot{M}_{\rm Edd}c^2$, others use $L_{\rm Edd} = \dot{M}_{\rm Edd}c^2/12$ or $\dot{M}_{\rm Edd}c^2/16$, and yet others use $L_{\rm Edd} = \eta(a_*)\dot{M}_{\rm Edd}c^2$ where $\eta(a_*)$ is the relativistic radiative efficiency of a thin disk around a black hole with dimensionless spin parameter $a_* \equiv a/M$.

optically thick advection-dominated accretion flow (Katz 1977, Begelman 1979, Begelman & Meier 1982, Abramowicz et al. 1988, Chen & Taam 1993, Ohsuga et al. 2005). The slim disk model has been applied to narrow-line Seyfert galaxies (Mineshige et al. 2000), objects like SS433 (Fabrika 2004) and ultraluminous X-ray sources (Watarai et al. 2001).

The thin disk and slim disk both belong to the class of cold accretion flows. Both consist of optically thick gas. The first hot accretion flow model was described by Shapiro et al. (1976; hereafter SLE). In contrast to the thin disk and slim disk, the temperature of the gas in the SLE solution is much higher, approaching virial, and the gas is optically thin. A key innovation of the SLE model is the introduction of a two-temperature accreting plasma, where the ions are much hotter than the electrons. The main success of the SLE solution, indeed its motivation, is that, for the first time, it was able to explain the hard X-ray emission seen in some black hole sources. Unfortunately, soon after the SLE model was introduced, it was realized that it is thermally unstable, so the model as originally developed is unlikely to be realized in nature.

The important role of advection in hot accretion flows was first emphasized by Ichimaru (1977) who pointed out that, in certain regimes, the viscously dissipated accretion energy can go into heating the accretion flow rather than being radiated away. This is the most important feature of the general class of advection-dominated accretion flows (ADAFs), one of the hot accretion solutions we will discuss in this review. Ichimaru further argued that, because of the inclusion of advection, his hot accretion solution should be thermally stable. Similar ideas were described independently by Rees et al. (1982) in their two-temperature "ion torus" model, though they did not emphasize the relation between their model and those of SLE and Ichimaru, nor did they discuss stability. Sadly, these pioneering studies were not followed up for many years.

With the re-discovery of the ADAF solution in the mid-1990s (Narayan & Yi 1994, 1995a, 1995b; Abramowicz et al. 1995; Chen et al. 1995), and the subsequent detailed study of its properties, hot accretion flow models finally became established in the accretion literature.[2] The dynamical and radiative properties of the ADAF solution have been studied in significant detail, and the model has been applied to various black hole systems, including the supermassive black hole in our Galactic center, Sagittarius A* (Sgr A*), low-luminosity AGNs, and BHBs in the hard and quiescent states This article reviews our current understanding of hot accretion flows. The reader is encouraged to read other reviews (e.g., Narayan et al. 1998b, Lasota 1999, Quataert 2001, Narayan & McClintock 2008, Ho 2008, Abramowicz & Fragile 2013, Blaes 2013), which discuss certain aspects of ADAFs in greater detail than we can here.

Before concluding this introduction, we briefly explain some terminology. The most popular and widely-used name for hot accretion flows is "advection-dominated accretion flow" (ADAF). Two variants of the ADAF are advection-dominated inflow-outflow solution (ADIOS) and convection-dominated accretion flow (CDAF), which emphasize the roles of two distinct physical phenomena in hot accretion

[2]Note that "advection-dominated accretion" is not synonymous with "hot accretion". For instance, the slim disk is advection-dominated, although for a very different reason (long radiative diffusion time) compared to a hot ADAF (long cooling time). In this article, we classify accretion solutions as hot or cold, and focus our attention on the hot solutions. While our classification is somewhat arbitrary, at least in certain respects, e.g., Fig. 3, the two solution branches are clearly distinct.

flows: outflows and convection (§3.4). Hot accretion flows are usually radiatively inefficient. Perhaps to emphasize that the low efficiency is not just because of advection, but may also be the result of other effects such as outflows and convection, some authors use the name "radiatively inefficient accretion flow" (RIAF). However, as we will see in §2, the radiative efficiency of a hot accretion flow increases with increasing mass accretion rate. In fact, the efficiency can even be comparable to that of the standard thin disk. This is especially the case in the "luminous hot accretion flow" (LHAF, §2.5), an extension of the ADAF to accretion rates above the original range of validity of the ADAF solution. Since the common feature of all these accretion solutions is that the gas is very hot, we use the generic name of "Hot Accretion Flow." Nevertheless, because of its popularity, we sometimes also use the term ADAF.

2 One-dimensional dynamics and radiation

2.1 One-dimensional equations and self-similar solution

Consider a steady axisymmetric accretion flow, and focus for now only on the dynamics. Conservation of mass, radial momentum, angular momentum and energy are described by the following height-integrated differential equations (e.g., Abramowicz et al. 1988, Narayan & Yi 1994, Narayan et al. 1998b):

$$\frac{d}{dR}(\rho R H v) = 0, \tag{1}$$

$$v\frac{dv}{dR} - \Omega^2 R = -\Omega_K^2 R - \frac{1}{\rho}\frac{d}{dR}(\rho c_s^2), \tag{2}$$

$$v\,\frac{d(\Omega R^2)}{dR} = \frac{1}{\rho R H}\frac{d}{dR}\left(\nu\rho R^3 H\frac{d\Omega}{dR}\right), \tag{3}$$

$$\rho v\left(\frac{de}{dR} - \frac{p}{\rho^2}\frac{d\rho}{dR}\right) = \rho\nu R^2\left(\frac{d\Omega}{dR}\right)^2 - q^-, \tag{4}$$

where ρ is the mid-plane density of the gas, R is the radius, $H \approx c_s/\Omega_K$ is the vertical scale height, v is the radial velocity, Ω is the angular velocity, Ω_K is the Keplerian angular velocity, $c_s \equiv \sqrt{p/\rho}$ is the isothermal sound speed, p is the pressure, e is the specific internal energy, and q^- is the radiative cooling rate per unit volume. The kinematic viscosity coefficient ν may be parameterized via the Shakura & Sunyaev (1973) prescription,

$$\nu \equiv \alpha c_s H = \alpha\frac{c_s^2}{\Omega_K}, \tag{5}$$

where the dimensionless parameter α is generally assumed to be a constant.

Equations (1)–(4) are quite general in the sense that they encompass all accretion models, including the thin disk, the slim disk and the ADAF (§2.6). Note, however, that equation (1) implies the mass accretion rate $\dot{M} = 4\pi\rho R H|v|$ is independent of radius. While this may be a reasonable approximation for a thin disk (though even these systems can have non-constant $\dot{M}$ if there are radiatively- or magnetically-driven winds), numerical simulations of hot accretion flows indicate that outflows are almost inevitable (§3.4), causing the mass accretion rate to decrease with decreasing radius. Therefore, assuming a power-law variation

for simplicity, it is useful to generalize equation (1) to (Blandford & Begelman 1999)

$$\dot{M}(R) = 4\pi\rho RH|v| = \dot{M}_{\rm BH}\left(\frac{R}{R_S}\right)^s, \quad R_S \le R \le R_{\rm out}, \tag{6}$$

where $R_S = 2GM/c^2$ is the Schwarzschild radius of the black hole, $\dot{M}_{\rm BH}$ is the mass accretion rate at this radius and $R_{\rm out}$ is the outer radius of the accretion flow. The index s is a measure of the strength of the outflow; s cannot exceed 1 for energetic reasons (Blandford & Begelman 1999), while $s = 0$ corresponds to a constant mass accretion rate (no outflow). Equations (2)–(4) should also be modified when there is mass outflow (e.g., Poutanen et al. 2007, Xie & Yuan 2008). However, the main effect of an outflow is probably through the density profile. Hence, simply replacing equation (1) by equation (6) and retaining equations (2)–(4) as written is a reasonable first approximation. Another caveat is that the power-law variation of $\dot{M}$ with R is not likely to continue all the way down to R_S as written above, but probably ceases at some inner radius $R_{\rm in}$ of order ten (or even tens of) R_S (§3.4 and Fig. 5).

Equation (4) needs more discussion. The two terms on the left hand side represent the rate of change of the internal energy per unit volume and the work done by compression; we will call the latter q^c. Together, the two terms represent energy advection, which we write compactly as $q^{\rm adv}$. More precisely, $q^{\rm adv}$ corresponds to $\rho v T ds/dR$, where T and s are the temperature and specific entropy of the gas; $q^{\rm adv}$ is thus the radial rate of advection of entropy. The first term on the right hand side of equation (4) is the heating rate per unit volume, or more precisely the rate at which entropy is added to the gas via viscous dissipation. Calling this term q^+, equation (4) takes the simple form

$$\rho v\frac{de}{dR} - q^c \equiv q^{\rm adv} = q^+ - q^- \equiv fq^+, \tag{7}$$

where the parameter $f \equiv q^{\rm adv}/q^+$ measures the relative importance of advection. Out of the total heat energy q^+ released by viscous dissipation per unit volume per unit time, a fraction f is advected and the rest $(1 - f)$ is radiated. The standard thin disk and SLE models assume $q^+ = q^-$ and thus correspond to $f = 0$, i.e., vanishing energy advection. The slim disk and various hot accretion flows have non-zero f. Quite often, e.g., when $\dot{M}_{\rm BH} \gg \dot{M}_{\rm Edd}$ (slim disk) or $\dot{M}_{\rm BH} \ll \dot{M}_{\rm Edd}$ (hot accretion flow), one finds $q^+ \gg q^-$, $f \to 1$. These accretion flows are then strongly advection-dominated.

Assuming a Newtonian gravitational potential and taking the advection parameter f to be independent of radius, Narayan & Yi (1994, 1995b) showed that equations (1)–(4) have a self-similar solution.[3] Their solution corresponds to a constant mass accretion rate without outflows ($s = 0$). Including mass outflow via equation (6), and making the reasonable assumption that the only important change is in the density profile (Xie & Yuan 2008), the Narayan & Yi self-similar solution becomes approximately (Yuan et al. 2012b)

$$v \approx -1.1\times10^{10}\alpha r^{-1/2}\ {\rm cm\ s^{-1}}, \tag{8}$$

$$\Omega \approx 2.9\times10^{4}m^{-1}r^{-3/2}\ {\rm s^{-1}}, \tag{9}$$

$$c_s^2 \approx 1.4\times10^{20}r^{-1}\ {\rm cm^2\ s^{-2}}, \tag{10}$$

[3]The same solution was obtained earlier by Spruit et al. (1987) in a different context.

$$n_e \approx 6.3\times10^{19}\alpha^{-1}m^{-1}\,\dot{m}_{\rm BH}\,r^{-3/2+s}\ {\rm cm}^{-3}, \quad (11)$$

$$B \approx 6.5\times10^{8}(1+\beta)^{-1/2}\alpha^{-1/2}m^{-1/2}\,\dot{m}_{\rm BH}^{1/2}\,r^{-5/4+s/2}\ {\rm G}, \quad (12)$$

$$p \approx 1.7\times10^{16}\alpha^{-1}m^{-1}\,\dot{m}_{\rm BH}\,r^{-5/2+s}\ {\rm g\ cm^{-1}\ s^{-2}}, \quad (13)$$

where the black hole mass M, the mass accretion rate $\dot{M}$, and the radius R, have been scaled to solar, Eddington, and Schwarzschild units, respectively,

$$m \equiv \frac{M}{M_\odot}, \quad \dot{m} \equiv \frac{\dot{M}}{\dot{M}_{\rm Edd}}, \quad r \equiv \frac{R}{R_S}. \quad (14)$$

Correspondingly, $\dot{m}_{\rm BH} = \dot{M}_{\rm BH}/\dot{M}_{\rm Edd}$, where $\dot{M}_{\rm BH}$ is defined in equation (6). The parameter β is a measure of the strength of the magnetic field:[4]

$$\beta \equiv \frac{p_{\rm gas}}{p_{\rm mag}}, \quad (15)$$

where $p_{\rm gas}$ is the gas pressure and $p_{\rm mag} \equiv B^2/8\pi$ is the magnetic pressure. Numerical magnetohydrodynamic (MHD) simulations usually give $\beta \simeq 10$ (§3.2).

The advection parameter f is generally a function of radius r and, more importantly, the mass accretion rate $\dot{m}$. When $\dot{m}$ is very much smaller than unity (say $\lesssim 10^{-4}$), f is nearly equal to unity and the flow is well-described as a true ADAF. As $\dot{m}$ becomes larger, radiation plays an increasingly important role and f becomes smaller, even negative in some regimes (LHAF). §2.5 discusses the energetics of various kinds of hot accretion flows.

Apart from being convenient for estimating gas properties in hot accretion flows, the self-similar solution reveals several distinct features of these solutions, which distinguish hot flows from the standard (cool) thin disk.

- The temperature of a hot accretion flow is almost virial,

  $$T \simeq GMm_p/6kR \sim (10^{12}/r)\,{\rm K}, \quad (16)$$

  which is much larger than the temperature of a thin disk. Because of the near-virial temperature, the accretion flow is geometrically quite thick, $H/R \sim 0.5$. Nevertheless, the height-integrated equations used in the 1D analysis appear to be reasonably accurate (Narayan & Yi 1995a).
- The radial velocity is much larger than in a thin disk. This is because accretion theory predicts $v \sim \alpha c_s H/R$ (e.g., eq. 3), and both c_s and H/R are much larger in a hot accretion flow.
- The angular velocity is sub-Keplerian. This is because the pressure is much larger than in a thin disk (higher temperature) and so gravity is partially balanced by the radial pressure gradient (right hand side of eq. 2).
- The large radial velocity and the low mass accretion rate generally cause the optical depth of a hot accretion flow to be less than unity. Therefore, the emitted radiation is almost never blackbody, but is dominated by processes like synchrotron, bremsstrahlung and inverse Compton scattering. In addition, as we discuss in §2.4, the radiative efficiency,

  $$\epsilon \equiv \frac{L}{\dot{M}_{\rm BH}c^2}, \quad (17)$$

[4]This is the standard definition of β as used in plasma physics. However, following Narayan & Yi (1995b), much of the ADAF literature uses a different $\beta_{\rm ADAF} \equiv p_{\rm gas}/(p_{\rm gas}+p_{\rm mag})$, which is confusingly also called β. The two β's are related by $\beta_{\rm ADAF} = \beta/(\beta+1)$.

where L is the luminosity of the accretion flow, is much lower than the fiducial 10% efficiency of a standard thin accretion disk, especially when $\dot{m}$ is small.

- In the low radiative efficiency limit, since the gas is heated but hardly cools, the entropy increases with decreasing radius. Hot accretion flows are therefore potentially unstable to convection.[5]
- Finally, the self-similar solution implies that the Bernoulli parameter Be of the flow is positive, which suggests that hot accretion flows should have strong outflows and jets (Narayan & Yi 1994, 1995a; Blandford & Begelman 1999). Global solutions (§2.3) indicate that Be may be either positive or negative, depending on outer boundary conditions (Nakamura 1998, Yuan 1999).

While much work on hot accretion flows has focused on the time-steady self-similar solution described above, Ogilvie (1999) has derived a beautiful similarity solution which describes the radiatively inefficient evolution of an initially narrow ring of viscous orbiting fluid. This solution confirms several of the features discussed above. In addition, it avoids an annoying singularity that is present in the time-steady self-similar solution when the gas adiabatic index approaches 5/3 (Narayan & Yi 1994; Quataert & Narayan 1999a; Blandford & Begelman 1999).

2.2 Two-temperature flow: Thermal properties

2.2.1 The two-temperature scenario

In the discussion so far, we focused on the dynamics. When dealing with the thermodynamics of a hot accretion flow, it is customary to follow the pioneering work of SLE and to allow the ions and electrons to have different temperatures. For such two-temperature plasmas, the energy equation (4) or (7) is replaced by two coupled equations (e.g., Nakamura et al. 1997, Quataert & Narayan 1999b):

$$q^{\rm adv,i} \equiv \rho v \left(\frac{de_i}{dR} - \frac{p_i}{\rho^2} \frac{d\rho}{dR} \right) \equiv \rho v \frac{de_i}{dR} - q^{i,c} = (1-\delta) q^+ - q^{\rm ie}, \qquad (18)$$

$$q^{\rm adv,e} \equiv \rho v \left(\frac{de_e}{dR} - \frac{p_e}{\rho^2} \frac{d\rho}{dR} \right) \equiv \rho v \frac{de_e}{dR} - q^{e,c} = \delta q^+ + q^{\rm ie} - q^-. \qquad (19)$$

Here $e_i \equiv kT_i/[(\gamma_i - 1)\mu_i m_p]$ and $e_e \equiv kT_e/[(\gamma_e - 1)\mu_e m_p]$ are the internal energies of ions and electrons per unit mass of the gas. Similarly, γ_i, γ_e are the respective adiabatic indices; p_i, p_e are the respective pressures; $q^{i,c}$, $q^{e,c}$ are the respective compression work done per unit volume. The quantity $q^{\rm ie}$ is the rate of transfer of thermal energy from ions to electrons via Coulomb collisions. The parameter δ denotes the fraction of the viscously dissipated energy that directly heats electrons; the remainder $(1-\delta)$ goes into the ions. There have been attempts to estimate this important parameter from first principles (§2.2.2), but δ is often treated as a free parameter. The above energy equations are further modified when the contribution of the magnetic field is included (Quataert & Narayan 1999a), but we ignore this complication here.

It is important to note that the two-temperature nature of the gas in a hot accretion flow is not simply an assumption but rather a generic consequence of

[5] Rotation can stabilize a system against convection even if the entropy gradient is unstable. The role of magnetic fields is less clear (§3.4).

the physics of these solutions. First, electrons radiate much more efficiently than ions (which is why we include a cooling term q^- only in eq. 19), and thus have a tendency to be cooler. Second, the primary channel whereby ions cool is by transfering their energy to the electrons. Coupling via Coulomb collisions is inefficient at the low densities found in hot flows, thus Coulomb equilibration of temperatures is suppressed. Third, we see from the energy equation that gravitational energy is transformed into thermal energy of the gas via two comparably important channels: viscous heating (q^+) and compressional heating ($q^{i,c}$, $q^{e,c}$). As we discuss in §2.2.2, viscous heating probably deposits comparable amounts of energy in the ions and electrons, with electrons perhaps receiving a somewhat smaller share ($\delta \sim 0.1 - 0.5$). As for compressional heating, under adiabatic conditions this causes the temperature to scale as $T \propto \rho^{\gamma-1}$. Since the ions remain non-relativistic throughout the accretion flow (even at $T_i \sim 10^{12}\,\mathrm{K}$), they have $\gamma_i \sim 5/3$. However, in the inner regions of the accretion flow, the electrons become relativistic, $kT_e > m_e c^2$, and $\gamma_e \to 4/3$. Therefore, while ions heat up by compression as $T_i \sim \rho^{2/3}$, electrons heat up only as $T_e \sim \rho^{1/3}$. This drives the gas to a two-temperature state at radii $r \lesssim 10^3$.

Despite all these arguments, the gas would still be single-temperature if there were efficient modes of energy transfer (over and above Coulomb collisions) from ions to electrons. Only one mechanism has been discussed in the literature (Begelman & Chiueh 1988), and it is unclear how important this particular mechanism is in situations of interest (Narayan & Yi 1995b). Of course, plasmas are complicated and there may well be some as-yet unidentified mechanism that succeeds in maintaining the gas at a single temperature. On the other hand, the two-temperature nature of hot accretion flows seems to be supported by observations (Yuan et al. 2006). Furthermore, the plasma in the solar wind is found to be both two-temperature and anisotropic (Marsch 2012), and the plasma behind shocks in supernova remnants is also two-temperature (Rakowski 2005). So it is certainly not the case that nature abhors a two-temperature plasma.

2.2.2 Heating and acceleration of electrons and ions

Early work on the two-temperature ADAF model assumed that most of the turbulent viscous energy goes into the ions (Ichimaru 1977, Rees et al. 1982, Narayan & Yi 1995b), and that only a small fraction $\delta < 10^{-2}$ goes into the electrons. However, the existence of neither a two-temperature plasma (§2.2.1) nor a radiatively inefficient flow (§2.5) requires such a small value of δ. What is essential is that $\dot{m}$ needs to be low.

A few attempts have been made to estimate δ from microphysics, by considering magnetic reconnection (Bisnovatyi-Kogan & Lovelace 1997; Quataert & Gruzinov 1999; Ding et al. 2010; Hoshino 2012, 2013), or MHD turbulence (Quataert 1998, Quataert & Gruzinov 1999, Blackman 1999, Medvedev 2000, Lehe et al. 2009), or dissipation of pressure anisotropy in a collisionless plasma (Sharma et al. 2007a). There is no consensus at the moment, but the work so far generally suggests that $\delta \gg 10^{-2}$.

By modeling astrophysical observations of hot accretion flows, weak constraints have been obtained on the value of δ. In the case of Sgr A*, where we have perhaps the most detailed observations of a hot accretion flow, Yuan et al. (2003; see §4.1 for details) estimated $\delta \approx 0.5$. However, from modeling black hole sources at higher luminosities, it appears that $\delta \sim 0.1$ (Yu et al. 2011, Liu & Wu 2013).

The best we can say at the moment is that δ probably lies in the range $0.1 - 0.5$.[6]

Is the energy distribution of the hot electrons thermal or non-thermal? Obviously, this depends on the details of energy dissipation, particle acceleration and thermalization. Processes like magnetic reconnection, weak shocks and turbulent dissipation are all likely to accelerate a fraction of the ions and electrons into a non-thermal power-law distribution (e.g., Ding et al. 2010, Hoshino 2013). How rapidly are the distributions then thermalized?

Mahadevan & Quataert (1997) showed that Coulomb collisions are far too inefficient to thermalize the ions, so ions retain whatever energy distribution they acquire through viscous dissipation and heating. Coulomb coupling between ions and electrons is also inefficient (though less so), which is why hot accretion flows develop a two-temperature structure in the first place (§2.2.1). On the other hand, electrons can exchange energy quite efficiently through Coulomb collisions, as well as by the emission and absorption of synchrotron photons. Thus, for accretion rates $\dot{m} > 10^{-3}$, the electrons are expected to have a more or less thermal distribution throughout the accretion flow. However, very high-energy electrons are not easily thermalized and could, in principle, retain a power-law distribution even at these high accretion rates. The electron energy distribution may thus be Maxwellian for the bulk of the electrons, but power-law for a small population of electrons at higher energies.

At lower accretion rates, thermalization is less efficient and the electron distribution function is expected to retain a stronger memory of the heating/acceleration process. So a hybrid thermal-nonthermal energy distribution should form readily. Observationally, non-thermal electrons are needed to explain the quiescent low-frequency radio emission in Sgr A* (Mahadevan 1998, Özel et al. 2000, Yuan et al. 2003; see §4.1) and other low-luminosity AGNs (Liu & Wu 2013), as well as the X-ray emission in flares in Sgr A* (Yuan et al. 2004).

2.3 Global solutions

The great virtue of the self-similar solution presented in §2.1 is that it is analytic and provides a transparent way of understanding the key properties of an ADAF. However, since the self-similar solution is scale-free, it cannot describe the flow near the inner or outer boundary. Especially for calculating the radiation spectrum one requires a global solution, since most of the radiation comes from the region close to the inner boundary where the self-similar solution is invalid.

A global solution refers to a numerical solution obtained by solving directly the differential equations of the problem, e.g., equations (1)–(4). Usually, an integrated version of the angular momentum equation (3) is used,

$$\frac{d\Omega}{dR} = \frac{v\Omega_K(\Omega R^2 - j)}{\alpha R^2 c_s^2}, \tag{20}$$

where the integration constant j is the angular momentum per unit mass accreted by the central mass. This constant is an eigenvalue of the problem and is obtained as part of the numerical solution. If the model under consideration includes mass loss in a wind, then (at the simplest level) equation (1) is simply replaced by

[6]This revision in the value of δ means that our understanding of hot accretion flows has evolved significantly since the early work reviewed in Narayan et al. (1998b), which was based entirely on models with $\delta < 0.01$. One consequence is that the radiative efficiency of a hot accretion flow is not as low as previously imagined, even when $\dot{m}$ is small (§2.5).

equation (6) with the chosen value of s (which is assumed to be independent of radius[7]). If one wishes to study the thermodynamics of the two-temperature gas consistently, equation (4) is replaced by equations (18) and (19). If one wishes to go beyond the assumption of a constant value of f, then the radiative cooling term q^- is kept in the energy equation, with contributions from relevant radiative processes (§2.4). In many studies, a pseudo-Newtonian gravitational potential (see Paczyński & Wiita 1980) is adopted to mimic the effective potential of a Schwarzschild black hole.

Mathematically, obtaining a global solution involves a three-point boundary value problem. Since the radial velocity of the accreting gas at large radius is highly subsonic, whereas the gas falls into the black hole horizon at the speed of light, there has to be an intermediate sonic radius $R_{\rm sonic}$ where the radial velocity equals the sound speed. The global solution must satisfy two boundary conditions at this radius, one of which is $v = c_s$. In addition, since the black hole cannot support a shear stress, the viscous torque must be zero at the horizon. This boundary condition is not always applied at the horizon; sometimes it is transferred to the sonic radius. Finally, at the outer edge of the solution ($R = R_{\rm out}$), the flow should match the properties of the gas flowing in from the outside.

The above boundary value problem is usually solved by one of two numerical methods (see Press et al. 1992, 2002 for details): relaxation (Narayan et al. 1997c, Chen et al. 1997, Esin et al. 1997), or shooting (Nakamura et al. 1996, 1997; Manmoto et al. 1997; Yuan 1999, 2001; Yuan et al. 2003). The main parameters are: black hole mass M, mass accretion rate $\dot{M}_{\rm BH}$, viscosity parameter α, magnetization parameter β, wind parameter s, and electron heating parameter δ. Among these, M is usually known through observations, δ was discussed in §2.2.2, and rough values of α, β and s may be obtained from numerical simulations, though s in particular is somewhat uncertain (§3.4); $\dot{M}_{\rm BH}$ is a free parameter which is either allowed to range over many values if one is doing a parameter study (e.g., Fig. 1) or is fitted to observations such as the luminosity and spectrum of a source. The global solution then gives the radial distributions of v, Ω, c_s, ρ, T_i, T_e and B, together with the eigenvalue j and the sonic radius $R_{\rm sonic}$. Away from the boundaries, global solutions generally agree well with the self-similar solution (Narayan et al. 1997c, Chen et al. 1997), confirming the validity and value of the latter.

The relativistic global problem, where the Newtonian equations discussed here are replaced by their general relativistic versions corresponding to the Kerr metric, has been solved by several authors (Abramowicz et al. 1996, Peitz & Appl 1997, Gammie & Popham 1998, Popham & Gammie 1998, Manmoto 2000). Solutions of the relativistic equations are similar to those of the Newtonian problem for radii $R \gtrsim 10R_S$, but differ significantly at smaller radii. In addition, the black hole's spin has a substantial effect at small radii, and this can impact the observed spectrum (Jaroszynski & Kurpiewski 1997).

2.4 Radiation processes, spectrum, and radiative efficiency

Since gas close to the black hole in a hot accretion flow has a very high temperature and is moreover optically thin and magnetized, the relevant radiation

[7]Numerical simulations suggest that mass loss begins only at radii greater than ten or tens of R_S (§3.4), so it is an oversimplification to assume a constant s all the way down to R_S (eq. 6). Presumably, the error introduced is not large, though this has not been checked.

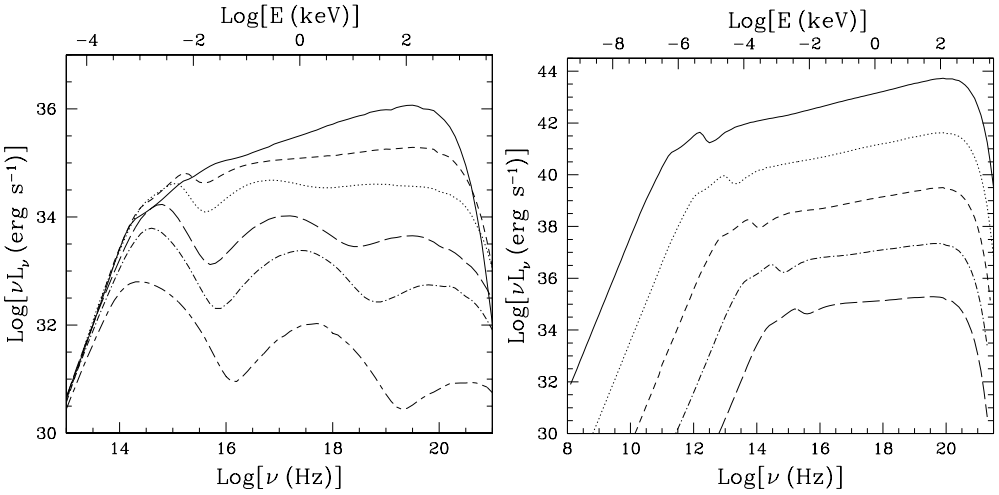

Figure 1: Model spectra of hot accretion flows for the following parameters: viscosity parameter $\alpha = 0.1$, magnetization parameter $\beta = 9$, electron heating parameter $\delta = 0.5$, wind parameter $s = 0.4$ (§§2.1, 2.2). *Left:* Spectra corresponding to a $10M_\odot$ black hole accreting with a mass accretion rate, from bottom to top, $\dot{m}_{\rm BH} = 8 \times 10^{-6}$, 5×10^{-5}, 1.6×10^{-4}, 8×10^{-4}, 2.4×10^{-3} and 5×10^{-3}, respectively. *Right:* Spectra corresponding to $\dot{m}_{\rm BH} = 2.4 \times 10^{-3}$ for black hole masses, from bottom to top, $M/M_\odot = 10$, 10^3, 10^5, 10^7 and 10^9, respectively. The model spectra shown here are for hot thermal accretion flows. When there is a cool outer disk beyond a transition radius, the spectrum has an additional thermal blackbody-like component (see Fig. 8). If there is a jet with non-thermal electrons, or if the hot flow itself has non-thermal particles, there is enhanced emission at radio and infrared wavelengths, and the prominent inverse Compton bumps shown here at low mass accretion rates are smoothed out to some degree (Figs. 6, 8). (Adapted from Narayan 1996, but with modern parameters.)

processes are synchrotron emission and bremsstrahlung, modified by Comptonization. The radiative cooling rate, the shape of the spectrum, the different components in the spectrum, and how all these scale with parameters, are described in various papers (e.g., Narayan & Yi 1995b; Narayan 1996; Mahadevan 1997; Esin et al. 1997; Nakamura et al. 1997; Manmoto et al. 1997; Narayan et al. 1998b; Quataert & Narayan 1999b; Yuan et al. 2003).

Figure 1 shows model spectra for hot accretion flows with different mass accretion rates $\dot{m}$ (left) and black hole masses m (right). The results can be understood as follows (based on Mahadevan 1997). At photon energies below and up to the first peak in the spectrum, the radiation is primarily due to synchrotron emission from the thermal electrons. The emission is highly self-absorbed and is very sensitive to the electron temperature ($\nu L_\nu \propto T_e^7$). The emission at the peak comes from gas near the black hole, while the radiation at lower frequencies comes from larger radii. The peak frequency scales roughly as $\nu_{\rm peak} \propto m^{-1/2}\dot{m}^{1/2}$. Synchrotron photons are Compton-upscattered by the hot electrons and produce hard radiation extending up to about the electron temperature: $kT_e \gtrsim 100\,{\rm keV}$ for typical two-temperature models. The importance of this Compton component depends on $\dot{m}$. At high values of $\dot{m}$, it dominates the spectrum, becoming even stronger than the primary synchrotron peak. As $\dot{m}$ decreases, the Compton

component is softer and becomes weaker (bolometrically) than the synchrotron component. At a sufficiently low $\dot{m}$, Comptonization is so weak that the X-ray spectrum is dominated by bremsstrahlung emission, which again cuts off at $h\nu \sim kT_e$.

The above discussion pertains to a pure hot accretion flow. If the hot flow is surrounded by a standard thin disk at larger radii (§4.2.2), there will be an additional multicolor blackbody component in the spectrum from the thermal disk. Also, the Compton component will be modified because, in addition to synchrotron photons, there is a second source of soft photons from the outer disk. The importance of the latter depends on where the transition radius $R_{\rm tr}$ between the hot flow and the thin disk is located.

In addition to thermal radiation from hot electrons, proton-proton collisions in a hot accretion flow can create pions, whose decay will give gamma-rays (Mahadevan et al. 1997). The same collisions will also produce a population of relativistic nonthermal electrons whose synchrotron radiation might explain the excess radio emission observed in Sgr A* (Mahadevan 1998, 1999),[8] although other processes can also produce such nonthermal electrons (§2.2.2). Interestingly, although the electrons in a hot accretion flow reach relativistic temperatures, pair processes are generally unimportant (Björnsson et al. 1996; Kusunose & Mineshige 1996; Esin 1999; Mościbrodzka et al. 2011), since the low opacity and low radiation energy density mean that there are very few pair-producing interactions in the medium.

At radii $\gtrsim 10^4 R_S$, the gas in a hot accretion flow is cool enough that heavier atomic species, especially iron-peak elements, are able to retain one or two electrons. As a result, the X-ray emission from these regions is expected to show emission lines on top of the inverse Compton and bremsstrahlung continuum (Narayan & Raymond 1999). The utility of these lines lies in their ability to constrain the run of gas density with radius and to thereby provide an observational estimate of the outflow parameter s (Perna et al. 2000, Xu et al. 2006, Wang et al. 2013).

Figure 2 shows the radiative efficiency of a hot accretion flow as a function of the mass accretion rate for various values of the electron heating parameter δ. Mass loss has been included via eq. (6) with $s = 0.4$. As can be seen, the efficiency depends strongly on the assumed value of δ. Also, for a given δ, the efficiency increases steeply with increasing mass accretion rate. Indeed, near the upper end, the efficiency of a hot accretion flow approaches the efficiency $\epsilon_{\rm SSD} \approx 10\%$ of a standard Shakura-Sunyaev disk. Xie & Yuan (2012) give piecewise power-law fitting formulae for the dependence of the radiative efficiency on $\dot{m}$ and δ.

2.5 Energetics: eADAF, ADAF, LHAF, and beyond

We now consider the energy equation of a hot accretion flow and discuss the role of the various terms that appear in it: viscous heating, compressional heating, energy advection, Coulomb energy transfer, radiative cooling. For simplicity, we begin with the simple energy equation (7), which corresponds to a single-temperature flow.

When $\dot{M}_{\rm BH}$ is very low, the gas density ρ is also low, and the radiative cooling rate q^- (which decreases rapidly with decreasing ρ) becomes negligibly small

[8] This process is less important in current models, which use higher values of δ than in the past and thus have lower mass accretion rates.

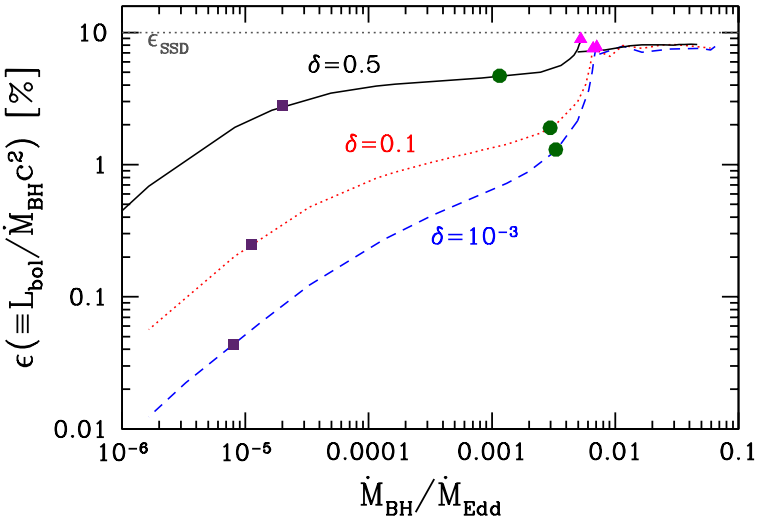

Figure 2: Radiative efficiency (eq. 17) of a hot accretion flow as a function of the mass accretion rate at the black hole $\dot{M}_{\rm BH}$ for three values of the electron heating parameter δ. Model parameters: $\alpha = 0.1$, $\beta = 9$, $s = 0.4$. The nominal radiative efficiency of a standard thin disk, $\epsilon_{\rm SSD} = 10\%$, is indicated by the horizontal dotted line at the top. When δ is large, the efficiency of a hot accretion flow is within a factor of a few of $\epsilon_{\rm SSD}$ for a wide range of $\dot{M}_{\rm BH}$ down to $\sim 10^{-5}\dot{M}_{\rm Edd}$. In contrast, when δ is small, the efficiency drops precipitously for $\dot{M}_{\rm BH} \lesssim 10^{-2}\dot{M}_{\rm Edd}$. Squares, filled circles and triangles indicate $\dot{M}_{\rm eADAF}$, $\dot{M}_{\rm crit,ADAF}$ and $\dot{M}_{\rm crit,LHAF}$, respectively, for each value of δ (§2.5 defines these quantities). The horizontal extensions of the curves above $\sim 7\times10^{-3}\dot{M}_{\rm Edd}$ show approximate radiative efficiencies assuming a two-phase accretion flow. (Adapted from Xie & Yuan 2012.)

(§2.4). The viscous heating rate is then balanced primarily by energy advection rather than cooling. Hence we have

$$q^+ \approx q^{\rm adv} \gg q^-, \quad f \approx 1. \tag{21}$$

That is, most of the viscous heat energy is stored in the flow and advected into the black hole rather than being radiated away. This is the classic regime of an ADAF. In the terminology used in this field, advection plays a "cooling" role.

With increasing $\dot{M}_{\rm BH}$, the radiative cooling q^- increases faster than $q^{\rm adv}$, and thus advective cooling becomes progressively less dominant. At a critical accretion rate $\dot{M}_{\rm crit,ADAF}$, the condition,

$$q^+ = q^-, \quad f \approx 0, \tag{22}$$

is satisfied. An ADAF is allowed only for $\dot{M}_{\rm BH} \le \dot{M}_{\rm crit,ADAF}$.

What happens when $\dot{M}_{\rm BH} > \dot{M}_{\rm crit,ADAF}$? Clearly we will have $q^+ < q^-$, i.e., radiative cooling will be stronger than the rate of heating by viscosity ($f < 0$). Yuan (2001) showed that hot accretion flows are still permitted in this regime up to a second critical accretion rate $\dot{M}_{\rm crit,LHAF}$, which is determined by the condition

$$q^c + q^+ = q^-. \tag{23}$$

Solutions over the range $\dot{M}_{\rm crit,ADAF} < \dot{M}_{\rm BH} < \dot{M}_{\rm crit,LHAF}$ are called luminous hot accretion flows (LHAFs) — they are hot, but unlike ADAFs, they are radiatively

efficient and luminous. The gas in these solutions remains hot despite the strong cooling because of the action of compressional heating q^c. Even though the entropy of the gas decreases with decreasing radius, the quantity $\rho v(de/dR) = q^+ + q^c - q^-$ is still positive. Thus the gas temperature continues to increase inward, and the flow remains hot (provided it starts out hot at a large radius). Over the entire LHAF branch, we have

$$q^c + q^+ > q^- > q^+. \tag{24}$$

Thus, $q^{\rm adv} = q^+ - q^- < 0$ and $f < 0$, so energy advection plays a "heating" role. In other words, the extra energy to heat the gas is supplied, not by viscous dissipation, but by the entropy already stored in the gas at large radius. Because of the high radiative efficiency and relatively large $\dot{M}_{\rm BH}$, LHAFs are expected to be much more luminous than ADAFs.

Consider now the more realistic case of a two-temperature hot accretion flow, where eq. (7) is replaced by eqs. (18) and (19). In the early literature on ADAFs, this case was treated in an approximate fashion by considering only the energy equation (18) of the ions. The neglect of the electron energy equation (19) is valid whenever δ is small, as was the case in these early studies which assumed $\delta \approx 0-0.01$. In this limit, almost all of the viscous heat goes into the ions. Moreover, the critical bottleneck that prevents gas from radiating is the rate of transfer of energy from ions to electrons, $q^{\rm ie}$; whenever $q^{\rm ie}$ is substantial (as happens at larger values of $\dot{M}_{\rm BH}$), the electrons have no trouble radiating whatever energy they receive from the ions, i.e., $q^{\rm ie} \approx q^-$. Thus, the approximation is self-consistent, though it does require very small values of δ. Numerically, in this regime it is found that $\dot{M}_{\rm crit,ADAF} \approx 0.4\alpha^2\dot{M}_{\rm Edd}$ and $\dot{M}_{\rm crit,LHAF} \approx \alpha^2\dot{M}_{\rm Edd}$ (Narayan 1996, Esin et al. 1997, Yuan 2001)[9].

As discussed in §2.2.2, the current consensus is that hot accretion flows have a larger value of $\delta \sim 0.1-0.5$. Viscous heating of electrons is then no longer negligible, nor is the Coulomb energy transfer rate $q^{\rm ie}$ the sole bottleneck. Consequently, it is now necessary to consider both the ion and electron energy equations (see Nakamura et al. 1997; Mahadevan & Quataert 1997; Yuan 2001 for early works on electron advection). As before, the two critical mass accretion rates, $\dot{M}_{\rm crit,ADAF}$ and $\dot{M}_{\rm crit,LHAF}$, may still be defined by the conditions given in equations (22) and (23).[10] However, a third critical accretion rate, $\dot{M}_{\rm eADAF}$, appears, which is explained below. By computing global models for δ in the range $0.1-0.5$, Xie & Yuan (2012) obtain the following rough estimates for the three critical accretion rates (measured at the black hole),[11]

$$\dot{M}_{\rm eADAF} \approx 0.001\,\alpha^2\dot{M}_{\rm Edd}, \tag{25}$$

[9] Another way to define $\dot{M}_{\rm crit,ADAF}$ is to require the timescale for ion-electron equilibration via Coulomb collisions to be equal to the accretion timescale (Narayan et al. 1998b). The two definitions are physically slightly different but give approximately the same result.

[10] Xie & Yuan (2012) adopt $(1-\delta)q^+ = q^{\rm ie}$ to define $\dot{M}_{\rm crit,ADAF}$. But the definition (23) is more physical. There is little difference in the numerical results.

[11] Two caveats should be mentioned. First, all quantities such as $q^{\rm adv}$, q^c, q^+, q^- are functions of radius. So we should, in principle, define a "local" critical accretion rate as a function of radius (e.g., see the review of Narayan et al. 1998b). Here we adopt a simpler and more "global" definition where we check if the relevant condition is satisfied at any radius within the range of interest. For example, we call a solution an LHAF whenever the condition $q^+ < q^-$ is satisfied at any radius. Second, the results quoted here are from Xie & Yuan (2012), who assume $s = 0.4$ and $\beta = 9$. The results are likely to change for other choices of the parameters.

$$\dot{M}_{\rm crit,ADAF} \approx (0.1-0.3)\,\alpha^2\dot{M}_{\rm Edd}, \quad (26)$$

$$\dot{M}_{\rm crit,LHAF} \approx (0.06-0.08)\,\alpha\dot{M}_{\rm Edd}. \quad (27)$$

In Figure 2, these critical rates are indicated by squares, filled circles, and triangles, respectively. Note that $\dot{M}_{\rm crit,ADAF}$ is smaller than the value $(0.4\alpha^2\dot{M}_{\rm Edd})$ mentioned above for $\delta \approx 0-0.01$. This is because electrons now receive more energy directly by viscous heating and hence radiate more efficiently.

The three critical mass accretion rates listed above separate different regimes of hot accretion as follows:

- $\dot{M}_{\rm BH} < \dot{M}_{\rm eADAF}$: Here both ions and electrons are radiatively inefficient. In particular, the electrons are unable to radiate either the viscous heat they acquire directly (δq^+) or the small amount of energy they receive from ions via Coulomb collisions ($q^{\rm ie}$). Systems in this regime are truly radiatively inefficient since even the electrons are advection-dominated; we call this regime "electron ADAF" or eADAF. These systems correspond to the dimmest black hole accretion sources known, e.g., Sgr A* at the Galactic Center and quiescent BHBs.
- $\dot{M}_{\rm eADAF} < \dot{M}_{\rm BH} < \dot{M}_{\rm crit,ADAF}$: Here electrons radiate efficiently their own viscous energy (δq^+) as well as any energy they receive from the ions ($q^{\rm ie}$). However, Coulomb collisions are inefficient. So the ions transfer only a small fraction of their energy to the electrons, and therefore remain advection-dominated. Systems in this regime are expected to be fairly radiatively efficient, with an efficiency of the order of a percent or more (depending on the value of δ). They are thus substantially brighter than classic ADAF models (see Fig. 2). However, the flows are hot and geometrically thick, and are still ADAFs in the sense that $q^+ > q^-$.
- $\dot{M}_{\rm crit,ADAF} < \dot{M}_{\rm BH} < \dot{M}_{\rm crit,LHAF}$: Here we have an LHAF with $q^+ < q^-$. All the energy terms in the ion energy equation are roughly comparable in magnitude. The entropy decreases as the gas flows in, but the gas remains hot because of compressional heating. The radiative efficiency increases rapidly with increasing $\dot{M}_{\rm BH}$, as shown in Fig. 2. This plot further shows that, when $\delta \ll 1$, the LHAF branch is restricted to quite a narrow range of $\dot{M}_{\rm BH}$. However, for currently accepted values of $\delta \sim 0.1-0.5$, the LHAF solution extends over a factor of several in $\dot{M}_{\rm BH}$.
- $\dot{M}_{\rm BH} > \dot{M}_{\rm crit,LHAF}$: In this regime, the one-dimensional global equations have no hot accretion flow solution. Radiative cooling is too strong, and even compressional heating is insufficient to keep the gas hot. In the traditional view, the accretion flow transitions to a standard thin accretion disk. However, there are large uncertainties, and Yuan (2003) speculates that the gas may transition to a two-phase medium with cold dense clumps embedded in hot gas. Alternatively, Oda et al. (2010) propose that a magnetically dominated accretion flow may form (see §3.2.3).

2.6 Stability and relationship to other accretion solutions

Hot optically thin gas generally tends to be thermally unstable. Therefore, all hot accretion flows are potentially unstable. What saves them is the fact that the accretion time scale is shorter than the instability growth time.

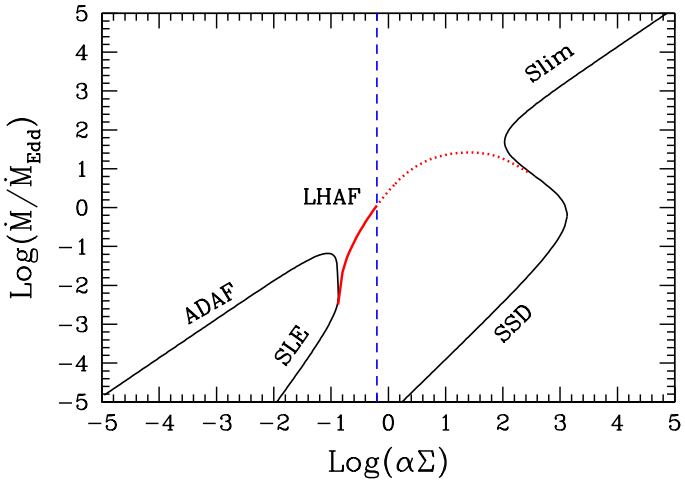

Figure 3: Thermal equilibrium curves of various accretion solutions for the following parameter values: $M = 10M_\odot$, $\alpha = 0.1$, $r = 5$. The accretion rate is normalized to $\dot{M}_{\rm Edd}$ and the surface density is in units of g cm^{-2}. The black solid lines correspond to the classic solution branches, viz., the hot branch consisting of ADAF and SLE, and the cold branch consisting of Slim disk and SSD. The blue vertical dashed line separates optically thin solutions on the left from optically thick solutions on the right. The red line corresponds to the LHAF solution. While the LHAF branch appears to go all the way across from the hot to the cold branch, global models indicate that this solution is self-consistent only to the left of the vertical line (shown by the solid red segment). (Adapted from Yuan 2003; see Abramowicz et al. 1995, Chen et al. 1995, for similar plots without the LHAF solution branch.)

Narayan & Yi (1995b) and Abramowicz et al. (1995) showed that ADAFs are stable to long wavelength perturbations. For small scale perturbations, however, the results are somewhat subtle. Wu & Li (1996) and Wu (1997) showed that ADAFs are stable under most reasonable conditions, while Kato et al. (1996, 1997) showed that ADAFs are potentially unstable at short wavelenghts. Using a time-dependent analysis, Manmoto et al. (1996) showed that small scale density perturbations in a one-temperature ADAF grow as the gas flows in, but not sufficiently quickly to affect the global viability of the solution. All these results were derived assuming that advection dominates. Hence they do not apply to the SLE or LHAF solutions.

In the case of the SLE solution, Piran (1978) showed that the model is thermally unstable. Yuan (2003) studied the thermal stability of LHAFs and concluded that these flows are thermally unstable. However, if the accretion rate is below $\dot{M}_{\rm crit,LHAF}$, the growth timescale of the instability remains longer than the accretion timescale and the solution can survive. Above this accretion rate, however, the instability will grow quickly. It is possible that the instability will not destroy the solution but will lead instead to a two-phase medium in which cold dense blobs are intermixed with hot gas (§2.5). Dynamically, the hot phase would behave like an LHAF with radiative cooling stronger than viscous heating. Xie & Yuan (2012) estimated the luminosity of such a two-phase accretion flow and found that, very approximately, the radiative efficiency is expected to be

around 10%, as indicated by the horizontal extensions in Fig. 2.

The above discussion deals with thermal stability. What about viscous stability? The most convenient way to investigate this is by plotting the locus of accretion solutions in the two-dimensional plane of accretion rate $\dot{M}$ and surface density $\Sigma \equiv 2\rho H$ (e.g., Frank et al. 2002). If the solution track has a positive slope, the solution is viscously stable, and vice versa. By including all solutions (both hot and cold) in such a diagram, one can appreciate the relationship between the various solutions.

Figure 3 shows an example of such a plot, taken from Yuan (2003; see also Abramowicz et al. 1995, Chen et al. 1995). The various solution tracks shown have been obtained by solving simple equations such as (1)–(4), or more complex versions of these that include radiative transfer, two-temperature plasma, etc. Usually, approximations are needed, e.g., assuming $\Omega = \Omega_K$ and $q^{\rm adv} = \xi(\dot{M}c_s^2/2\pi R^2 H)$ with a constant ξ (see Abramowicz et al. 1995). Then, for a given set of parameters, α, M, R, ξ, one can solve for $\dot{M}$ as a function of Σ.

The black solid lines in Fig. 3 show all the standard solution branches: the ADAF and SLE solutions belong to the sequence of hot solutions on the left, and the Shakura-Sunyaev disk (SSD) and slim disk solutions belong to the sequence of cold solutions on the right. All four of these solution branches are viscously stable since each track has a positive slope. At a given Σ, if there are multiple solutions, the uppermost (highest $\dot{M}$) solution is thermally stable to long wavelength perturbations, the next one below is unstable, and the next is stable. Therefore, the ADAF, slim disk and SSD solutions are thermally stable. However, the SLE solution on the left is thermally unstable, as is the segment between the SSD and slim disk on the right.[12] The latter solution is also viscously unstable (Lightman & Eardley 1974) since this branch has a negative slope. In terms of the advection parameter f, we have $f \approx 0$ for SSD and SLE, and $f \approx 1$ for ADAF and slim disk. The red line in Fig. 3 corresponds to the LHAF solution. Here ξ is negative, advection plays a heating role (§2.5) and $f < 0$.

The results presented in Fig. 3 are approximate since they are based on a single-temperature model (however, see Fig. 1c in Chen et al. 1995 for equivalent results for a two-temperature model) and are, moreover, based on a local rather than a global analysis. Nevertheless, these plots are believed to be qualitatively correct and therefore raise an important question. For certain ranges of the mass accretion rate, both hot and cold solutions are available, and both are thermally stable. Which solution does nature pick? Narayan & Yi (1995b) discussed a number of options, of which the following two deserve mention.

One option is that, if the accreting gas is hot at the outer feeding radius where mass first enters the accretion disk, and if a hot accretion solution is permitted at that radius, then the gas will start off in the hot mode of accretion and will remain in the hot accretion state all the way down to the black hole. On the other hand, if the gas starts out on the cool SSD branch on the outside, then it will remain in that branch down to the black hole unless the disk enters the Lightman & Eardley (1974) viscous instability zone (where the gas would become

[12] Recently, there has been considerable interest in the thermal stability of this solution branch, which corresponds to a radiation pressure dominated thin disk. Using numerical radiation MHD simulations, Hirose et al. (2009) concluded that a thin disk in this regime is thermally stable. However, later work by Jiang et al. (2013) showed that the disk is, in fact, thermally unstable. The reason for the discrepancy is discussed by the latter authors. Viscous stability of this solution branch is yet to be investigated via numerical simulations.

a hot accretion flow, the only stable solution remaining).

The second, more revolutionary, option is that the accretion flow will switch to the hot accretion branch whenever the latter solution is allowed, i.e., whenever $\dot{M} < \dot{M}_{\rm crit,LHAF}(R)$ corresponding to the local radius R. In other words, accretion occurs via the SSD solution only if it is the sole stable solution available. This so-called "strong ADAF principle" appears to be generally consistent with observations (§4.2.2).

3 Numerical simulations

The one-dimensional solutions considered so far are easy to calculate and often capture the important physics. However, hot accretion flows are geometrically thick, so one cannot be sure that the vertically integrated equations from which 1D solutions are derived are valid. In particular, height-integration eliminates multidimensional structures such as outflows.

Analytical two-dimensional solutions have been obtained by a number of authors over the years (e.g., Begelman & Meier 1982, Narayan & Yi 1995b, Xu & Chen 1997, Blandford & Begelman 2004, Xue & Wang 2005, Tanaka & Menou 2006, Jiao & Wu 2011, Begelman 2012). However, these models make simplifying assumptions such as self-similarity, and therefore have limited applicability. If we wish to understand the multidimensional structure of hot accretion flows, numerical simulations are the only way.

3.1 Hydrodynamic simulations

Although it is known that angular momentum transport in hot accretion flows is via magnetohydrodynamic (MHD) turbulence driven by the magnetorotational instability (§3.2.1), early computer simulations were carried out without magnetic fields, using 2D hydrodynamic (HD) codes and an α-like prescription for the viscous stress (Igumenshchev et al. 1996, Igumenshchev & Abramowicz 1999, Stone et al. 1999, Igumenshchev & Abramowicz 2000; Igumenshchev et al. 2000, De Villiers & Hawley 2002; Fragile & Anninos 2005). There were some differences in the adopted form of the shear stress, e.g., Stone et al. (1999) assumed that only the azimuthal component of the shear stress tensor is present, while Igumenshchev & Abramowicz (1999) included also poloidal components.

HD simulations of hot accretion flows reveal rich and complicated time-dependent structures. In particular, there are convective motions (Igumenshchev & Abramowicz 1999, Stone et al. 1999, Igumenshchev et al. 2000), confirming an early prediction of Narayan & Yi (1994; §2.1). The level of convective turbulence depends on details; for example, convection becomes weaker if a larger value of α is used or if poloidal components of the shear stress are included (Igumenshchev & Abramowicz 1999, Stone et al. 1999, Yuan & Bu 2010). The radial dynamic range of simulations is usually fairly limited (even more so for the 3D MHD simulations discussed below), but Yuan et al. (2012b) recently achieved an unprecedented four decades of dynamic range in a HD simulation using a "two-zone" approach.

The time-averaged "steady-state" flow in HD simulations is usually well described by a radial power law distribution of various quantities, with the power law indices depending on the specific form of the adopted shear stress. For the usual Shakura & Sunayev α-prescription, the radial scalings are consistent with the self-similar solution (eqs. 8–13, see Stone et al. 1999). On the other hand,

the initial conditions used in the simulations appear to affect some results such as the streamline structure and the Bernoulli parameter (Yuan et al. 2012a).

3.2 Magnetohydrodynamic simulations

3.2.1 Magnetorotational instability (MRI)

It is now widely accepted that the mechanism of angular momentum transport in ionized accretion flows is the magnetorotational instability (MRI; Balbus & Hawley 1991, 1998). This instability takes a seed magnetic field in the accreting gas and amplifies it exponentially, until the system becomes nonlinear and develops MHD turbulence. The Maxwell and Reynolds stresses in the turbulent state transport angular momentum outward, causing gas to accrete inward.

While the basic MRI is a linear instability and can be understood analytically, the nonlinear turbulent state relevant for disk accretion can be studied only with numerical simulations. A number of codes have been used, notably, ZEUS (Stone & Norman 1992a, 1992b), HARM (Gammie et al. 2003), the GRMHD code of De Villiers & Hawley (2003a), COSMOS++ (Anninos et al. 2005), and ATHENA (Stone et al. 2008). Many studies have been done in the limit of a local shearing box, which permits high spatial resolution (e.g., Hawley & Balbus 1991; Hawley et al. 1995, 1996; Brandenburg et al. 1995; Matsumoto & Tajima 1995; Stone et al. 1996). These show that MHD turbulence is inevitable so long as the gas and the magnetic field are well-coupled, and that the Maxwell stress dominates over the Reynolds stress by a factor of several.

When data from different published 3D shearing box simulations are combined, a tight correlation is seen between the parameter β (eq. 15) and the viscosity parameter α, viz., $\alpha\beta \sim 0.5$ (Blackman et al. 2008, Guan et al. 2009, Sorathia et al. 2012, see also Hawley & Balbus 1996). However, the individual values of β and α vary substantially from one numerical experiment to the next; for example, Hawley et al. (2011) obtained β values in the range $10 - 200$, corresponding to $\alpha \sim 0.01 - 0.003$, and other authors have found even larger variations. The value of α is thus not constrained. It seems to depend on the magnitude of the net initial magnetic field (Hawley et al. 1995, 1996; Pessah et al. 2007), a dependence that is confirmed also in localized regions of global simulations (Sorathia et al. 2010). Some shearing box simulations even find α values larger than unity (e.g., Bai & Stone 2013). Numerical resolution also plays a role. Generally, better resolution gives a larger α (up to some saturation value). However, when the net magnetic flux is zero, increasing the resolution actually causes α to decrease (Fromang & Papaloizou 2007, Fromang et al. 2007), with α going to zero in the limit of infinite resolution.

Interestingly, the uncertainty in the value of α is eliminated if shearing box simulations include vertical stratification to mimic the effect of vertical disk gravity (Davis et al. 2010, Bai & Stone 2013). Perhaps because of this, global disk simulations, which automatically include vertical gravity, show less variations in the effective value of α. These simulations generally evolve to steady state with $\alpha \sim 0.05 - 0.2$ (Hawley & Balbus 2002, Penna et al. 2013b).

3.2.2 Global simulations: General results

Global MHD simulations of hot accretion flows are more realistic than global HD simulations as they self-consistently generate shear stress through MRI-induced

MHD turbulence, whereas HD simulations must include an ad hoc viscosity. Early pioneers in global MHD simulations include Matsumoto & Shibata (1997), Armitage (1998), Hawley (2000), Machida et al. (2000), Stone & Pringle (2001), Hawley & Krolik (2001), and Igumenshchev & Narayan (2002).

Compared to shearing box simulations, global simulations enable the MRI to sample much larger radial and azimuthal wavelengths. The largest radial dynamic ranges are achieved in 2D[13]. However, 2D simulations do not treat the MRI accurately because of Cowling's antidynamo theorem (Cowling 1933), which limits the growth of the poloidal magnetic field and causes turbulence to die away. Thus, no steady accretion is possible in 2D and one has to carefully select a period of time after the disk has become turbulent but before the turbulence dies out. There has been no systematic study of how well the properties of this intermediate period in 2D simulations agree with those of 3D simulations with sustained turbulence. Qualitatively, it appears that the differences are not large.

Hawley (2000) compared the results of local shearing box and global simulations using two different initial configurations of the magnetic field: toroidal and vertical. In terms of growth of the MRI and transition to MHD turbulence, he found global and shearing box simulations to behave similarly. The magnetic shear stress $T_{R\phi}$ is directly proportional to the magnetic pressure, $2\langle B_R B_\phi\rangle \approx (0.4-0.5)\langle B^2\rangle$; this is equivalent to $\alpha\beta \approx 0.5$ mentioned earlier. Depending on the value of β, the resulting $\alpha \approx 0.05-0.2$ in the interior of the disk (e.g., Penna et al. 2013b). The Maxwell (magnetic) stress is always larger than the Reynolds stress by a factor of several. Also, the toroidal component of the field is significantly larger than the radial component, which is itself somewhat larger than the vertical component. While most global simulations start with a weak magnetic field (initial $\beta \sim 100$), Machida et al. (2000) used a strong initial toroidal field with $\beta = 1$. There was no MRI in their simulation, but they found the Parker instability, which led to the formation of a magnetized corona.

Global 3D MHD simulations have been run by various groups, and the results are fairly similar. Early work assumed Newtonian dynamics and modeled the black hole at the center via a pseudo-Newtonian potential (Armitage 1998; Hawley 2000; Machida et al. 2000, 2004; Hawley & Krolik 2001; De Villiers & Hawley 2003b; Igumenshchev et al. 2003). General relativistic MHD (GRMHD) codes were later developed (Koide et al. 1999, Gammie et al. 2003, De Villiers & Hawley 2003a, Fragile et al. 2007). Much of the recent work in this field is based on the latter codes, which provide a more realistic description of phenomena close to the black hole. Nevertheless, pseudo-Newtonian simulations are still useful for studying large scale properties of the accretion flow.

Representative results from 3D GRMHD simulations can be found in the series of early papers by De Villiers and collaborators (De Villiers et al. 2003, 2005; Hirose et al. 2004; Krolik et al. 2005) and Gammie and collaborators (Gammie et al. 2004, McKinney & Gammie 2004, McKinney 2006). The simulations are initialized with a rotating torus in hydrostatic equilibrium and embedded with a weak poloidal magnetic field. Accretion occurs self-consistently as a result of MHD turbulence generated by the MRI, and the accretion flow separates into three qualitatively different regions (Fig. 4): disk body, corona, axial funnel.

[13]With current computer resources, 3D simulations can reach inflow equilibrium over at best only about 2 orders of magnitude in radius (e.g., Pang et al. 2011, McKinney et al. 2012, Narayan et al. 2012b, Sadowski et al. 2013a), a substantial part of which is dominated by either inner or outer boundary conditions. 2D simulations can achieve a factor of several larger dynamic range.

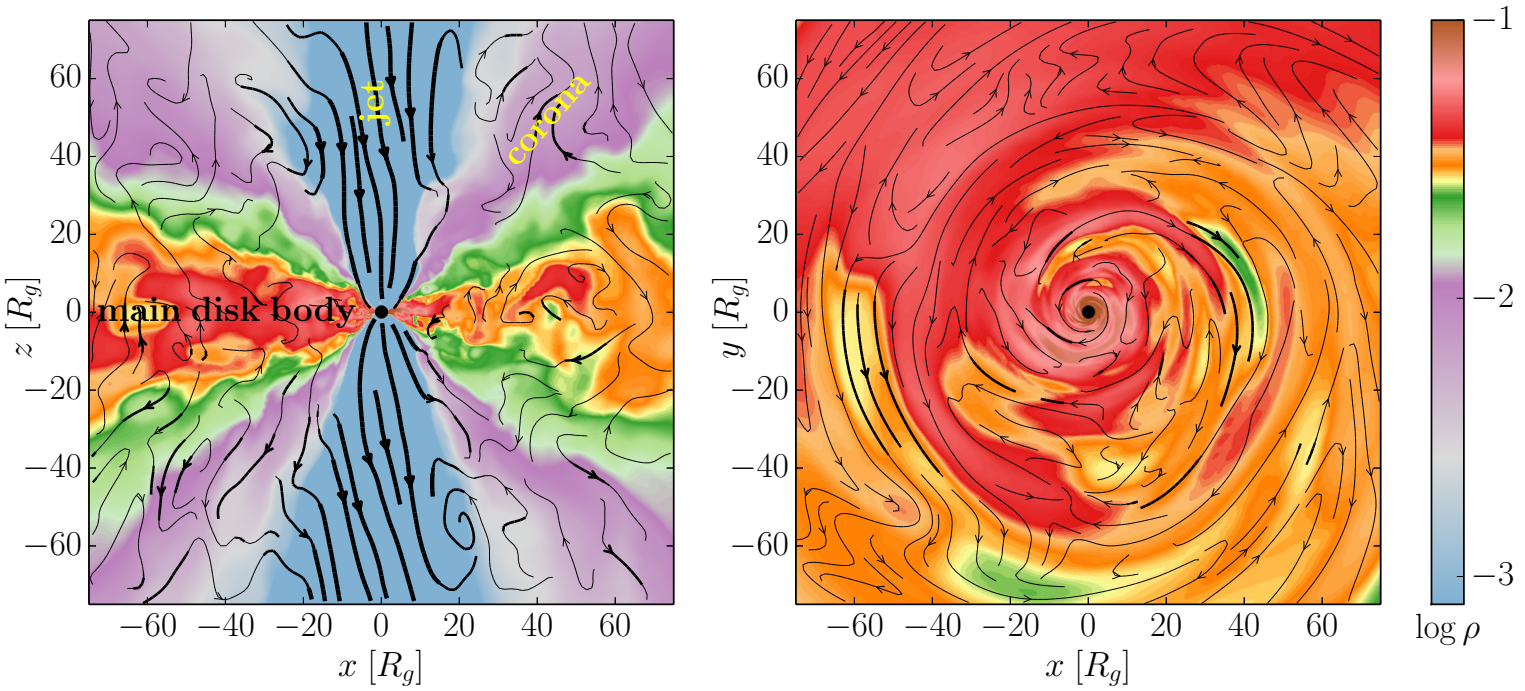

Figure 4: An instantaneous poloidal slice at a fixed azimuthal angle (*left*) and a slice through the equatorial plane (*right*) from a 3D GRMHD simulation of a hot accretion flow around a spinning black hole ($a_* \equiv a/M = 0.7$). The black hole is at (0,0) and lengths are in units of $R_g = GM/c^2$. Three regions of the flow are identified: main disk body, corona, jet. Color indicates density, with fluctuations evident due to turbulence. Lines trace the magnetic field in the two image planes, with the out-of-plane component ignored. Arrows show the direction of the magnetic field and line thickness indicates magnetic energy density relative to other energy densities: the thickest lines correspond to regions with comoving $B^2/4\pi > \rho c^2$ (found primarily in the region of the jet), intermediate thickness lines indicate regions with (see eq. 15) $\beta < 4$ (mostly in the corona), and thin lines correspond to regions with the weakest magnetization, $\beta > 4$ (primarily in the main disk body). (Figure courtesy of A. Tchekhovskoy, based on data from Sadowski et al. 2013a.)

The disk body is turbulent and dense and has a roughly constant value of H/R, consistent with 1D self-similar and global solutions (§2). The magnetic field within the disk is sub-equipartition ($\beta \sim 10 - 100$), and both the magnetic field and velocity streamlines are chaotic, as expected for turbulence. Inside the innermost stable circular orbit (ISCO) is the plunging region. Here the flow spirals in rapidly toward the black hole horizon and the motion is almost laminar. While the ISCO is roughly where the turbulent gas in the disk transitions to laminar inflow, there is no other specific signature in the flow dynamics associated with the ISCO. This is in contrast to the case of thin disks, where the flow changes dramatically across the ISCO (Reynolds & Fabian 2008, Shafee et al. 2008, Penna et al. 2010, but see Noble et al. 2010).

Above and below the main disk is the corona, where the gas density is much lower. The magnetic field here is more regular than in the disk body, and tends to be toroidal. The magnetic and gas pressure are roughly comparable ($\beta \sim 1$). The value of β decreases with increasing distance away from the midplane, with $\beta \sim 0.1$ above about two density scale heights (De Villiers et al. 2003, 2005). The corona is the launchpad for the disk wind (§3.4).

The axial funnel is a magnetically dominated region in which the gas is very tenuous. This is the location of the jet (§3.3). The magnetic field is predominantly radial close to the black hole, where the jet extracts rotational energy from the black hole spin (§3.3.1). Far from the black hole the field becomes mostly toroidal and carries the jet power in the form of a Poynting flux. The boundary of the funnel (the funnel wall) corresponds to the centrifugal barrier associated with material originating from the innermost region of the disk. The jet here is less relativistic and is powered at least partly by the rotation of the accretion flow (§3.3.2). Hence it is less sensitive to the black hole spin. Overall, there is a smooth variation of properties, going from highly magnetically dominated conditions at the axis to progressively larger gas content with increasing distance from the axis. Past the funnel wall, the jet merges with the corona where the disk wind is launched (§3.4)

The effect of different initial magnetic field geometries has been investigated by a number of authors (e.g., Hawley & Krolik 2002, Igumenshchev et al. 2003 with a pseudo-Newtonian potential; and Beckwith et al. 2008, McKinney & Blandford 2009 with GRMHD). Models with a purely toroidal initial field evolve much more slowly than those with poloidal initial field. This is because the former have neither an initial vertical field, which is needed for the linear MRI, nor a radial field, which is needed for field amplification via shear. Inflow begins only after the MRI has produced turbulence of sufficient amplitude (Hawley & Krolik 2002), which happens much later when the initial field is toroidal. Generally, once saturation has been reached, the disk properties do not depend much on the initial field topology. On the other hand, jet properties are very sensitive (§3.3).

In the case of geometrically thin accretion disks, it is believed that Lense-Thirring precession causes a tilted disk to align with the spin axis of the black hole out to a fairly large radius (Bardeen & Petterson 1975, Scheuer & Feiler 1996, Lodato & Pringle 2006). Fragile and collaborators have carried out a number of numerical simulations of tilted hot accretion flows (Fragile et al. 2007, 2009; Fragile 2009; Dexter & Fragile 2011, 2013). They find that the disk does not align with the black hole, in agreement with theoretical predictions for a geometrically thick disk (Papaloizou & Lin 1995). Instead the disk precesses as a whole out to some radius. Alignment does happen when accretion occurs in the

MAD regime (§3.2.3) and might have observational implications for relativistic jets (McKinney et al. 2013).

The precession of a tilted disk will lead to time-dependence in the observed radiation from a hot accretion flow, and could potentially explain some low frequency quasi-periodic oscillations (QPOs) seen in BHBs (Ingram et al. 2009, Ingram & Done 2011, Veledina et al. 2013). It is unlikely that high frequency QPOs can be explained in a similar fashion (Dexter & Fragile 2011). A number of authors (e.g., Bursa et al. 2004, Blaes et al. 2006, Abramowicz et al. 2006) have explored oscillation modes of tori in this connection. Recently, high frequency QPOs have been reported in numerical GRMHD simulations of geometrically thick hot accretion flows (Dolence et al. 2012) and magnetic arrested disks (§3.2.3, McKinney et al. 2012, Shcherbakov & McKinney 2013).

A few authors have carried out simulations of magnetized spherical accretion (Igumenshchev & Narayan 2002, Igumenshchev 2006) as well as accretion of low-angular momentum gas (Proga & Begelman 2003, Mościbrodzka et al. 2007, Janiuk et al. 2009). These topics are beyond the scope of this review.

We conclude with some general remarks on numerical accuracy. Since energy advection plays a key role in hot accretion flows, it is important to ensure that numerical codes conserve energy accurately. Early numerical simulations were based on codes that evolve the internal energy of the gas. Such codes do not conserve total energy and can introduce an effective numerical cooling that is hard to quantify. An alternative Godunov-based approach has come to the fore in recent years. This enforces strict mass, momentum and total energy conservation, as exemplified by the pioneering relativistic MHD code of Komissarov (1999, 2001), the GRMHD codes HARM (Gammie et al. 2003) and COSMOS++ (Anninos et al. 2005), and the Newtonian MHD code ATHENA (Stone et al. 2008). Direct comparison of simulations using both techniques shows that accretion flows simulated with non-energy conserving codes tend to be geometrically thinner than they should be.

The effect of numerical resolution on global simulation results has been investigated recently by a number of authors (Sorathia et al. 2010; Hawley et al. 2011, 2013; Shiokawa et al. 2012). These studies achieved numerical convergence in terms of shell-averaged quantities, azimuthal correlation length of fluid variables, and synthetic spectra. It appears that most previous global simulations might have been somewhat under-resolved.

3.2.3 Magnetically arrested disk

Magnetically dominated hot accretion flows have recently come to the fore, thanks to the advent of numerical MHD simulations. One version of these models, called a "magnetically arrested disk" (MAD, Narayan et al. 2003, Igumenshchev et al. 2003, Igumenshchev 2008) or a "magnetically choked accretion flow" (MCAF, McKinney et al. 2012), is based on an idea originally proposed by Bisnovatyi-Kogan & Ruzmaikin (1974), in which a strong vertical bipolar magnetic field is pushed into the central black hole by the thermal and ram pressure of the accreting gas. A significant amount of magnetic flux threads the horizon. As a result, the field outside the black hole becomes so strong that it disrupts the axisymmetric accretion flow, forcing the gas to move inward via streams and blobs through an interchange instability. This behavior was first noted by Igumenshchev et al. (2003) in 3D Newtonian MHD simulations and was later confirmed in 3D

GRMHD simulations (Tchekhovskoy et al. 2011, 2012; McKinney et al. 2012). Current interest in MAD accretion is driven by the discovery that it leads to very powerful relativistic jets (§3.3).

All magnetized accretion flows cause a certain amount of magnetic flux to thread the black hole. The MAD state is special in that the flux threading the hole is at its maximum saturation value for the given mass accretion rate $\dot{M}_{\rm BH}$. This saturation flux is approximately[14] (Tchekhovskoy et al. 2011, 2012)

$$\Phi_{\rm MAD} \approx 50\, \dot{M}_{\rm BH}^{1/2} R_g c^{1/2} = 1.5\times 10^{21}\, m^{3/2} \dot{m}_{\rm BH}^{1/2}\ {\rm G\,cm^2}, \tag{28}$$

where m and $\dot{m}$ are defined in eq. (14) and $R_g = GM/c^2 = R_S/2$ (half the Schwarzschild radius) is the gravitational radius of the black hole. The corresponding field strength at the horizon is roughly[15] (compare eq. 12)

$$B_{\rm MAD} \approx \frac{\Phi_{\rm MAD}}{2\pi R_g^2} = 10^{10}\, m^{-1/2} \dot{m}_{\rm BH}^{1/2}\ {\rm G}. \tag{29}$$

Systems that have not reached the MAD limit have been referred to as SANE ("standard and normal evolution", Narayan et al. 2012b). They span a one-parameter family of models extending from $\Phi = 0$ up to a magnetic flux just below $\Phi_{\rm MAD}$. Structural differences are evident between MAD and SANE models (Narayan et al. 2012b, Sadowski et al. 2013a), most notably in the jet.

It should be noted that, unlike small-scale fields, a large-scale vertical magnetic field cannot be dissipated locally (since the plasma has negligible resistivity), nor can it be absorbed by the central black hole (e.g., even when field lines thread the horizon, the external magnetic flux is unaffected, see Igumenshchev et al. 2003). But how does vertical field reach the center in the first place? Presumably the field is advected in from whatever external mass reservoir feeds the accretion flow. Such advection happens quite efficiently in numerical simulations, especially in the case of geometrically thick hot accretion flows. However, most simulations are limited to radii relatively close to the black hole and it is not clear that the same physics will necessarily operate at larger radii. If outward diffusion of the magnetic field via reconnection is inefficient (Spruit & Uzdensky 2005, Bisnovatyi-Kogan & Lovelace 2007, Rothstein & Lovelace 2008, Cao 2011), as seems especially likely for geometrically thick accretion flows (Livio et al. 1999; Guilet & Ogilvie 2012, 2013), magnetic field should be readily advected in from large radii. Magnetic field can also be brought in efficiently via the corona (Beckwith et al. 2009). At least in the case of supermassive black holes accreting from an external medium, plenty of magnetic flux is available in the mass reservoir (e.g., Narayan et al. 2003). Therefore, all supermassive black holes with hot accretion flows should quickly approach the MAD limit, provided flux is advected efficiently. The situation is less clear in the case of BHBs, since the supply of net

[14] $\Phi_{\rm MAD}$ has a weak dependence on the black hole spin as well as the disk thickness (see Tchekhovskoy et al. 2013), but we ignore this complication for clarity.

[15] Simulation results are often given in Heaviside-Lorentz units, whereas numerical estimates in this article are in gaussian units. The two differ by a factor of $\sqrt{4\pi}$. For instance, the magnetic pressure is $B^2/8\pi$ in gaussian units but $B^2/2$ in Heaviside-Lorentz units. Note also that the magnetic field strength is frame-dependent. For instance, when evaluating the magnetic pressure, especially for computing the value of β (eq. 15, Fig. 4), one must consider the field strength in the comoving fluid frame, i.e., $B^2/4\pi \rightarrow b^2$ in the notation of Komissarov (1999) and Gammie et al. (2003). On the other hand, $B_{\rm MAD}$ and $\Phi_{\rm MAD}$ in eq. (29) are evaluated in the stationary coordinate frame or "lab frame".

magnetic flux depends on the properties of the companion star and the details of the mass transfer.

Two additional magnetically dominated accretion models have been discussed. Meier (2005, see also Fragile & Meier 2009) proposed that the inner regions ($R \lesssim 50R_S$) of a hot accretion flow may be converted into a magnetically-dominated magnetosphere-like phase in which a strong, well-ordered field is present rather than the weak, turbulent field usually seen in a hot flow. A different possibility is the "magnetically supported accretion flow" model proposed by Oda et al. (2010), stimulated by MHD simulations described in Machida et al. (2006). This kind of flow exists only when the accretion rate is relatively high, well above $\dot{M}_{\rm crit,ADAF}$. Both of these models have a magnetic field geometry dominated by radial and toroidal fields, which is different from the vertical poloidal field envisaged in the MAD model.

3.3 Jets in hot accretion flows

It was conjectured already in early papers (Narayan & Yi 1994, 1995a; Blandford & Begelman 1999) that hot accretion flows should have strong winds and, by extension, jets. Observational evidence for such an association has accumulated in recent years with the recognition that essentially all low-luminosity AGNs are radio loud (Nagar et al. 2000, Falcke et al. 2000, Ho 2002) and the parallel discovery that virtually every BHB in the hard state has radio emission (Corbel et al. 2000; Fender 2001, 2006; Fender et al. 2004). Since all these systems are believed to have hot accretion flows (§4.2), it seems likely that there is a direct causal connection between hot flows and radio-emitting jets. In contrast, jets are much weaker, and often not seen at all, in systems that have cool geometrically thin disks. While there is no definitive explanation for this dichotomy, it is likely that three effects play a role: (i) geometrically thick disks more easily advect magnetic field to the black hole compared to thin disks (Livio et al. 1999, Guilet & Ogilvie 2012); (ii) the Bernoulli parameter of the gas in hot accretion flows is larger, hence enhancing winds in these systems (Narayan & Yi 1994, 1995a; Blandford & Begelman 1999); (iii) strong winds help to collimate and stabilize the jet (Appl & Camenzind 1992, 1993; Beskin & Malyshkin 2000).

Although many models of jets have been proposed over the years, the current consensus is that jets arise from a combination of magnetic fields and rotation. Especially influential in this field are the Blandford-Znajek model (BZ, Blandford & Znajek 1977; see also Ruffini & Wilson 1975, Lovelace 1976, MacDonald & Thorne 1982; Phinney 1983; Thorne et al. 1986; Punsly & Coroniti 1989; Komissarov & McKinney 2007, Tchekhovskoy et al. 2011; Penna et al. 2013a) and the Blandford-Payne model (BP, Blandford & Payne 1982; see also Pudritz & Norman 1983; Heyvaerts & Norman 1989; Li et al. 1992; Contopoulos & Lovelace 1994; Ostriker 1997; Vlahakis & Konigl 2003). The primary distinction between the two models is the energy source of the jet. In the BZ model, the source is the rotational energy of the black hole, while in the BP model, it is the rotational energy of the accretion flow. Numerical simulations suggest that truly relativistic jets are produced primarily by the BZ mechanism, while quasi-relativistic jets and non-relativistic winds may be driven by a combination of the BP and other mechanisms. In the following discussion we use the term "BZ jet" for the truly relativistic BZ-powered outflow, and refer to the quasi-relativistic outflow from the inner region of the accretion flow as the "disk jet".

3.3.1 Relativistic BZ jet

In the BZ model a large-scale poloidal magnetic field passes through the ergosphere of the rotating black hole and threads the horizon (cf §3.2.3). Frame dragging by the rotating hole leads to the creation of toroidal field and hence a Poynting flux. The key to the BZ process, which goes back to the influential work of Penrose (1969) and subsequently Ruffini & Wilson (1975), is the fact that, within the ergosphere, it is possible to have a negative inward electromagnetic energy flux as measured at infinity. This negative energy flux enters the horizon, thereby reducing the mass-energy and angular momentum of the hole. Correspondingly, there is an outgoing Poynting-dominated jet which carries positive energy and angular momentum. At its most basic, the outflowing power in the BZ model is given by (Blandford & Znajek 1977; see Tchekhovskoy et al. 2010 for more accurate approximations)

$$P_{\rm BZ} = \frac{\kappa}{4\pi c}\Phi^2\Omega_{\rm H}^2, \tag{30}$$

where Φ is the magnetic flux threading the horizon, $\Omega_{\rm H} = a_* c/2R_{\rm H}$ is the angular velocity of the horizon, $a_* \equiv a/M$ is the dimensionless spin parameter of the black hole, and $R_{\rm H} = R_g(1+\sqrt{1-a_*^2})$ is the radius of the horizon. The numerical coefficient κ depends weakly on the magnetic field geometry and is approximately ≈ 0.05. The above formula highlights the fact that the BZ mechanism requires two key ingredients: an ordered magnetic flux at the horizon (Φ), and rotation of the black hole ($\Omega_{\rm H}$).

Many MHD simulations of hot accretion flows have been performed to study jet formation (e.g., Kudoh et al. 1998; Koide et al. 1999, 2000; Kuwabara et al. 2000; Hawley & Balbus 2002; Koide 2003; McKinney & Gammie 2004; Kato et al. 2004a, 2004b; De Villiers et al. 2005; McKinney 2005, 2006; Hawley & Krolik 2006; Komissarov et al. 2007; McKinney & Blandford 2009; Tchekhovskoy et al. 2011; McKinney et al. 2012, Sadowski et al. 2013a). The simulations are typically initialized with a gas torus threaded with a weak magnetic field. It is found that a large-scale magnetic field forms self-consistently at the black hole horizon, as required by the BZ model, even though such a field is not present in the initial state (e.g., Igumenshchev et al. 2003; De Villiers et al. 2003, 2005; McKinney 2006; Tchekhovskoy et al. 2011), and that the magnetic flux is trapped within a funnel, causing the outgoing power to be collimated in a relativistic jet. However, a powerful jet forms only if the initial field in the simulation has a favorable poloidal configuration. A dipolar field is ideal. If a quadrupolar initial field is adopted, the field in the funnel is much weaker, and if a toroidal field is adopted, no funnel field at all develops (Igumenshchev et al. 2003, De Villers et al. 2005, Beckwith et al. 2008, McKinney & Blandford 2009). In the latter case there is no BZ jet.

The jet power measured in simulations shows good agreement with the predictions of the BZ model (eq. 30), modulo modest changes in the coefficient due to the presence of the surrounding thick disk. A rough estimate of the BZ jet power

is obtained by combining equations (28) and (30)[16],

$$P_{\rm jet} \approx 2.5 \left(\frac{a_*}{1+\sqrt{1-a_*^2}} \right)^2 \left(\frac{\Phi}{\Phi_{\rm MAD}} \right)^2 \dot{M}_{\rm BH} c^2, \tag{31}$$

where $\Phi_{\rm MAD}$ is the limiting magnetic flux defined in equation (28) and Φ is the actual flux threading the black hole horizon. As is evident from this relation, the most favorable situation is when the magnetic flux has reached the MAD limit ($\Phi \rightarrow \Phi_{\rm MAD}$) and the black hole spin is maximum ($a_* \rightarrow 1$). In this limit, the BZ jet power can exceed the total accretion energy budget of $\dot{M}_{\rm BH} c^2$ (Tchekhovskoy et al. 2011, 2012; Tchekhovskoy & McKinney 2012). Although at first sight this might appear to violate energy conservation, there is no inconsistency since most of the jet energy comes directly from the spinning black hole via a generalization of the Penrose (1969) process.

Many studies have been published over the years, providing estimates of the jet power as a function of black hole spin (e.g., Hawley & Balbus 2002; De Villers et al. 2005; McKinney 2005, 2006; Hawley & Krolik 2006). While the numerical values given do not always agree, the results are consistent with the above BZ-derived relation, once the dependence on magnetic flux is taken into account. Modest differences are seen between prograde and retrograde disks, with prograde producing somewhat stronger jets (Tchekhovskoy & McKinney 2012). In addition, the physics near the horizon in the simulations matches very closely the physics of the BZ mechanism (Penna et al. 2013a) as described in the membrane paradigm (Thorne et al. 1986). It also satisfies all the requirements to be viewed as a form of generalized Penrose process (Lasota et al. 2014).

Another quantity of interest is the asymptotic Lorentz factor of the jet, $\gamma_{\rm jet}$. Unfortunately, the value of $\gamma_{\rm jet}$ depends on how much mass is loaded on magnetic field lines, the physics of which is very poorly understood. The current best guess is that mass-loading occurs via pair creation through breakdown of a vacuum gap (Beskin et al. 1992; Hirotani & Okamoto 1998). However, in simulations, mass-loading is treated in an entirely ad hoc fashion by applying a minimum "floor" value for the gas density. The resulting jet Lorentz factor tends to be large on the axis and to decrease outward, but the values obtained do not mean much without a physical model of mass-loading. Mass loss in the jet $\dot{M}_{\rm jet}$ and jet Lorentz factor $\gamma_{\rm jet}$ are related by $P_{\rm jet} \approx \gamma_{\rm jet} \dot{M}_{\rm jet} c^2$ (including the rest mass energy of the ejected gas). Whereas $P_{\rm jet}$ can be calculated with reasonable confidence from simulations, neither $\dot{M}_{\rm jet}$ nor $\gamma_{\rm jet}$ can be estimated reliably.

3.3.2 Quasi-relativistic disk jet

Surrounding the relativistic BZ jet discussed in the previous subsection is a quasi-relativistic disk jet. The key distinctions are: (i) the disk jet is matter-dominated, not Poynting flux dominated,[17] and (ii) the disk jet is powered by the inner regions of the accretion disk, not directly by the black hole. There is no unambiguous

[16] This formula slightly underestimates the jet power for slow spins and overestimates the power for rapid spins. A better approximation is $P_{\rm jet} \approx 0.65 a_*^2 (1 + 0.85 a_*^2)(\Phi/\Phi_{\rm MAD})^2 \dot{M}_{\rm BH} c^2$ (A. Tchekhovskoy, private communication).

[17] The recent detection of Doppler-shifted X-ray emission lines in the candidate black hole binary, 4U1630–47 (Diaz Trigo et al. 2013), suggests that at the time of the observations this system might have had a baryon-loaded jet. What was observed was conceivably a disk-jet, and perhaps also an episodic jet (§3.3.3).

way to demarcate the two regions, and different authors have used different prescriptions to identify the boundary (e.g., Hawley & Krolik 2006, Tchekhovskoy et al. 2011). The outflow power of the disk jet is typically $< 0.1\dot{M}_{\rm BH}c^2$, and it varies only modestly with the parameters Φ and a_*, in contrast to the steep dependence in the case of the BZ jet (eq. 31). As a result, when $\Phi \ll \Phi_{\rm MAD}$ (extreme SANE limit), the power in the disk jet can be larger than that in the BZ jet even though the black hole may be spinning rapidly (De Villiers et al. 2005, Sadowski et al. 2013a). Observationally, the disk jet will produce radio emission and will behave in many respects like a relativistic jet. However, its Lorentz factor is usually modest.

The quasi-relativistic disk jet receives energy from the disk via magnetic fields anchored in the accretion flow. In the BP model, if the field lines are angled outward sufficiently with respect to the disk rotation axis, there is a net outward centrifugal force on matter threading the field. As gas is accelerated outward along the rotating field lines, its angular momentum increases, thereby causing further acceleration. The relevance of the BP mechanism to quasi-relativistic outflows in GRMHD simulations has not been explored systematically.

An alternative magnetic tower mechanism has been proposed in which a strong toroidal magnetic field is produced by the differential rotation of the accretion flow, and the resulting magnetic pressure gradient causes gas to be accelerated away from the disk surface (Lynden-Bell 2003). Structures analogous to a magnetic tower have been seen in some MHD simulations (e.g., Shibata & Uchida 1985, 1986; Kato et al. 2004b). In addition, there is a suggestion (Hawley & Krolik 2006) that acceleration of the disk jet is caused, not by centrifugal force (BP), but by the gradient of magnetic and gas pressure (magnetic tower).

3.3.3 Episodic jet

Observations show that BHBs have two distinct kinds of jets (Fender & Belloni 2004): steady jets and episodic (or ballistic) jets. Episodic jets are most obviously observed in BHBs during the transition from the hard to the soft state (McClintock & Remillard 2006, Remillard & McClintock 2006), often at luminosities close to Eddington. However, there is a hint that these jets can occur also at lower luminosities (Cyg X-1, Fender et al. 2006; Sgr A*, Yusef-Zadeh et al. 2006, §4.1.3; other examples are reviewed in Yuan et al. 2009a). The most distinctive difference between the two jets is that the episodic jet is transient and is in the form of discrete, isolated blobs, while the steady jet behaves like a continuous outflow. Other differences have been noted in the polarization, spectrum, and power (Fender & Belloni 2004).

It is unclear whether the models reviewed in §3.3.1 and §3.3.2 are applicable to episodic jets since the simulations discussed there generally give quasi-steady jets. Numerical MHD simulations of accretion disks in other contexts do produce episodic ejections of magnetized blobs from the disk surface (e.g., Romanova et al. 1998, Kudoh et al. 2002, Kato et al. 2004a, Dyda et al. 2013), although the underlying physics has not been identified clearly[18].

By analogy with coronal mass ejections in the Sun, which is another example of episodic mass ejection, Yuan et al. (2009a) proposed an MHD model for the

[18]Interestingly, similar episodic ejection have also been found in MHD simulations of accretion disks around young stellar objects, and are possibly better understood there (e.g., Hayashi et al. 1996, Goodson et al. 1999, Goodson & Winglee 1999).

formation of episodic jets.[19] In this model, a flux rope is first formed in the corona due to the twisting of magnetic loops emerging from the disk body via the Parker instability. The flux rope is initially in force equilibrium between magnetic tension and magnetic pressure. However, with further twisting of the field lines, a threshold energy is reached. The flux rope jumps upward, causing a reconnection event to occur. This results in a substantial enhancement of the magnetic pressure force and weakening of the tension force, causing the flux rope to be ejected. This model is similar to the magnetic tower model (Lynden-Bell 2003) discussed earlier, except that here it is time-dependent and involves a flux rope.

3.4 Disk Wind from hot accretion flows

Outside the quasi-relativistic disk jet and above the main disk body lies the bulk of the mass outflow from the disk (Yuan et al. 2012a, Narayan et al. 2012b, Sadowski et al. 2013a). We call this the disk wind. In contrast to the BZ jet and the disk jet, the disk wind is non-relativistic and moves slowly. However, it occupies a much larger solid angle. The mass loss rate is also quite high, although the rate of outflow of energy is small compared to the power in the BZ jet or the disk jet (Yuan et al. 2012a, Sadowski et al. 2013a). As in the case of the boundary between the BZ jet and the disk jet, here again there is no unabiguous way to identify the boundary between the disk jet and the disk wind.

The likelihood that ADAFs will have strong winds was pointed out by Narayan & Yi (1994, 1995a), but these authors were unable to come up with a quantitative prediction for the amount of mass loss in the wind. Blandford & Begelman (1999) described a family of self-similar solutions with a wide range of assumed outflow efficiencies, again emphasizing the inability of analytical models to say anything definite about the magnitude of mass and energy loss in winds. This uncertainty has been a serious bottleneck in the development of one-dimensional models of hot accretion flows, and is an important motivation for doing numerical simulations. From a practical standpoint, it is essential to understand the nature of disk winds in hot accretion flows because (i) mass loss can strongly affect the dynamics of the accreting gas, and (ii) disk winds canx be a powerful contributor to AGN feedback (§5).

In an important pioneering study of winds from hot accretion flows, Stone et al. (1999) carried out numerical 2D HD simulations and calculated the mass inflow, outflow and net accretion rates via the following integrals,

$$\dot{M}_{\rm in}(r) = -2\pi r^2 \left\langle \int_0^\pi \rho \min(v_r, 0) \sin\theta d\theta \right\rangle_{t\phi}, \quad (32)$$

$$\dot{M}_{\rm out}(r) = 2\pi r^2 \left\langle \int_0^\pi \rho \max(v_r, 0) \sin\theta d\theta \right\rangle_{t\phi}, \quad (33)$$

$$\dot{M}_{\rm net} = \dot{M}_{\rm in} - \dot{M}_{\rm out}, \quad (34)$$

where the angle brackets represent an average over time (and also azimuthal angle ϕ in the case of 3D simulations). The quantity $\dot{M}_{\rm net}$ is the net mass accretion rate; in steady state, it is equal to the accretion rate on the black hole $\dot{M}_{\rm BH}$. Stone et al. (1999) found, as has been confirmed in many later simulations (see

[19] Massi & Poletto (2011) discuss other interesting similarities between coronal mass ejections and AGN jets.

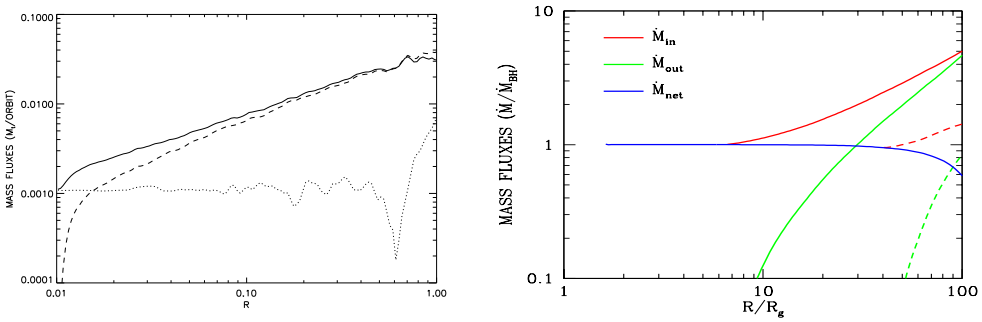

Figure 5: Radial profiles of mass inflow rate $\dot{M}_{\rm in}$, mass outflow rate $\dot{M}_{\rm out}$ and net mass accretion rate $\dot{M}_{\rm net}$ (eqs. 32, 33, 34). *Left:* Results from a 2D Newtonian HD simulation of a hot accretion flow (Stone et al. 1999). Solid, dashed, and dotted lines correspond to $\dot{M}_{\rm in}$, $\dot{M}_{\rm out}$ and $\dot{M}_{\rm net}$, respectively. Note the rapid increase of $\dot{M}_{\rm out}$ with increasing radius. *Right:* Solid lines show equivalent results from a 3D GRMHD simulation of a hot accretion flow around a non-spinning black hole ($a_* = 0$, Narayan et al. 2012b). Mass outflow becomes important only beyond a radius $\sim 30R_g$, though the slope outside this radius is similar to that in the panel on the left. Dashed lines show results for a different kind of time-averaging, as described in the text. Here the estimated mass outflow rate is very much smaller (see also the top-left panel of Fig. 14 in Yuan et al. 2012a). The true mass outflow rate is likely to be in between the solid and dashed green lines.

references below), that both $\dot{M}_{\rm in}$ and $\dot{M}_{\rm out}$ decrease inward, following roughly a power-law behavior (see eq. 6),

$$\dot{M}_{\rm in}(r) = \dot{M}_{\rm in}(r_{\rm out}) \left(\frac{r}{r_{\rm out}}\right)^s, \qquad s > 0. \tag{35}$$

This is illustrated in the left panel in Fig. 5. Correspondingly, the radial profile of density becomes flatter than in a self-similar ADAF solution: $\rho(r) \propto r^{-p}$ with $p < 1.5$. These statements appear to be true regardless of whether one considers hydro simulations (Stone et al. 1999, Yuan & Bu 2010, Yuan et al. 2012b, Li et al. 2013a) or MHD simulations (Stone & Pringle 2001, Machida et al. 2001, Hawley et al. 2001, Hawley & Balbus 2002, Igumenshchev et al. 2003, Pen et al. 2003, Kato et al. 2004b, Pang et al. 2011, Yuan et al. 2012a).

The values of s and p in various simulations are summarized in Yuan et al. (2012b): $s = 0.4 - 0.8$, $p = 0.5 - 1$. The variations between different simulations seem to be due to differences in the value of the viscosity parameter α (in the case of hydro simulations), choice of Newtonian gravity versus general relativity, initial configuration of the magnetic field (toroidal or poloidal), and the strength of the initial field (weak or strong). Observationally, there is support for a value of $s \sim 0.3$, $p \sim 1$ (see the discussion of Sgr A* in §4.1). The apparent discrepancy between theory and observations may be due to low angular momentum of the accretion flow in Sgr A* (Bu et al. 2013) or dynamical importance of thermal conduction (§3.6; Johnson & Quataert 2007).

Competing models have been proposed to explain the radially varying inflow and outflow rates seen in numerical simulations. In the adiabatic inflow-outflow

solution (ADIOS; Blandford & Begelman 1999, 2004; Begelman 2012), the inward decrease of $\dot{M}_{\rm in}$ is due to a genuine mass loss in a wind. What drives the wind is unspecified in the model. Assuming merely that a mechanism exists for draining energy from the interior of the accretion flow to launch a wind, the authors construct 1D and 2D self-similar solutions. In their models, the index s is left as a free parameter, limited only by the condition $0 \leq s \leq 1$. In the most recent version of the ADIOS model, however, Begelman (2012) considers the inflow and outflow zones on an equal footing and, using a conserved outward energy flux, finds that s should be close to unity. This is somewhat larger than the range of values seen in numerical simulations.

An alternative scenario is the convection-dominated accretion flow (CDAF) model (Narayan et al. 2000, Quataert & Gruzinov 2000, Abramowicz et al. 2002a, Igumenshchev 2002), which is based on the assumption that a hot accretion flow is convectively unstable (Narayan & Yi 1994). In this model, inward angular momentum transport by convection and outward transport by viscous stresses almost cancel each other. A convective envelope solution can then be constructed which has a conserved (outward) convective luminosity and automatically produces a flat density profile. The gas constantly moves in and out in turbulent convective eddies, and this motion gives the impression that there are large fluxes of inflowing and outflowing matter. However, none of the outgoing gas really escapes, and the net accretion rate is quite small. There is unresolved discussion in the literature on whether the CDAF model can be applied to MHD accretion flows (Stone & Pringle 2001, Hawley & Balbus 2002, Narayan et al. 2002).

The ADIOS and CDAF scenarios are very different from each other and it would seem that numerical simulations ought to be able to discriminate between them easily. In this context, the key question is: how strong is the "real" wind in a simulated hot accretion disk? This is not easy to answer. Returning to equations (32), (33), note that the integrals are computed at each instant of time using instantaneous velocities, and the integrals are then averaged over t and ϕ to obtain $\dot{M}_{\rm in}(r)$ and $\dot{M}_{\rm out}(r)$. This procedure gives undue importance to turbulent motions. Especially at large radii, where a given turbulent eddy will consist of roughly half the gas moving in and half moving out, one is likely to overestimate both the inflow rate and outflow rate. A parcel of gas that is moving out at a particular time will likely soon turn around and begin to flow in. Thus, the inflow and outflow rates estimated via equations (32) and (33) will both be overestimates of the true values.

An alternative approach is to move the $t\phi$ average inside the integrals, i.e., to integrate $\min(\langle \rho v_r \rangle_{t\phi}, 0)$ and $\max(\langle \rho v_r \rangle_{t\phi}, 0)$ (see Narayan et al. 2012b). This eliminates contributions from the to-and-fro motion due to turbulence, and not surprisingly produces substantially lower estimates for the mass outflow rate (see the dashed lines in the right panel of Fig. 5). However, this procedure too is problematic — it could underestimate the real outflow rate if some genuine outflowing streams wander around in three-dimensional space (Yuan et al. 2012a). Therefore, the estimated mass outflow rate obtained by this method is a lower limit.

Yuan et al. (2012a) present an alternative way to roughly estimate the strength of the wind. They calculate and compare the various properties of inflow and outflow such as angular momentum and temperature. They find that the properties are quite different whereas, if the inflowing and outflowing motion were domi-

nated by turbulence, the properties would be roughly similar[20]. They therefore conclude that systematic outflow must exist and the rate of real outflow should be a significant fraction of that indicated by eq. (33). Yuan et al. (2012a) investigate the production mechanism of the wind. Based on the much larger angular momentum of outflow compared to inflow, they argue that the magneto-centrifugal force must play an important role. They also briefly discuss the velocity of the wind (see also Li et al. 2013a).

An influential concept in theoretical discussions of outflows is the Bernoulli parameter Be, which is the sum of the kinetic energy, potential energy and enthalpy. It measures the ratio of energy flux to mass flux. For a steady inviscid hydrodynamic flow, Be is conserved along streamlines. Therefore, any parcel of gas with a positive Be can escape to infinity while a parcel with negative Be cannot. One-dimensional hot accretion flow models often have $Be > 0$ (Narayan & Yi 1994, 1995a; Blandford & Begelman 1999), which is interpreted as a strong clue that these flows should experience heavy mass loss in winds. However, note that Be is not conserved if the flow is either viscous or non-steady. Therefore, Be is not a useful parameter for describing gas in the interior of a turbulent disk. The situation is somewhat better in the case of outflows, which tend to be more laminar and quasi-steady.

In the area of numerical simulations of non-radiative accretion flows, Igumenshchev & Abramowicz (2000) were among the first to explore the connection between the Bernoulli parameter and outflows. They found that HD simulations with a large value of the viscosity parameter $\alpha \gtrsim 0.3$ have well-defined outflows with $Be > 0$, whereas simulations with a smaller $\alpha \lesssim 0.1$ have outflowing gas with $Be < 0$, i.e., the outward-moving gas in the latter models is gravitationally bound and cannot escape to infinity. More recently, Yuan et al. (2012a) have carried out a detailed study of Be in HD and MHD simulations. They find that in the HD case the value of Be of outflowing gas is always larger than that of inflowing gas.

In the case of MHD flows, the definition of Be must be modified to include the contribution of the magnetic field. The necessary expression is well-known in the theory of relativistic hydromagnetic winds, e.g., the "total energy-to-mass flux ratio" μ in Vlahakis & Konigl (2003; also J in Lovelace et al. 1986). Sadowski et al. (2013a) analyzed 3D GRMHD simulations using a general relativistic version of μ and found that gas with $\mu > 0$ has an outward-pointing velocity (outflow), while gas with $\mu < 0$ has an inward-pointing velocity (inflow). This result appears to confirm the usefulness of the Bernoulli parameter as a diagnostic for MHD winds in hot accretion flows. Note that the analysis was carried out using time-averaged quantities in quasi-steady state, where the Bernoulli parameter is expected to be particularly well conserved.

In addition to directly estimating the strength of mass outflows in simulated hot accretion flows, the convective stability of the gas in MHD simulations may be analyzed using the Hoiland criteria (Narayan et al. 2012b, Yuan et al. 2012a). This reveals that gas is convectively stable over most of the accretion flow, in contrast to HD accretion simulations which are convectively unstable (§3.1). It thus appears that the magnetic field in MHD simulations stabilizes the gas against convection. Pen et al. (2003) named this state of affairs "frustrated convection".

[20] In the case of convection (the HD case in Yuan et al. 2012a), some differences are expected between inflow and outflow, but perhaps this will not affect the final conclusion.

On the whole, current results seem to favor the ADIOS model over the CDAF model, but not overwhelmingly. It is likely that the truth involves some combination of the two models. More work is required to clarify this issue. In particular, simulations covering a significantly larger dynamic range in radius than currently possible will be required before we can hope to obtain unambiguous results.

Large dynamic range 3D simulations are especially important for estimating two critical parameters: (i) the mass-loss index s, and (ii) the radius $R_{\rm in}$ inside which mass loss is unimportant. It is vital to know the values of these parameters if we wish to calculate quantitative global models of hot accretion flows (§2.3) and to apply these models to real systems (§4).

3.5 Effect of radiation

Radiation is nearly always ignored in hydro and MHD simulations of hot accretion flows. However, a few studies have considered optically thin radiative cooling. Yuan & Bu (2010) included bremsstrahlung radiation in the energy equation in their HD simulations and recovered the ADAF and LHAF solutions when they varied the mass accretion rate. Surprisingly, their simulated LHAF was convectively unstable, whereas 1D models predict that the entropy gradient should be stable (§2.5). Apparently, the 2D structure of the flow permits an unstable entropy gradient to survive, although this behavior is not understood. Li et al. (2013a) again included bremsstrahlung cooling and showed that, by changing the mass supply rate outside the Bondi radius, they could successfully reproduce both a cool thin disk at high $\dot{M}_{\rm BH}$ and a hot accretion flow at lower $\dot{M}_{\rm BH}$.

Ohsuga and collaborators (e.g., Ohsuga et al. 2009, Ohsuga & Mineshige 2011) have carried out simulations with full radiative transfer and have studied a wide range of accretion rates. They recover both the cold and hot accretion flow solutions at appropriate values of $\dot{M}_{\rm BH}$. Radiation generally does not appear to have a significant effect on the dynamics of their hot solutions. However, in a recent study, Dibi et al. (2012) include optically thin cooling and find that, when $\dot{M}_{\rm BH} \gtrsim 10^{-7}\dot{M}_{\rm Edd}$, radiative cooling can significantly affect the density and temperature. Their result is likely to be sensitive to the particular prescription they used to fix the electron temperature in the two-temperature plasma. Nevertheless, their study highlights the fact that, above some accretion rate, numerical simulations need to include radiation self-consistently.

3.6 Effect of low collisionality

Most studies of hot accretion flows are based on a fluid approximation, specifically MHD. However, the density of the accreting gas is often so low that the flow is macroscopically collisionless, and one must carry out a kinetic analysis to determine whether MHD simulations can capture the relevant physics.

In the case of the MRI, a kinetic treatment is in principle required whenever the wavelength of the fastest growing mode is smaller than the collisional mean free path. Quataert et al. (2002) found that, while the MRI instability criterion is the same in kinetic theory as in MHD, the growth rates of modes are different. The nonlinear development of the kinetic MRI has been studied using numerical simulations based on a fluid model with kinetic effects added (Sharma et al. 2006) as well as the more precise particle-in-cell technique (Riquelme et al. 2012). The non-linear evolution of the axisymmetric kinetic MRI is found to be qualitatively

similar to that of the standard MHD MRI.

The low collisionality of hot accretion flows also has an effect on thermal conduction. For a magnetized collisionless accretion flow, the collisional mean free path of electrons is larger than the electron Larmor radius, and thermal conduction is the dominant mode of heat transport. Conduction tends to be primarily along the magnetic field lines (though cross-field diffusion is not as small as often imagined, Narayan & Medvedev 2001). Among other things, anisotropic conduction modifies the convective stability criterion, as shown by Balbus (2001). The instability in this case is usually referred to as the magnetothermal instability (MTI). Local MHD simulations with anisotropic electron thermal conduction have demonstrated that the MTI amplifies the magnetic field and causes a substantial convective heat flux (Parrish & Stone 2007). Sharma et al. (2008) investigated the effects of the MTI on non-rotating accretion flows and confirmed the main results of local simulations. Bu et al. (2011) extended this study to the case of a rotating accretion flow and found that the MTI and MRI operate independently and can cooperatively amplify the magnetic field.

Thermal conduction in a hot collisionless accretion flow can directly affect the dynamics by flattening the temperature profile (e.g., Quataert 2004, Tanaka & Menou 2006, Johnson & Quataert 2007). This mechanism has been invoked as an alternative explanation for the very low mass accretion rate in Sgr A* (§4.1; Shcherbakov & Baganoff 2010).

4 Applications

*4.1 Galactic Center black hole: Sgr A**

Sagittarius A* (hereafter Sgr A*), the compact radio source at the center of our Galaxy, is a unique laboratory for studying black hole accretion. Observations of O and B stars orbiting the Galactic Center (Schödel et al. 2002; Ghez et al. 2003, 2008; Gillessen et al. 2009a, 2009b; Meyer et al. 2012) provide very strong evidence for the presence of a dark compact object of mass $(4.1 \pm 0.4) \times 10^6\ M_\odot$. Measurements of the size of Sgr A* (Bower et al. 2004, Shen et al. 2005, Doeleman et al. 2008) leave little doubt that this dark object must be a supermassive black hole. Since Sgr A* is relatively nearby, there is abundant data to constrain the nature of the accretion flow (for details on the observations, see Genzel et al. 2010 and references therein).

Sgr A* spends most of its time in a steady low-luminosity state, usually referred to as the "quiescent state" (§4.1.1). A few times each day, strong variations are seen in the infrared and X-ray bands, and sometimes also in other wavebands. These fluctuations are referred to as "flares" (§4.1.3). The ADAF model and its variants explain the main features of the quiescent state. However, despite important recent progress, the nature of the flares is still poorly understood.

4.1.1 Observational constraints on the quiescent state

The outer boundary of the accretion flow around Sgr A* is generally assumed to be located at the Bondi (1952) radius, $R_B \sim 10^5 R_S \approx 0.04\,\mathrm{pc} \approx 1"$, where the thermal energy of the external ambient gas is equal to its potential energy in the gravitational field of the black hole. Because of the high spatial resolution of the *Chandra X-ray Observatory*, the density and temperature of gas near R_B can be

measured using X-ray observations (Baganoff et al. 2003), and we can thereby estimate the Bondi mass accretion rate: $\dot{M}_B \sim 10^{-5} M_\odot \text{ yr}^{-1} \sim 10^{-4} \dot{M}_{\rm Edd}$. Independently, 3D numerical simulations of stellar winds accreting on to Sgr A* (Cuadra et al. 2008; see also Quataert 2004, Shcherbakov & Baganoff 2010) predict $\dot{M}_B \sim \text{few} \times 10^{-6} M_\odot \text{yr}^{-1}$, consistent with the above estimate. The simulations indicate that the gas has a reasonable amount of angular momentum at the Bondi radius, corresponding to a circularization radius $\sim 10^4 R_s$. Thus, gas cannot fall directly into the black hole, as in the classic Bondi model, but must accrete viscously via a hot accretion flow. The measured density and temperature of gas at the Bondi radius, and its estimated specific angular momentum, constitute outer boundary conditions that a successful accretion model must satisfy.

The spectral energy distribution of Sgr A* is shown in Fig. 6. The radio spectrum has two components: below $\sim 50\,$GHz the spectrum consists of a power-law, and above this frequency there is a "submillimeter bump". The X-ray emission in the quiescent state is spatially resolved ($\sim 1.4"$; Baganoff et al. 2003), consistent with the size of the Bondi radius. The most outstanding feature of Sgr A* is that its bolometric luminosity is extremely low: $L_{\rm bol} \sim 10^{36}\,\text{erg}\,\text{s}^{-1} \sim 2 \times 10^{-9} L_{\rm Edd}$. If gas accretes on the black hole at the Bondi accretion rate $\dot{M}_B$ estimated above, the radiative efficiency of the accretion flow must be extremely low: $\epsilon_{\text{Sgr A}*} \sim 10^{-6}$ instead of the traditional $\epsilon_{\rm SSD} \approx 10\%$. This ultra-low efficiency is the strongest argument for invoking an ADAF or other hot accretion flow model instead of a standard thin accretion disk. A second argument is that the observed spectrum does not look anything like the multi-temperature blackbody spectrum expected for a standard thin disk. Note, however, that strong extinction in the optical and UV could hide much of the emission from a thin disk, so constraints come mainly from infrared observations (Falcke & Melia 1997).

The radio emission at submillimeter and millimeter wavelengths is linearly polarized at a level of $2-9\%$ (Aitken et al. 2000; Bower et al. 2003; Marrone et al., 2006, 2007), and the mean rotation measure between 227 and 343 GHz is $-5.6 \pm 0.7 \times 10^5\,\text{rad}\,\text{m}^{-2}$. The latter measurement limits the mass accretion rate at the central black hole (Agol 2000, Quataert & Gruzinov 2000). Current constraints are $\dot{M}_{BH} < 2 \times 10^{-7} M_\odot \text{ yr}^{-1}$ if the magnetic field is near equipartition, ordered, and largely radial, and $\dot{M}_{BH} > 2 \times 10^{-9} M_\odot \text{ yr}^{-1}$ if the field is subequipartition, disordered, or toroidal (Marrone et al. 2007). Since these estimates of $\dot{M}_{BH}$ are very much smaller than $\dot{M}_B$, it is inferred that most of the gas available at R_B does not fall into the black hole. Recently, emission lines from relatively low ionization species were detected (Wang et al. 2013) in 3 million seconds of *Chandra* observations. The H-like Fe Kα line was extremely weak, indicating a flat radial density profile $\rho(r) \propto r^{-1}$ near the Bondi radius, rather than $r^{-3/2}$ as one expects for the classic ADAF model. The flat density profile seems to confirm that the mass accretion rate decreases with decreasing radius (§3.4), consistent with millimeter wave polarization results. Both observations suggest that the accretion flow has a significant outflow which causes $\dot{M}$ to decrease with decreasing radius (§3.4).

4.1.2 ADAF model for the quiescent state of Sgr A*

Narayan et al. (1995; see also Manmoto et al. 1997; Narayan et al. 1998a) applied the ADAF model to Sgr A* and showed that the model explains the main features of the source, viz., an ultra-low radiative efficiency and an unusual (non thin disk)

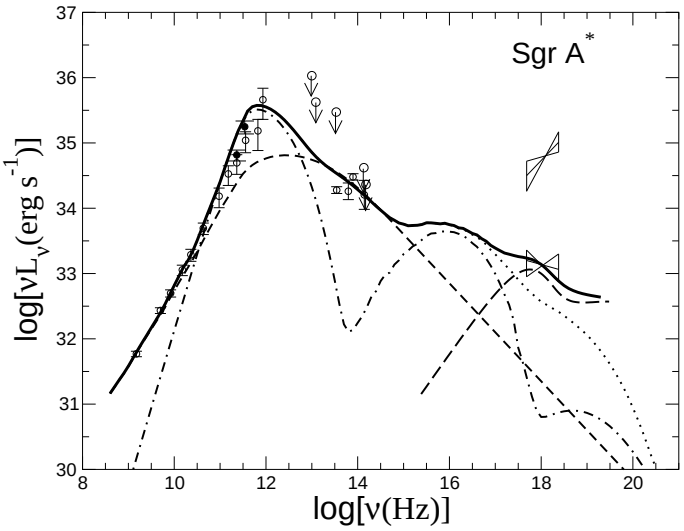

Figure 6: Spectrum corresponding to an ADAF model of the quiescent state of Sgr A*, the supermassive black hole at the Galactic Center (from Yuan et al. 2003). Circles with errorbars show measurements at radio and millimeter wavelengths, circles with arrows correspond to infrared upper limits, and the two "bowties" show X-ray data in the quiescent state (below) and during a bright flare (above). Additional data are shown in the infrared waveband (from Schödel et al. 2011), which were not available when the model was originally developed. The model spectrum (thick solid line) is the sum of three components: synchrotron emission and its Compton humps from thermal electrons (dot-dashed line), synchrotron emission from a population of non-thermal electrons (short-dashed line), and bremsstrahlung emission from electrons near the Bondi radius (long-dashed line). The dotted line shows the total synchrotron and inverse Compton emission.

spectrum. In these early studies, the accretion rate was taken to be independent of radius, and viscous dissipation was assumed to heat only ions ($\delta \ll 1$, §2.2.2). The most serious defect of this model is that it predicts a rotation measure orders of magnitude larger than that observed (§4.1.1).

In the years following this early work, three separate developments led to a new paradigm. (1) Numerical simulations demonstrated that outflows are important (§3.4). (2) Electron heating was recognized to be more efficient than previously assumed ($\delta \sim 0.1 - 0.5$, §2.2.2). (3) Faraday rotation measurements indicated that $\dot{M}_{BH} \ll \dot{M}_B$ (§4.1.1). Yuan et al. (2003, 2004) presented an updated ADAF model of Sgr A* (sometimes called a RIAF model to distinguish it from the "old" ADAF model) which allowed for an outflow and assumed more efficient electron heating. The model spectrum is shown in Fig. 6. The submillimeter bump is produced by synchrotron emission from thermal electrons in the ADAF (dot-dashed line in the figure – the additional bumps at higher frequencies are due to inverse Compton scattering), while the low-frequency power-law radio spectrum (short-dashed line) is produced by synchrotron radiation from a small population of nonthermal electrons (following earlier suggestions by Mahadevan 1998 and Özel et al. 2000). The nonthermal electrons are usually introduced into the model in an ad hoc fashion, but are thought to be the result of electron-positron production via proton-proton collisions (Mahadevan 1998, 1999), magnetic reconnection, or weak shocks (e.g., Machida & Matsumoto 2003). Bremsstrahlung emission of thermal gas near the Bondi radius (long-dashed line) is responsible

for the X-ray emission (Quataert 2002). Sazonov et al. (2012) recently proposed that the extended X-ray emission may be dominated by coronal radiation from a population of low-mass stars. However, Wang et al. (2013) did not detect the predicted level of Fe Kα emission.

The net radiative efficiency of the Yuan et al. (2003) model is very low: $L_{\rm bol}/[\dot{M}_{\rm in}(R_B)c^2] \approx 2\times10^{-5}$. The low efficiency is the result of two effects: (i) mass loss in an outflow gives an effective $\epsilon_{\rm outflow} \equiv \dot{M}_{\rm BH}/[\dot{M}_{\rm in}(R_B)] \sim 4\times10^{-2}$, and (ii) energy advection gives an additional "real efficiency" (eq. 17) $\epsilon \equiv L_{\rm bol}/\dot{M}_{\rm BH}c^2 \sim 4\times10^{-4}$. The inclusion of an outflow in the model is consistent with independent modeling of X-ray emission lines (Wang et al. 2013) as well as numerical MHD simulations (§3.4). However, there is no direct observational evidence for any outflowing gas. Overall, the success of this (by no means unique) model provides strong evidence for the presence of a hot advection-dominated accretion flow around Sgr A*. It has also been used to argue for the existence of an event horizon in this object (Narayan et al. 1998a, Broderick & Narayan 2006, Narayan & McClintock 2008, Broderick et al. 2009; see also Narayan et al. 1997b, Menou et al. 1999a, Garcia et al. 2001, McClintock et al. 2004 for related arguments in the case of quiescent BHBs, and Abramowicz et al. 2002b for a counter-argument).

More constraints on model parameters such as the mass accretion rate, the relative importance of the disk versus the jet (§4.1.4), the orientation and magnitude of the BH spin and the magnetic field, could be obtained by considering additional millimeter-VLBI observations and polarization data (§4.1.5). This has been done using the Yuan et al. (2003) semianalytical model (Huang et al. 2007, Broderick et al. 2011) and in numerous studies based on MHD simulations (Goldston et al. 2005; Noble et al. 2007; Sharma et al. 2007b, 2008; Mościbrodzka et al. 2009; Chan et al. 2009; Kato et al. 2009; Dexter et al. 2010; Shcherbakov et al. 2012; Dexter & Fragile 2013). In most of the latter studies the simulations do not include radiation, so the emergent spectrum is calculated separately by post-processing the simulation output.

4.1.3 Multiwaveband flares

Flares have been observed in Sgr A* in many wavebands, but are strongest in X-rays (Baganoff et al. 2001) and infrared (Genzel et al. 2003, Ghez et al. 2004, Gillessen et al. 2006), where the flux can increase by up to a factor of 100 and 5, respectively. The variability timescale ranges from several minutes to three hours, indicating that the flares must be produced close to the black hole; for comparison, the light-crossing time of the black hole is $2R_S/c \approx 30\,{\rm s}$, and the orbital period at the ISCO for a non-rotating black hole is $2\pi/\sqrt{GM/R_{\rm ISCO}^3} \approx 2000\,{\rm s}$. Many multiwaveband campaigns (e.g., Eckart et al. 2004, 2006; Yusef-Zadeh et al. 2006, 2009; Dodds-Eden et al. 2009; Trap et al. 2011) have provided valuable information on flare spectra, polarization, time lags between different wavebands, and occurrence rates. The observations suggest that flares in different wavebands are likely physically related.

So far, most theoretical flare models are phenomenological and have focused mainly on interpreting the observed spectrum (e.g., Markoff et al. 2001; Yuan et al. 2004; Dodds-Eden et al. 2009, 2010). While the IR flare is generally believed to be due to pure synchrotron emission, there is still some debate on whether the X-ray flare is due to synchrotron (Yuan et al. 2003, 2004; Dodds-Eden et

al. 2009), synchrotron self-Compton, or inverse Compton of external radiation (Markoff et al. 2001; Eckart et al. 2004, 2006; Yusef-Zadeh et al. 2009). Yusef-Zadeh et al. (2006) found that, in the radio band, the peak flare emission at 43 GHz leads that at 22 GHz by $\sim 20 - 40$ minutes. They interpret this in terms of a van der Laan (1966)-like expanding plasma blob model. The blob is ejected from the accretion flow and becomes optically thin as it expands. The maximum emission at any given frequency occurs when the blob transitions from optically thick to thin at that frequency. Thus, the peak naturally occurs later at longer wavelengths. A similar process may be happening in GRS 1915+105 and other black hole sources (Fender & Belloni 2004; see references in Yuan et al. 2009a), and strongly suggests episodic jet ejections (§3.3.3). In analogy with coronal mass ejections associated with solar flares, the ejections in Sgr A* might be caused by magnetic reconnection in a corona, and the same process may also be responsible for the flares (Yuan et al. 2009a).

More multiwaveband observations will clarify many remaining puzzles. At the same time, there is a need for theoretical models that combine detailed gas dynamics with radiative processes.

4.1.4 Alternative models of Sgr A*

Two alternative models of Sgr A* have been discussed in the literature: the jet model (Falcke & Markoff 2000, Markoff et al. 2001, Yuan et al. 2002a, Markoff et al. 2007), and the spherical accretion model (Melia 1992, Melia et al. 2001).

In one version of the jet model (Falcke & Markoff 2000, Markoff et al. 2007), it is proposed that all the emission from radio to X-rays is produced by the jet. In an alternate version, called the jet-ADAF model (Yuan et al. 2002a), only the radio spectrum below ~ 50 GHz is produced by the jet while the rest of the emission is assumed to come from the ADAF. No radio jet has been convincingly detected in Sgr A* (but see Li et al. 2013b), even though this supermassive black hole is right in our Galaxy and has been observed in the radio with both high sensitivity and very high spatial resolution.

The spherical accretion model (Melia 1992) is similar to the ADAF model in that the accretion flow is assumed to be very hot, with the temperature being nearly virial. However, in contrast to the ADAF and other hot accretion flow models, the gas here is one-temperature. In addition, the angular momentum of the gas is assumed to be extremely small, with a circularization radius of only $\sim 5 - 10R_s$, which is rather extreme. If gas at the Bondi radius has any reasonable angular momentum, as seems likely (e.g., the numerical work of Cuadra et al. 2008), accretion cannot take place spherically but must proceed via a viscous rotating flow.

4.1.5 Future Observations

As the nearest supermassive black hole, Sgr A* has always been a favorite target for observational campaigns. Two near-term opportunities may provide significant new information on the nature of the accretion flow around this black hole.

Gillessen et al. (2012) discovered a dense cloud of gas called G2 on a highly eccentric orbit around Sgr A*. Pericentric passage is expected in early 2014 at a distance of $\sim 2000R_S$ from the black hole (Phifer et al. 2013, Gillessen et al. 2013). The interaction of G2 with the hot accretion flow could potentially be observed

in radio, infrared or X-rays (Narayan et al. 2012a, Sadowski et al. 2013b, Saitoh et al. 2013, Yusef-Zadeh & Wardle 2013, Crumley & Kumar 2013, Shcherbakov 2013). If a signal is detected, it will provide information on the properties (density, temperature, magnetic field) of the accretion flow in a region ($R \gtrsim 10^3 R_S$) where we have hitherto had no observational constraint. In addition, gas stripped from G2 is expected to accrete on the black hole on a viscous time, causing the quiescent radio and millimeter emission of Sgr A* to increase. A detection of this increase will provide a direct measurement of the viscous time at the orbit pericenter, which currently is poorly constrained. A number of HD and GRMHD simulations of the G2 encounter have already been carried out (e.g., Moscibrodzka et al. 2012, Anninos et al. 2012, Burkert et al. 2012, Schartmann et al. 2012, 2013, Sadowski et al. 2013b, Abarca et al. 2013). Coupled with future observations, such work should provide new information on the nature of the accretion flow in Sgr A* at intermediate radii.

In recent years, ultra-high angular resolution millimeter wave interferometry has become a reality and the first detections have been made of event-horizon scale structure in Sgr A* (Doeleman et al. 2008, Fish et al. 2011) and M87 (Doeleman et al. 2012). From these observations some inferences have already been made on the spins of the black hole and the nature of the accretion flow and jet near the horizon (e.g., Fish et al. 2009, 2011; Broderick et al. 2009, 2011ab). Future plans are focused on commissioning the Event Horizon Telescope (Doeleman et al. 2010), which will carry out long baseline millimeter wave interferometry using a network of up to eight telescopes spread all around the world. With this array, images of Sgr A* will be measured with unprecedented sensitivity and angular resolution, and information will be obtained both on polarization and time variability. It is anticipated that the Event Horizon Telescope will finally provide direct information on the physics of the hot accretion flow in the vicinity of Sgr A*'s horizon. Questions such as the relative importance of the disk versus the jet; the density, temperature and optical depth (at millimeter wavelengths) of the accreting plasma; and the direction and topology of the magnetic field will hopefully be answered by means of direct observations. In anticipation, numerical codes are being developed and a number of numerical simulations have already been carried out (e.g., Moscibrodzka et al. 2009, Dexter et al. 2010, Shcherbakov et al. 2012, Dexter & Fragile 2013, Chan et al. 2013). Much more work is anticipated in the future.

4.2 Other low-luminosity sources

The hot accretion flow solution is essentially independent of black hole mass. If $\dot{M}_{\rm BH}$ is scaled by the Eddington rate and radius is scaled by the Schwarzschild radius, many properties of the solution, notably the gas temperature and the Eddington-scaled luminosity, are independent of mass (see §2.1). Because of this, hot accretion flow systems, such as low-luminosity active galactic nuclei (LLAGNs) and black hole binaries (BHBs) in the hard and quiescent state, show similar properties, despite the large disparity in their black hole masses. We begin by introducing LLAGNs and BHBs, and then describe the role of hot accretion flows in determining their properties.

4.2.1 Introduction

LLAGNs. Although virtually every galaxy with a bulge has a supermassive black hole in its nucleus, at any given time only a small fraction of these black holes have luminosities close to Eddington. The vast majority are LLAGNs with luminosities spanning the range $L_{\rm bol}/L_{\rm Edd} \approx 10^{-9} - 10^{-1}$ (Ho 2008, 2009). As in the case of Sgr A*, most of these black holes have considerable gas available for accretion close to their Bondi radii (Fabian & Canizares 1988). The fact that the black holes are dim thus suggests that they must be accreting via a radiatively inefficient mode, i.e., a hot accretion flow (Fabian & Rees 1995, Di Matteo et al. 2000, Ho 2009, Russell et al. 2013b). Other distinctive features of LLAGNs confirm this suspicion.

The "big blue bump", a characteristic spectral feature associated with a thin accretion disk around a supermassive black hole, is absent in LLAGNs (Ho 1999, 2008; Chiaberge et al. 2006; Eracleous et al. 2010; Younes et al. 2012). In the language of $\alpha_{\rm ox}$, defined as the two-point spectral index between 2500 Å and 2 keV, LLAGNs have $\alpha_{\rm ox} \gtrsim -1$ while quasars and Seyferts have $\alpha_{\rm ox} \approx -1.4$ and -1.2, respectively. The optical-UV slope is also exceptionally steep (Ho 2008). These observations strongly suggest that LLAGNs do not have a thin disk in their inner regions; however, a disk may be present at larger radii, as indicated by a "big red bump" in their spectra (Lasota et al. 1996a, Quataert et al. 1999, Gammie et al. 1999, Yuan et al. 2002b, Chiang & Blaes 2003, Ptak et al. 2004, Yuan & Narayan 2004, Nemmen et al. 2006, Wu et al. 2007, Yu et al. 2011).[21] As further confirmation, the iron Kα line, which is commonly attributed to X-ray fluorescence off a cold accretion disk extending close to the black hole, is weak or absent (e.g., Fabbiano et al. 2003, Ptak et al. 2004, Binder et al. 2009, Younes et al. 2011, Kawamuro et al. 2013).

BHBs. BHBs have a number of distinct spectral states (see Zdziarski & Gierliński 2004, McClintock & Remillard 2006, Done et al. 2007, Zhang 2013, Poutanen & Veledina 2014 for reviews). The most notable among these, in order of decreasing luminosity, are the soft or thermal state, the hard state, and the quiescent state.[22] The soft state is found at luminosities down to $\sim 1.5\% L_{\rm Edd}$ (Kalemci et al. 2013). It is characterized by a strong blackbody or thermal spectrum, and is well described by the standard thin disk model. The hard state is found at lower luminosities and differs dramatically. Its spectrum has only a weak blackbody component and is dominated instead by a strong hard power-law with a cutoff at ~ 100 keV. While the soft state has little time variability, the hard state is highly variable and often exhibits quasi-periodic oscillations (QPOs, Remmilard & McClintock 2006). In addition, the hard state has a continuous, steady jet, whereas the soft state almost never has jets (Fender 2006). All of these differences indicate that the hard state must correspond to a very different regime of accretion compared to the thin disk.

Many studies over the years have shown that the power-law component in the hard state must be produced by thermal Comptonization in a hot plasma

[21] Based on the fact that LLAGNs lie on the low-luminosity extrapolation of the well-known relation between α_{ox} and luminosity, Maoz (2007) argues that LLAGNs do not differ appreciably from luminous AGNs, and hence that LLAGN accretion disks are similar to disks in luminous AGNs. However, he does not provide a physical explanation for the correlation, whereas Yu et al. (2011) show that the trend is naturally explained in the framework of hot accretion flows.

[22] There is also a very high state or steep power-law state which usually, but not always, occurs at an even higher luminosity than the thermal state. This state is poorly understood.

with a temperature $kT \sim 100\,\mathrm{keV}$ and optical depth $\tau \sim 1$ (e.g., Zdziarski et al. 1998). The ADAF model has the correct density, electron temperature and optical depth needed to reproduce the observed spectrum. Moreover, the luminosity at which a fading thermal state source switches to the hard state ($\sim 1.5\% L_{\rm Edd}$) is reasonably consistent with the maximum mass accretion rate of a hot accretion flow (Fig. 2). At luminosities below $\sim 10^{-3} L_{\rm Edd}$, the hard state merges smoothly with the quiescent state, which then extends down to as low as $L \sim 10^{-9} L_{\rm Edd}$. There is no clear boundary between the hard and quiescent states, so it is likely that the same accretion physics operates in both.

BHBs show a very interesting hysteresis effect in their transitions between the soft and hard state. Whereas with decreasing luminosity the soft-to-hard transition in most sources happens at roughly the same luminosity $\sim 1.5\% L_{\rm Edd}$, with increasing luminosity the hard-to-soft transition can occur at any of a wide range of luminosities extending up to $L \sim 30\% L_{\rm Edd}$ (Zdziarski & Gierliński 2004, Done et al. 2007, Yu & Yan 2009). There is as yet no convincing physical explanation for this hysteresis phenomenon, though Meyer-Hofmeister et al. (2005) and Liu et al. (2005) show that their disk evaporation model can reproduce the observations when Compton cooling is included. Done et al. (2007) have an alternative explanation, arguing that it is simply a matter of time scales. As $\dot{M}_{\rm BH}$ increases, it takes a viscous time for the truncated thin disk (see §4.2.2 below) to move down to the ISCO, and during this time the luminosity continues to increase and goes well above the threshold value before the transition is completed. This plausible scenario needs to be confirmed with detailed models.

4.2.2 Accretion geometry: Truncated thin disk plus hot accretion flow

Most BHBs in the hard and quiescent state, as well as many LLAGNs, are deduced to have a two-zone accretion flow consisting of a cool thin disk at large radii and a hot accretion flow at small radii[23]. This configuration is illustrated in the left panel of Fig. 7. The main parameter that controls the transition radius $R_{\rm tr}$ between the two zones is the mass accretion rate $\dot{M}_{\rm BH}$. When $\dot{M}_{\rm BH}$ is above the maximum allowed for the hot accretion flow solution (§2.6), only the thin disk solution is available, so the thin disk extends all the way down to the ISCO. This corresponds to the soft state. When $\dot{M}_{\rm BH}$ becomes smaller, the source first enters an intermediate state and then, with decreasing $\dot{M}_{\rm BH}$, progresses to the hard state and finally the quiescent state. In these latter states, the thin disk is truncated at a radius $R_{\rm tr} > R_{\rm ISCO}$ and the region inside $R_{\rm tr}$ is occupied by a hot accretion flow. The radial extent of the hot zone increases with decreasing $\dot{M}_{\rm BH}$. This "truncated thin disk plus hot inner accretion flow" configuration was first proposed by Shapiro et al. (1976) to explain the hard state of Cyg X-1; however, their model was based on the unstable SLE solution. A similar concept, but using the ADAF solution, was later developed by Narayan (1996, see also Poutanen et al. 1997 and Esin et al. 1997) to explain the various spectral states of BHBs.

[23] In the case of Sgr A* and some elliptical galaxies such as M87, the flow starts out hot at the Bondi radius and remains hot throughout, so there is apparently no thin disk at large radii.

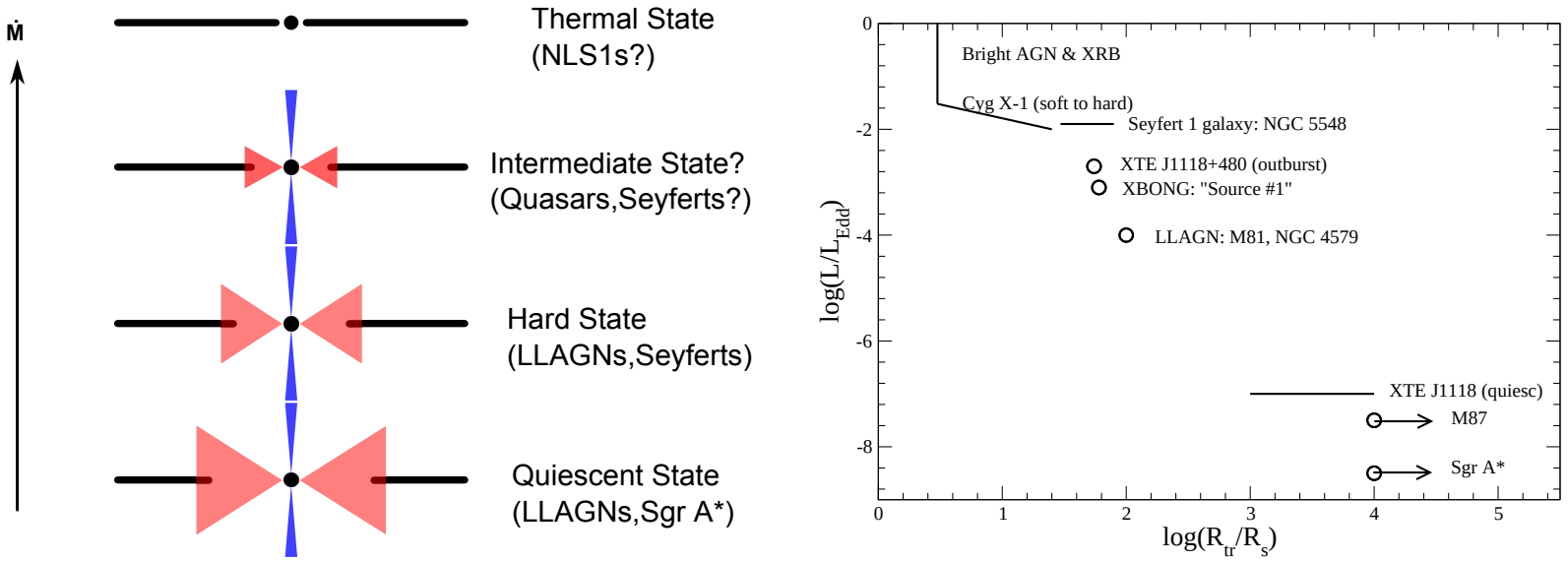

Figure 7: *Left*: Schematic diagram showing as a function of the mass accretion rate $\dot{M}_{\rm BH}$ the configuration of the accretion flow in different spectral states of BHBs (adapted from Esin et al. 1997, Narayan & McClintock 2008). Possibly equivalent AGN classes are indicated in parentheses. Red triangles indicate the hot accretion flow while thick black horizontal lines represent the standard thin disk. The transition radius $R_{\rm tr}$ where the thin disk is truncated becomes smaller with increasing $\dot{M}_{\rm BH}$. In the thermal state, the disk is not truncated and its inner edge is located at the ISCO. *Right*: Plot of the Eddington-scaled accretion luminosity $L/L_{\rm Edd}$ versus $R_{\rm tr}$ as deduced from observations. The transition radii were estimated by modeling spectra of individual LLAGNs and BHBs (from Yuan & Narayan 2004).

While there is some understanding of the dynamics of the transition from the outer thin disk to the inner hot accretion flow (e.g., Abramowicz et al. 1998, Manmoto et al. 2000), the physical reason why cold gas in the outer disk is converted into hot gas on the inside is not fully understood. It is likely that some combination of the following models is responsible: "evaporation" model (Meyer & Meyer-Hosmeister 1994; Liu et al. 1999, 2011; Meyer et al. 2000, 2007; Różańska & Czerny 2000; Spruit & Deufel 2002; Mayer & Pringle 2007; Taam et al. 2012); "turbulent diffusion" model (Honma 1996, Manmoto & Kato 2000, Manmoto et al. 2000); "large viscosity" model (Gu & Lu 2000, Lu et al. 2004). Of these, the evaporation model has been studied most extensively, though all three models predict that $R_{\rm tr}$ should increase with decreasing $\dot{M}_{\rm BH}$. As the panel on the right in Fig. 7 shows, this prediction is in agreement with empirical data based on modeling spectra of individual sources (Yuan & Narayan 2004).[24]

4.2.3 Modeling observations of LLAGNs

Following the initial application of the ADAF model to Sgr A* (Narayan et al. 1995), a number of authors used similar ideas to explain a variety of observations of other LLAGNs: nearby elliptical galaxies (Fabian & Rees 1995; Reynolds et al. 1996; Di Matteo et al. 2000, 2001; Loewenstein et al. 2001; Ho et al. 2003; Fabbiano et al. 2003), LINERs (Lasota et al. 1996a, Quataert et al. 1999, Gammie et al. 1999, Yuan et al. 2002b, Pellegrini et al. 2003, Ptak et al. 2004, Nemmen et al. 2006, Xu & Cao 2009, Liu & Wu 2013, Nemmen et al. 2014), BL Lac objects (Maraschi & Tavecchio 2003), FR I sources (Reynolds et al. 1996, Begelman & Celotti 2004, Wu et al. 2007, Yuan et al. 2009c, Yu et al. 2011), X-ray Bright Optically Normal Galaxies (Yuan & Narayan 2004), and even Seyferts (Chiang & Blaes 2003; Yuan & Zdziarski 2004).

NGC 1097, a famous LINER, is an interesting case. It is the first and best-studied LLAGN to display broad, double-peaked Hα and Hβ emission lines (e.g., Storchi-Bergmann et al. 1997). Such double-peaked lines are believed to be the result of irradiation of a truncated thin disk, most likely by radiation from the inner hot accretion flow (Chen & Halpern 1989). In the case of NGC 1097, the Hα line profile requires the transition radius to be at $R_{\rm tr} \approx 225 R_S$ (Storchi-Bergmann et al. 1997). Using the truncated thin disk plus hot accretion flow model, Nemmen et al. (2006) successfully modeled the optical-to-X-ray continuum spectrum of the source. In their model, the truncated thin disk dominates the optical-UV emission while the inner hot accretion flow produces the X-ray emission. Impressively, the $R_{\rm tr}$ they require to fit the continuum spectrum agrees very well with the $R_{\rm tr}$ estimated from fitting the double-peaked Hα line.

[24] Not all systems follow the trend shown in the right panel of Fig. 7. For BHBs with short orbital periods, the mass transfer stream from the companion star circularizes at a fairly small radius $R_{\rm circ}$. When these systems go into the quiescent state, the continued supply of cold gas at $R_{\rm circ}$ will ensure that the transition radius is pinned close to $R_{\rm circ}$ (Menou et al. 1999b). A similar situation is possible even in the case of very low luminosity AGN. If the AGN is fueled from the external medium by cold gas clouds with low angular momentum, the gas clouds will first circularize and form a thin disk before "evaporating" into a hot accretion flow (Inogamov & Sunyaev 2010).

The value of $R_{\rm tr}$ in the case of XTE J1118+480 shown in Fig. 7 is significantly smaller than that obtained in later work by Yuan et al. (2005; see §4.2.4 for details). The reason for the discrepancy is explained in Yuan et al. (2005). This does not affect the main conclusion.

4.2.4 Modeling observations of BHBs

In the field of BHBs, the truncated thin disk plus hot accretion flow scenario was first applied to the quiescent state (Narayan et al. 1996, 1997a; Menou et al. 1999ab)[25] and soon after to the hard state (Esin et al. 1997, 1998, 2001). The source XTE J1118+480 is a spectacular example where there is (i) good EUV data which is crucial for constraining the radius of the inner edge of the thin disk (McClintock et al. 2003), and (2) good timing information, including a low-frequency QPO (~ 0.1Hz) and measurements of time lags between different wavebands (see review in Yuan et al. 2005). Spectral fitting of the EUV data indicates that the thin disk must be truncated (Esin et al. 2001, Chaty et al. 2003). Figure 8 shows a comprehensive model (Yuan et al. 2005) which uses a more modern hot accretion flow model, including a jet. In this model, the radio/infrared emission is dominated by the jet, the optical–EUV by the truncated thin disk, and the X-ray region of the spectrum is produced by the hot accretion flow. The transition radius is constrained to be $R_{\rm tr} \approx 300 R_S$. The same truncated thin disk scenario can also explain the low-frequency QPO. In the model proposed by Giannios & Spruit (2004; see also Rezzolla et al. 2003 for a similar idea), the QPO arises from a global p-mode oscillation of the hot ADAF.[26] The QPO frequency is roughly determined by the Keplerian frequency at $R_{\rm tr}$ and agrees well with the observed frequency for $R_{\rm tr} \approx 300 R_s$. In addition, the model also qualitatively explains other timing features such as time-lags between different wavebands (Yuan et al. 2005, see also Malzac et al. 2004 for a similar model with similar conclusions).

A number of observations have confirmed the basic features of the truncated thin disk scenario in BHBs (see reviews by Zdziarski & Gierliński 2004, McClintock & Remillard 2006, Done et al. 2007, Poutanen & Veledina 2014): (1) A truncated thin disk is required to model the thermal spectral component observed in BHBs in the quiescent state (Narayan et al. 1996, 1997a; Yuan & Cui 2005) and hard state (Esin et al. 2001, Di Salvo et al. 2001, Chaty et al. 2003, Yuan et al. 2005, Cabanac et al. 2009, Tomsick et al. 2009). (2) The observed transient behavior of BHBs requires a truncated disk (Lasota et al. 1996b, Menou et al. 2000, Dubus et al. 2001), as does the time delay between the optical and X-ray outbursts (Hameury et al. 1997). (3) A reflection component is seen in the X-ray continuum spectrum in the hard state. When the X-ray spectrum steepens, both the solid angle subtended by the reflection material and the amount of relativistic smearing increase, consistent with the truncation radius moving in and thereby increasing the flux of soft photons irradiating the inner hot accretion flow (Gilfanov et al. 1999, Zdziarski et al. 2003). (4) The truncated disk model explains the correlation between the luminosity and the photon index of the X-ray spectrum in the hard state (Qiao & Liu 2013, Gardner & Done 2013). (5) The model naturally explains why the QPO frequency increases with increasing X-ray luminosity (Cui et al. 1999, Ingram & Done 2011). (6) Across the soft-hard state transition, there is a sharp change in observational features such as variability (Kalemci et al. 2013, and references therein), photon index and X-ray flux (see Fig. 6 in Zdziarski & Gierliński 2004), and high-energy cut-off of the

[25] When the source is extremely dim, the X-ray radiation is likely to come primarily from the jet rather than the ADAF (see §4.2.6).

[26] As mentioned in §3.2.2, another QPO model invokes the precession of the ADAF, with the frequency again determined by the size of the ADAF.

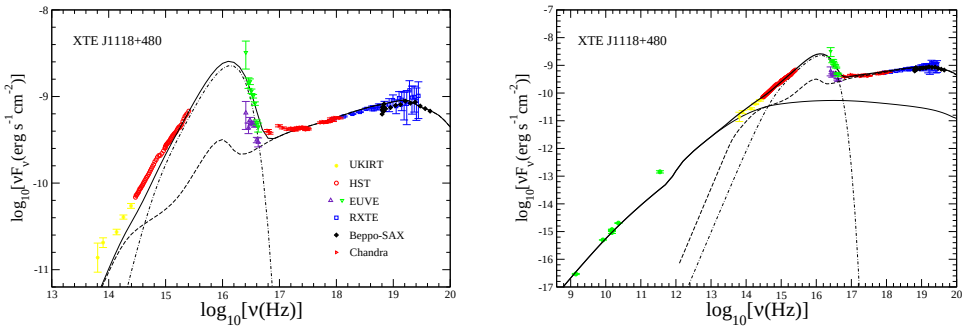

Figure 8: Modeling the spectrum of the BHB XTE J1118+480 in the hard state (from Yuan et al. 2005). *Left*: Calculated spectrum for a model consisting of an ADAF (dashed line) plus a truncated thin disk (dot-dashed line). The thin disk is essential to fit the optical–EUV part of the spectrum, while the hot ADAF is needed to fit the power-law X-ray emission. The model fails to explain the infrared and radio data. *Right*: A model that includes an additional jet component (thin solid line). This model explains all the observations.

X-ray spectrum (Belloni et al. 2006), all of which suggest that there must be a substantial qualitative change in the mode of accretion during this transition.

Most investigations of hot accretion flows tend to focus on thermal electrons. However, it is quite plausible that some nonthermal electrons will also be present (§2.2.2). Compared to a pure thermal model, a hybrid thermal-nonthermal model can explain a wider range of observations, with the nonthermal electrons playing a role similar to the jet component in disk-jet models. For instance, the hybrid model explains the MeV tail in the hard state spectrum of some BHBs (Poutanen & Vurm 2009), the power-law like optical/infrared spectrum, and the concave shape of the X-ray spectrum (Poutanen & Veledina 2014).

The hard state often reaches luminosities $\sim 10\% L_{\rm Edd}$ during the hard-to-soft transition. This is a factor of several too high for an ADAF (§2). Yuan & Zdziarski (2004) suggested that such luminous hard state systems, and also some Seyfert galaxies, might be explained by the LHAF model. This is confirmed in detailed modeling of XTE J1550−564 (Yuan et al. 2007), where the X-ray spectrum is naturally explained by the LHAF model. Features such as the slope of the X-ray spectrum, the cutoff energy, and the normalization are reproduced well. The agreement in the cutoff energy indicates that the predicted electron temperature is consistent with that required by observations (e.g., Fig. 3 in Yuan et al. 2007), although in some cases it is claimed that the ADAF model is too hot and that a hybrid thermal-nonthermal electron distribution is required to reconcile the model with observations (e.g., Poutanen & Veledina 2014). Some BHBs achieve even higher luminosities of up to $\sim 30\% L_{\rm Edd}$ in the "bright hard state" (Gierliński & Newton 2006). Oda et al. (2010) propose that a magnetically supported accretion flow model might explain these systems.

4.2.5 Assessment of arguments against disk truncation

The hard state sometimes shows a dim blackbody-like thermal component and also a broad iron Kα line at X-ray luminosities $L_{0.5-10\,\rm keV} > 10^{-3}L_{\rm Edd}$. These observations have been used to argue that the thin disk is not truncated but extends down to the ISCO (e.g., Miller et al. 2006, Rykoff et al. 2007, Ramadevi & Seetha 2007, Reis et al. 2010). However, the soft component in the spectrum typically has only 10% of the total observed luminosity. It is hard to understand how a radiatively efficient thin disk can extend down to the ISCO and yet contribute so little to the emitted luminosity. In fact, other groups have obtained different estimates of the disk inner radius using the same data (e.g., Done & Gierliński 2006, Done et al. 2007, Gierliński et al. 2008). Cabanac et al. (2009) carried out a detailed analysis of systematic uncertainties in spectral fitting and concluded that, when $L_{0.5-10\,\rm keV} \gtrsim 0.01L_{\rm Edd}$ one has $R_{\rm tr} \lesssim 10R_g$; while, when $10^{-3}L_{\rm Edd} \lesssim L_{0.5-10\,\rm keV} \lesssim 10^{-2}L_{\rm Edd}$, the disk inner edge recedes well away from the ISCO.

Alternate explanations have been proposed for the weak thermal spectral component in the hard state. These do not require the thin disk to extend down to the ISCO. One possibility is that the thermal component might originate near the inner edge of the truncated thin disk which is illuminated by hard X-rays from the hot flow (D'Angelo et al. 2008). Another possibility is that the emission is from cold clumps in the hot accretion flow (Chiang et al 2010). The same clumps may also explain timing features in the X-ray emission such as the power spectrum of rapid aperiodic variability (Böttcher & Liang 1999). Note that, at accretion rates approaching the upper limit of the hot accretion flow solution, cold clumps are expected to form naturally as a result of thermal instability in the hot gas (Yuan 2003; see §2.6) or condensation of the hot flow (Różańska & Czerny 2000; Meyer et al. 2007; Liu et al. 2007, 2011; Mayer & Pringle 2007; Meyer-Hofmeister et al. 2009).

Disk inner radii derived from iron line profile are even more controversial. Hartnoll & Blackman (2001) showed that iron lines can be readily produced in a two-phase (hot gas plus cold clumps) accretion flow. Provided the clumps are able to survive long enough, the line profiles are similar to those produced by a thin disk extending down to the ISCO.

Done & Diaz Trigo (2010) re-analyzed MOS iron line data in GX 339−4 in the hard state. Miller et al. 2006 (see also Reis et al. 2008) had previously claimed that the data indicated an extremely broad iron line. However, Done & Diaz Trigo (2010) showed that the line shape is strongly affected by pile-up. Furthermore, using the simultaneous PN timing-mode data, which should not be affected by pile-up, they obtained a significantly narrower line, which is easily consistent with a truncated disk. Recently, Plant et al. (2013) have carried out a systematic study of the iron line in GX 339−4 and have tracked the evolution of the thin disk inner radius over a range of two orders of magnitude in luminosity. They find that the data are consistent with the thin disk being truncated throughout the hard state, with the truncation radius moving closer to the black hole as the luminosity increases. In another recent study, Kolehmainen et al. (2013) used data on both the weak thermal component and the iron line to constrain the inner radius of the thin disk. They find that the data are consistent with a truncated disk.

The question of whether or not the disk is truncated in the hard state is

crucially important for efforts to measure black hole spin using X-ray reflection spectroscopy (see Reynolds 2013 for a current review). A key assumption of this method is that reflection occurs from a cool disk that extends down to the ISCO. Effectively, the measured profile of the iron Kα emission line is used to fit for the radius of the inner edge of the disk. Then, assuming that the disk edge is located at the ISCO, the black hole spin is estimated. However, almost all applications of the reflection method to stellar mass black holes have been carried out on X-ray data in the hard state. If the cool disk in BHBs in the hard state is truncated outside the ISCO, as the preponderence of evidence suggests (in the authors' view), most spin measurements by the reflection method will be affected. Measurements of the spins of supermassive black holes (where the reflection method originated and where considerable work has been done over many years, Reynolds 2013) are not affected by this criticism unless those systems also have truncated disks.

4.2.6 Radio/X-ray correlation and the role of jet radiation

Corbel et al. (2003) and Gallo et al. (2003) discovered a remarkable correlation between the radio luminosity L_R and X-ray luminosity L_X of BHBs in the hard state. Soon after, Merloni et al. (2003) and Falcke et al. (2004) considered the effect of black hole mass M and showed that the correlation extends also to LLAGNs (see Fig. 9; and also Körding et al. 2006, Wang et al. 2006, Li et al. 2008, Gültekin et al. 2009, Yuan et al. 2009c, de Gasperin et al. 2011, Younes et al. 2012 for later work). Their generalized correlation takes the form (Gültekin et al. 2009),

$$\log\left(\frac{L_R}{\mathrm{erg\,s^{-1}}}\right) = (0.7\pm0.1)\,\log\left(\frac{L_X}{\mathrm{erg\,s^{-1}}}\right) + (0.8\pm0.3)\,\log\left(\frac{M}{M_\odot}\right) + (4.8\pm0.2), \tag{36}$$

and is referred to as the "fundamental plane of black hole activity".

Using a simple model in which thermal gas in a hot accretion flow is responsible for the X-ray emission and relativistic electrons in a jet produce the radio emission, Heinz & Sunyaev (2003) showed that the fundamental plane can be naturally explained (see also Merloni et al. 2003, Heinz 2004, Yuan et al. 2005, Yuan & Cui 2005, Li et al. 2008). An alternative explanation has also been advanced in which the radio and X-ray emission are both produced by the jet (Markoff et al. 2003)[27].

Most sources in the Merloni et al. (2003) sample are relatively luminous and correspond to the upper range of allowed $\dot{M}_{\rm BH}$ for the hot accretion flow solution. Yuan & Cui (2005) extrapolated the coupled ADAF-jet model of Yuan et al. (2005) to lower luminosities and predicted that, below a critical luminosity $L_{\rm X,crit}$ given by $\log\left(L_{\rm X,crit}/L_{\rm Edd}\right) \approx -5.36 - 0.17\,\log(M/\,M_\odot)$, the correlation

[27]Heinz (2004) pointed out that, if the "cooling break" is properly taken into account for the electron energy distribution, the predicted correlation is different from that obtained by Markoff et al. (2003). This is confirmed by Yuan & Cui (2005), who find a steeper correlation when radiation from the jet dominates both the radio and X-ray emission (eq. 37). Plotkin et al. (2012) therefore suggest that supermassive black holes should be excluded from the sample since the cooling break "is a concern" for these objects. However, Zdziarski et al. (2012) find that the cooling break is independent of black hole mass, so the cooling break should be equally important for both LLAGNs and BHBs.

should steepen to (see segment "CD" in the middle panel of Fig. 9),

$$\log\left(\frac{L_R}{\mathrm{erg\,s^{-1}}}\right) = 1.23\,\log\left(\frac{L_X}{\mathrm{erg\,s^{-1}}}\right) + 0.25\,\log\left(\frac{M}{M_\odot}\right) - 13.45. \qquad (37)$$

This is because radiation from a hot accretion flow at low $\dot{M}_{\rm BH}$ is roughly $\propto \dot{M}_{\rm BH}^2$ (§2.4) while that from the jet is $\propto \dot{M}_{\rm BH}$ (Heinz 2004, Yuan & Cui 2005). Therefore, at a low enough $\dot{M}_{\rm BH}$, the X-ray emission from the jet will dominate. This can explain some otherwise puzzling observations of quiescent black holes (Yuan & Cui 2005). Early models of M87, for example, assumed that the X-ray emission is produced by the ADAF (e.g., Reynolds et al. 1996, Di Matteo et al. 2003). However, *Chandra* observations suggest that the emission is dominated by the jet (Wilson & Yang 2002), which is consistent since M87 has $L_X < L_{\rm X,crit}$.

On the whole, there is not enough data on quiescent BHBs to verify eq. (37). The two most promising sources are V404 Cyg (Corbel et al. 2008) and A0620-00 (Gallo et al. 2006), but the former is not dim enough to explore the low-luminosity end of the correlation, while the latter has data only in the quiescent state, not the hard state. The situation is much better in the case of LLAGNs, where recent work has confirmed the change of slope of the L_R-L_X correlation at low luminosities (Pellegrini et al. 2007, Wu et al. 2007, Wrobel et al. 2008, Yuan et al. 2009c, de Gasperin et al. 2011, Younes et al. 2012). Yuan et al. (2009c) considered 22 LLAGNs with $L_{\rm X} < L_{\rm X,crit}$ and found a correlation slope ~ 1.22 (Fig. 9 bottom), in excellent agreement with eq. (37).

4.2.7 Jets and black hole spin

The fundamental plane of black hole activity (Fig. 9 top, eq. 36) involves only the mass accretion rate $\dot{M}_{\rm BH}$ (through the luminosities L_R and L_X) and the black hole mass M; it does not involve the black hole spin. While there is a large scatter in most of the data, van Velzen & Falcke (2013) have recently obtained a very homogeneous sample of radio quasars in which they claim that most of the remaining scatter is due to environment, leaving little room for additional scatter due to variations in the black hole spin. If jets are powered by black hole spin (BZ jet, §3.3.1), we expect a strong dependence of jet power on the angular velocity of the black hole Ω_H (eqs. 30, 31). Why do the data not show this?

One possibility is that the range of black hole spins is not very large. Since the data are usually shown in a log-log plot, any modest variations due to spin could be hidden. Even the van Velzen & Falcke (2013) data are potentially consistent with equation (31), provided the black hole population does not span the full range of spin values but is restricted to a smaller range, say from 0.3 to 1.

Alternatively, perhaps hot accretion flows in nature do not approach anywhere near the MAD limit discussed in §3.2.3. If the flux Φ around the black hole is sufficiently below $\Phi_{\rm MAD}$, the BZ jet mechanism will be sub-dominant. The quasi-relativistic disk jet will then take over and we no longer expect a strong correlation between jet power and spin (§3.3.2). Note that jets in BHBs in the hard state do not appear to be relativistic (Fender 2006) and may well be disk jets rather than BZ jets. Even in the case of LLAGNs, only a few sources (e.g., M87: Hada et al. 2011) are known to have relativistic jets.

As discussed in §3.3.3, BHBs have two distinct kinds of jets: (i) steady quasi-relativistic jets which are associated with the hard state, and (ii) episodic jets which are most obviously seen when black holes undergo state transitions from

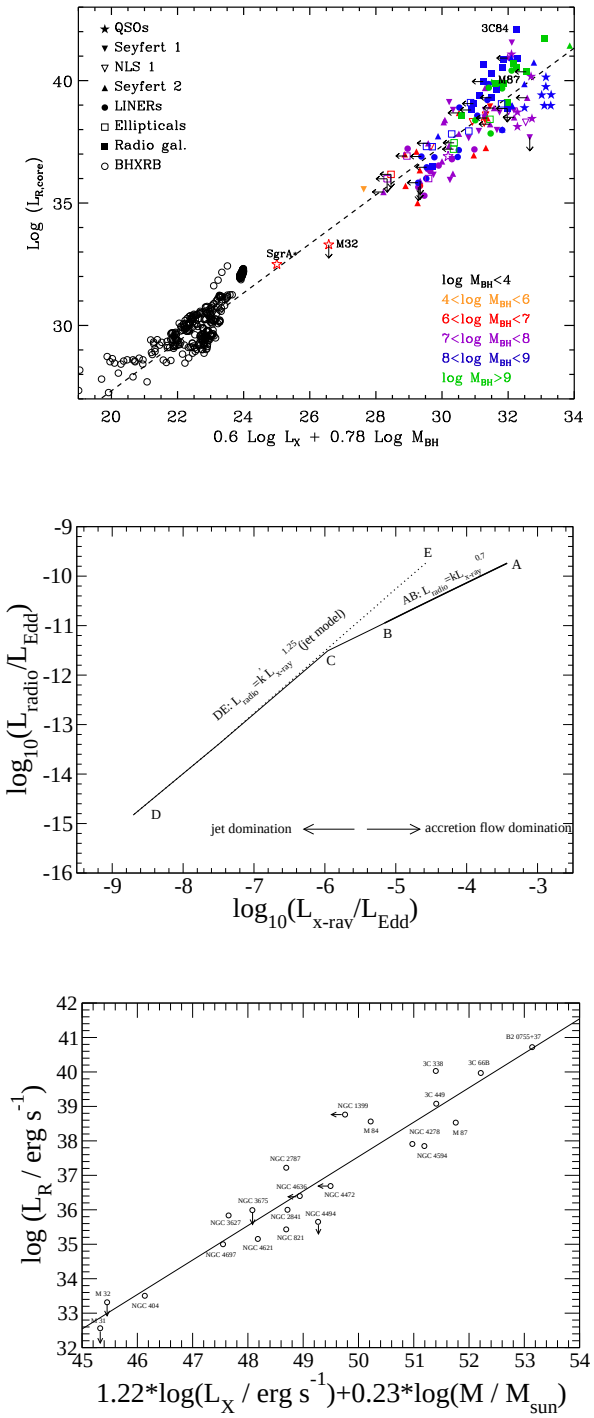

Figure 9: *Top*: The "fundamental plane of black hole activity" (from Merloni et al. 2003). Note that the correlation extends over many decades of black hole mass and accretion luminosity, and includes many different source types. (Figure courtesy of A. Merloni.) *Middle*: The predicted radio/X-ray correlation according to the ADAF-jet model (from Yuan & Cui 2005). The segment AB, which represents luminous sources, has the same slope (~ 0.6) as the top panel. The segment CD corresponds to objects at lower luminosities, where the jet is expected to dominate both the radio and X-ray emission. *Bottom*: Observational data on 22 LLAGNs with luminosities corresponding to CD in the middle panel (from Yuan et al. 2009c). The measured slope (~ 1.22) agrees well with the theoretically predicted slope (~ 1.23).

hot to cold mode accretion. So a third possibility is that the van Velzen & Falcke (2013) sample, which consists of radio loud quasars, is dominated by episodic jets (e.g., Merloni et al. 2003, Nipoti et al. 2005). If episodic jets are powered by the disk mechanism proposed by Yuan et al. (2009a; see §3.3.3 for details), no strong correlation between jet power and black hole spin is expected.

In the case of BHBs, thanks to recent progress in measuring the spins of black holes (McClintock et al. 2011, 2013), it is now possible to check directly for a correlation between spin and jet power. A strong correlation has been seen in the case of episodic jets (Narayan & McClintock 2012, Steiner et al. 2013, McClintock et al. 2013; but see Fender et al. 2010, Russell et al. 2013a, who question the reality of the correlation). However, the episodic jets in question are all associated with the transition from a hard to a soft state (i.e., from a hot accretion flow to a cold disk) rather than with a pure hard state. Hence the simulation results discussed in §3.3.1 may not be relevant. Also, since the jets were produced when the source luminosities were close to Eddington (Steiner et al. 2013), it is possible that additional physical effects, e.g., radiation, play an important role. There have been no investigations of the effect of radiation on the BZ mechanism.

4.2.8 Alternative models for the hard state

An alternative to the hot accretion flow model of hard state BHBs and LLAGNs is the "disk-corona" model. Here the thin disk extends down to the ISCO and the hard radiation is produced above the disk in a hot corona which is heated perhaps by magnetic reconnection (Liang & Price 1977; Haardt & Maraschi 1991, 1993). Because of the abundance of soft photons from the disk, coupled with the strong reprocessing of the coronal emission in the disk, the "slab" geometry of disk-corona models generally gives relatively soft X-ray spectra (photon indices $\Gamma \gtrsim 2$). This is not consistent with observed spectra (Stern et al. 1995, Zdziarski et al. 2003, Done et al. 2007). One way out is to postulate that the corona forms the base of an outward-moving jet (Beloborodov 1999, Malzac et al. 2001, Merloni & Fabian 2002). In this case, relativistic beaming reduces the amount of reprocessing in the cold disk and it is possible to obtain hard spectra. A patchy corona is another possibility (e.g., Malzac et al. 2001). In a recent study, Schnittman et al. (2013) calculated spectra for the disk-corona model using MHD simulation data. They claim to obtain relatively hard X-ray spectral slopes, although their spectra are inconsistent with observations in certain other respects. Apart from the spectral slope, the corona model also has trouble explaining the observed correlations between the spectral slope, iron line width and characteristic variability frequencies (Poutanen & Veledina 2014).

Another model for the hard state is the "jet model". As in the standard hot accretion flow models, the thin disk here is truncated. The main difference is that, not only the radio emission but also the X-ray emission is produced by the jet. In early work, it was proposed that the X-ray emission is due to synchrotron radiation (Markoff et al. 1999, 2003). However, it has been pointed out that a pure synchrotron model cannot reproduce the observed shape of the high-energy cutoff of the X-ray spectrum (Zdziarski et al. 2003). Later versions of the jet model invoke synchrotron self-Compton radiation from the base of the jet to explain the X-ray emission (Markoff et al. 2005). The model is then similar to the standard hot accretion flow model, except that the required electron temperature is much

higher, $\sim$ several MeV. Of course, a jet involves outflowing gas, so one way to distinguish between the models is by measuring the velocity of the X-ray-emitting gas. However, the outflowing gas at the base of the jet is only weakly relativistic. Therefore, while there may be some modest beaming (as in the Beloborodov 1999 model cited above), it is not expected to be a dominant effect. Observationally, there is no evidence that X-ray emission in the hard state has any dependence on the inclination of the system (Fender et al. 2004, Narayan & McClintock 2005). Other problems with the jet model are pointed out in Malzac et al. (2009) and Poutanen & Veledina (2014).

5 Hot accretion and AGN feedback

There is considerable observational evidence that AGN feedback plays an important role in the evolution of galaxies and galaxy clusters (Fabian 2012, Kormendy & Ho 2013). Arguments usually mentioned include: (1) the famous correlation between the black hole mass and the luminosity of the host galaxy or the velocity dispersion of the galaxy bulge (Magorrian et al. 1998, Ferrarese & Merritt 2000, Gebhardt et al. 2000, Kormendy & Ho 2013); (2) the observed exponential cutoff in the number density of galaxies at the high mass/luminosity end (Schechter 1976), even though there is no cutoff at the same mass scale in the distribution of dark matter halos; (3) the "downsizing" puzzle, where the most massive galaxies and black holes are the oldest (Cowie et al. 1996, Kriek et al. 2007, Babić et al. 2007, Fanidakis et al. 2012); and (4) the "cooling flow problem" in galaxy clusters, where the lack of any significant cooling in cluster cores (Peterson et al. 2001), despite a short cooling time, suggests that a central AGN serves as an extra source of energy (Pedlar et al. 1990; Churazov et al. 2000, 2002; Ciotti & Ostriker 2001; Brüggen & Kaiser 2002).

Two major modes of AGN feedback have been identified (Fabian 2012, Kormendy & Ho 2013): (1) "Radiative" mode, also known as "quasar" mode, which operates when the black hole accretes at a good fraction ($\gtrsim 0.1$) of the Eddington rate. (2) "Kinetic" mode, also known as "radio" mode or "maintenance" mode, which typically operates when $\dot{M}_{\rm BH}$ is low, i.e., when the AGN is fed by a hot accretion flow (the topic of this review). Maintenance mode feedback has been considered in the context of the cooling flow problem in galaxy clusters (Churazov 2002, Ruszkowski & Begelman 2002), it is included in semi-empirical models of galaxy formation (Croton et al. 2006, Hopkins et al. 2006, Somerville et al. 2008), and incorporated in hydrodynamical simulations of galaxy formation and evolution (Ciotti et al. 2010, Novak et al. 2011, Gaspari et al. 2012). We review here some of the physics of maintenance mode feedback, highlighting simplifications in current models that could be improved using our current knowledge of hot accretion flows.

5.1 Feedback from jets and outflows

Since the majority of supermassive black holes accrete at highly sub-Eddington rates via hot accretion flows, maintenance mode feedback is much more prevalent in the universe compared to quasar mode feedback. In particular, most nearby galaxies contain LLAGNs (§4.2), and any feedback activity in these systems occurs via the maintenance mode. Hot accretion flows tend to be radiatively inefficient, so the maintenance mode is believed to be dominated by mechanical

feedback via jets and winds rather than radiation from the accretion disk (but see §5.2). Bubbles and cavities in X-ray and radio images (e.g., Fabian 2012, Morganti et al. 2013) provide direct observational evidence for interaction between jets and the interstellar or intracluster medium. The two *Fermi* bubbles detected above and below the Galactic center (Su et al. 2010) are also thought to be inflated by a jet or wind from Sgr A* during a period of activity in the last few million years (Zubovas et al. 2011, Guo & Mathews 2012).

Most studies of maintenance mode feedback in the literature focus on the role of a collimated jet rather than a more isotropic non-relativistic disk wind. In large part, this is driven by the fact that jets are easily observed in the radio and their power can be estimated directly from observations. In contrast, there is virtually no direct evidence for uncollimated winds in LLAGNs (but see Crenshaw & Kraemer 2012). In addition, jets have been investigated via simulations for a number of years (§3.3), whereas the study of winds from hot accretion flows has only just begun (§3.4).

The relevant quantities that determine the effectiveness of feedback are the rate of injection of energy and momentum into the external medium and the degree of collimation of the jet or wind. Numerical simulations of hot accretion flows can provide some useful information. There is relatively better information in the case of jets (§3.3) compared to winds (§3.4), but rapid progress is expected on both fronts. One important parameter for feedback studies is "feedback efficiency" ϵ, defined as the ratio of the kinetic power in the jet or wind to the accretion power $\dot{M}_{\rm BH}c^2$. In almost all current cosmological models of feedback, ϵ is regarded as a free parameter, but it could in principle be estimated via simulations. Typically, one requires $\epsilon \sim 10^{-3} - 10^{-4}$ to explain observations (e.g., Di Matteo et al. 2005, Springel et al. 2005, Ciotti et al. 2009, Ostriker et al. 2010, Gaspari et al. 2012)[28].

Both jets and winds carry with them substantial fluxes of energy and momentum. Typically, the jet dominates the energy output, whereas the wind dominates the momentum output (Yuan et al. 2012a, Sadowski et al. 2013a). By and large, studies of AGN feedback have tended to focus on energy feedback (e.g., Springel et al. 2005, Di Matteo et al. 2005). However, momentum feedback can more effectively push the surrounding gas and may be equally important for controlling the growth of the black hole and switching off star formation (King 2003, 2005, 2010; Ostriker et al. 2010; Debuhr et al. 2010; Silk 2013).

The jet and wind differ significantly in their degree of collimation. Even though the jet dominates the energy flux, it is not clear that this energy couples very well to the interstellar medium of the host galaxy. The jet might simply drill through the surrounding gas, depositing little energy within the galaxy. Indeed some simulations indicate that the jet is ineffective even on the scale of galaxy clusters (Vernaleo & Reynolds 2006), though the problem is much alleviated when shear, rotation and large-scale flows in the intracluster medium are included (Heinz et al. 2006). Models that invoke efficient jet heating generally require a relatively slow (sub-relativistic) jet and a mass loss rate in the jet as large as the Eddington rate, which seems unlikely (e.g., Omma et al. 2004). In contrast, the less collimated disk wind, despite its lower energy budget, may actually be more important for galaxy scale feedback.

One other difference between jets and winds is the dependence of feedback

[28]Note that many studies of AGN feedback on galaxies do not discriminate between quasar and maintenance mode feedback and adopt a single value of ϵ for both.

efficiency on the parameters of the system. Apart from the obvious dependence on mass accretion rate $\dot{M}_{\rm BH}$, jet power is strongly affected by the black hole spin and the magnetic flux around the hole (at least in numerical simulations, §3.3). Thus, realistic incorporation of jet feedback in cosmological simulations requires keeping track of the spins of supermassive black holes. It is also necessary to decide whether or not the MAD configuration is viable, which depends on whether advection of magnetic field into the black hole is efficient (§3.2.3). In contrast, the energy and momentum flux in winds is relatively insensitive to the black hole spin and magnetic flux, and is primarily determined by $\dot{M}_{\rm BH}$. Thus, wind feedback ought to be simpler to model. Unfortunately, estimating the mass accretion rate itself involves large uncertainties (§3.4).

5.2 Feedback from radiation

The most obvious output of black hole accretion is radiation, which can impart energy and momentum to the surrounding interstellar medium via electron scattering, photoionization, atomic resonance scattering, and absorption by dust grains. In some semi-analytical models and numerical simulations (e.g., Wyithe & Loeb 2003, Di Matteo et al. 2005, Croton et al. 2006), it is assumed that a small and constant fraction ~ 0.05 of the radiated luminosity from an AGN couples thermodynamically to the surrounding gas. In other studies, a more elaborate calculation is used to calculate the heating rate using the Compton temperature $T_{\rm C}$ of the radiation field, which measures the frequency-weighted average energy of the emitted photons. Usually $T_{\rm C} \sim 10^7$ K is adopted, as appropriate for typical spectra of quasars (Sazonov et al. 2005, Ciotti et al. 2010, Novak et al. 2011).

Whereas in quasar mode there is no doubt that feedback from radiation and radiatively-driven winds (Proga 2007, Proga et al. 2008, Liu et al. 2013) are very important, in the case of maintenance mode, radiative feedback is usually assumed to be negligible compared to mechanical feedback. Two reasons are invoked (e.g., Churazov et al. 2005): (1) The kinetic power of the outflow is larger than the radiative output of the disk. (2) The efficiency of radiative heating is low. However, the radiative luminosity may actually be larger than the kinetic outflow power for luminosities[29] $\gtrsim 10^{-4} L_{\rm Edd}$ (Fender et al. 2003). In addition, the efficiency of radiative heating is not as low as usually imagined, since the efficiency is proportional to T_c. The spectrum of a hot accretion flow is much harder than that of a quasar (§4.2). Hence the Compton temperature can be as high as $T_c \sim 10^9$ K (Yuan et al. 2009b)[30], which means that the radiative heating efficiency is much greater than in the quasar mode.

Although the effect of a larger T_c has not been included in studies of galaxy-wide feedback, Ostriker and collaborators (e.g., Park & Ostriker 2001, 2007; Yuan et al. 2009b) have for many years investigated its role on the scale of the accretion flow itself and have demonstrated its importance in that context. When the accretion rate is relatively high, non-local radiative feedback via Compton heating is dynamically important and can change the temperature profile of the accretion flow. Moreover, if $L \gtrsim 2\% L_{\rm Edd}$, radiative heating at and beyond the Bondi radius ($R \gtrsim 10^5 R_S$) can be so strong that the gas is heated above the virial temperature and wants to flow out rather than in. In this case, no steady accretion solution

[29] This transition luminosity is different from the "critical luminosity" mentioned in §4.2.6.

[30] The value of $T_c \sim 10^9$K is obtained for a pure hot accretion flow. When the contribution from a truncated thin disk is included (§4.2), the value will be somewhat lower.

can be found and the accretion flow oscillates between active and inactive phases (Cowie et al. 1978; Ciotti & Ostriker 1997, 2001, 2007; Yuan et al. 2009b). This "small-scale AGN radiative feedback" effect has also been invoked to explain the intermittent activity of compact young radio sources (Yuan & Li 2011).

5.3 Estimating the mass accretion rate

Both mechanical and radiative feedback depend strongly on the mass accretion rate $\dot{M}_{\rm BH}$ of the black hole. Various approaches have been adopted in the literature for estimating $\dot{M}_{\rm BH}$. These include assuming that $\dot{M}_{\rm BH}$ is equal to the Eddington rate, or the Bondi rate, or some variant of these (e.g., Springel et al. 2005, Debuhr et al. 2010). The Bondi accretion rate is more relevant for maintenance mode feedback. However, whether or not the Bondi model is a reasonable proxy for a hot accretion flow is still very much in debate (see Narayan & Fabian 2011 and references therein).

Given the density and temperature of the external gas at the Bondi radius $R_{\rm B} \sim 10^5 - 10^6 R_S$, it is straightforward to calculate the Bondi accretion rate $\dot{M}_{\rm B}$ at that radius. But how much of this gas actually reaches the black hole is highly uncertain. If the accretion rate declines with decreasing radius as r^s, with $s \sim 0.5$ (§3.4), then as little as $0.1 - 0.3\%$ of $\dot{M}_{\rm B}$ will make it to the black hole. Although this is on the low side, it is not inconsistent with some models of Sgr A* (§4.1). However, other systems with powerful jets seem to require much more gas to reach the black hole to power the observed jets (Allen et al. 2006, Rafferty et al. 2006, McNamara et al. 2009, Russell et al. 2013b). A possible solution is that the value of s depends on boundary conditions. Perhaps s is effectively lower whenever the accreting gas has very low angular momentum (Narayan & Fabian 2011, Bu et al. 2013) or when accretion occurs via the MAD mode (Narayan et al. 2012b; Sadowski et al. 2013a). Unfortunately, until one has a better understanding of the mapping between $\dot{M}_{\rm B}$ and $\dot{M}_{\rm BH}$, it is hard to imagine any kind of quantitative modeling of maintenance mode feedback.

Another complication is that the mass accretion rate may be dominated by cold gas from the external medium rather the hot gas usually considered in hot accretion flow models (Pizzolato & Soker 2005, Rafferty et al. 2006). This could potentially boost the accretion rate by up to two orders of magnitude compared to the Bondi rate calculated based purely on hot gas (Gaspari et al. 2013). The cold gas would presumably first form a thin accretion disk and then evaporate to become a hot accretion flow closer to the black hole. Modeling this mode of accretion would require an understanding of the multi-phase nature of the interstellar medium as well as the specific angular momentum of the external cold clouds (Inogamov & Sunyaev 2010).

6 Prospects and remaining open questions

The discovery of the self-similar ADAF solution 20 years ago (Narayan & Yi 1994), and the subsequent development of the ADAF model of hot accretion flows (Abramowicz et al. 1995, Narayan & Yi 1995b, Chen et al. 1995), triggered a flurry of activity which has contributed greatly to our understanding of the dynamics and thermodynamics of hot accretion flows, as well as the recognition that these flows are relevant for numerous astrophysical objects: Sgr A*, low luminosity AGNs, BHBs.

Despite the impressive progress of the last two decades, there are presently more questions than answers in this field. Below, in the authors' view, are some of the more important questions:

- How are electrons and ions heated in a hot accretion flow? What particle energy distributions do these processes generate? What role do non-thermal particles play in the dynamical and radiative properties of the system?
- Are there processes in addition to Coulomb collisions which transfer energy from ions to electrons, and how do they influence the temperatures of the two species?
- How strong are mass outflows from hot accretion flows, and how does the mass accretion rate at the black hole ($\dot{M}_{\rm BH}$) depend on boundary conditions at large radius? What if gas is supplied from an external two-phase (or even multi-phase) medium?
- Why do hot accretion flows produce jets, whereas cool thin disks apparently do not? What role does the black hole, especially its spin, play in determining the properties of the jet? What fraction of the observed radiation comes from the jet versus the hot accretion flow?
- How efficiently do hot accretion flows advect large-scale ordered magnetic field towards the center, and how often do accreting black holes approach the "magnetically arrested disk" limit?
- Why and how do state transitions in black hole binaries occur? What are the physical processes responsible for converting cold optically thick gas into hot optically thin gas in a "truncated thin disk and hot inner accretion flow" configuration, and how do they relate to the hysteresis phenomenon? How do the same processes behave in the case of supermassive black holes?
- What is the thermal state of a hot accretion flow when $\dot{M}_{\rm BH}$ is close to the upper limit for a hot solution? Does the accreting gas become a two-phase medium, and what observational signatures do the hot and cold phases produce?
- What determines whether a hot accretion flow produces a steady jet or an episodic jet, and why are the latter often associated with the hard to soft state transition in black hole binaries? How does this map to supermassive black holes, AGN jets and the radio loud/quiet dichotomy?
- What is the angular distribution of mass, momentum and energy outflow from a hot accretion flow around a supermassive black hole, and how do they determine the efficiency of feedback processes?
- How does the relative importance of mechanical versus radiative feedback depend on $\dot{M}_{\rm BH}$ and other parameters of the accretion flow?
- What are the properties of hot accretion flows around compact objects with a surface?[31]

[31] An object with a surface introduces two important modifications compared to the black hole flows considered in this review. First, since gas comes to rest at the stellar surface, the inner boundary condition on the dynamical equations is very different and will result in vastly different density, velocity, pressure, etc. at small radii. Second, radiation from the surface will Compton-cool the hot accreting gas and modify its temperature. There have been only a few applications of the ADAF model to accreting neutron stars and white dwarfs. For lack of space, we have not reviewed this work here. Much more could be done in this area.

The authors are grateful to M. C. Begelman, C. Done, J.-P. Lasota, J. E. McClintock, J. P. Ostriker, J. Poutanen, E. Quataert, J. Stone, A. Tchekhovskoy and A. Zdziarski for helpful comments on the manuscript. This work was supported by grants 11133005 and 11121062 from the NSFC (FY) and AST1312651 from the NSF (RN).

LITERATURE CITED

Abarca D, Sadowski A, Sironi L. 2013. *MNRAS* submitted. arXiv:1309.2313
Abramowicz MA, Blaes O, Horák J, Kluźniak W, Rebusco P. 2006. *Class. Quant. Grav.* 23:1689-96
Abramowicz MA, Chen X, Granath M, Lasota JP. 1996. *Ap. J.* 471:762-73
Abramowicz MA, Chen X, Kato S, Lasota, JP, Regev O. 1995. *Ap. J. Lett.* 438:L37-9
Abramowicz MA, Czerny B, Lasota JP, Szuszkiewicz E. 1988. *Ap. J.* 332:646-58
Abramowicz MA, Fragile PC. 2013. *Living Reviews in Relativity* 16:1-88
Abramowicz MA, Igumenshchev IV, Lasota JP. 1998. *MNRAS* 293:443-6
Abramowicz MA, Igumenshchev IV, Quataert E, Narayan R. 2002a. *Ap. J.* 565:1101-6
Abramowicz MA, Kluzniak W, Lasota JP. 2002b. *Astron. Astrophys.* 396:L31-L34
Agol E. 2000. *Ap. J. Lett.* 538:L121-4
Aitken DK, Greaves J, Chrysostomou A, et al. 2000. *Ap. J. Lett.* 534:L173-6
Allen SW, Dunn RJH, Fabian AC, Taylor GB, Reynolds CS. 2006. *MNRAS* 372:21-30
Anninos P, Fragile PC, Salmonson JD. 2005. *Ap. J.* 635:723-40
Anninos P, Fragile PC, Wilson J, Murray SD. 2012. *Ap. J.* 759:132
Appl S, Camenzind M. 1992. *Astron. Astrophys.* 256:354-70
Appl S, Camenzind M. 1993. *Astron. Astrophys.* 270:71-82
Armitage P. 1998. *Ap. J. Lett.* 501:L189-92
Babić A, Miller L, Jarvis MJ, et al. 2007. *Astron. Astrophys.* 474:755-62
Baganoff FK, Bautz MW, Brandt WN, et al. 2001. *Nature* 413:45-48
Baganoff FK, Maeda Y, Morris M, et al. 2003. *Ap. J.* 591:891-915
Bai X, Stone JM. 2013. *Ap. J.* 767:30
Balbus SA. 2001. *Ap. J.* 562:909-17
Balbus SA, Hawley JF. 1991. *Ap. J.* 376:214-33
Balbus SA, Hawley JF. 1998. *Rev. Mod. Phys.* 70:1-53
Bardeen JM, Petterson JA. 1975. *Ap. J. Lett.* 195:L65-L67
Beckwith K, Hawley J, Krolik JH. 2008. *Ap. J.* 678:1180-99
Beckwith K, Hawley J, Krolik JH. 2009. *Ap. J.* 707:428-45
Begelman MC. 1979. *MNRAS* 187:237-51
Begelman MC. 2012. *MNRAS* 420:2912-23
Begelman MC, Celotti A. 2004. *MNRAS* 352:L45-8
Begelman MC, Chiueh T. 1988. *MNRAS* 332:872-90
Begelman MC, Meier DL. 1982. *Ap. J.* 253:873-96
Belloni T, Parolin I, Del Santo M, et al. 2006. *MNRAS* 367:1113-20
Beloborodov AM. 1999. *Ap. J. Lett.* 510:L123-6
Beskin VS, Istomin YN, Parev VI. 1992. *Astronomicheskij Zhurnal* 69:1254-74
Beskin VS, Malyshkin LM. 2000. *Astronomy Letters* 26:208-18
Binder B, Markowitz A, Rothschild RE. 2009. *Ap. J.* 691:431-40

Bisnovatyi-Kogan G, Lovelace RVE. 1997. *Ap. J.* 486:L43-46
Bisnovatyi-Kogan G, Lovelace RVE. 2007. *Ap. J.* 667:L167-9
Bisnovatyi-Kogan GS, Ruzmaikin AA. 1974. *Ap&SS* 28:45-59
Björnsson G, Abramowicz MA, Chen, X. Lasota JP. 1996. *Ap. J.* 467:99-104
Blackman EG. 1999. *MNRAS* 302:723-30
Blackman EG, Penna RF, Varniére P. 2008. *New Astron.* 13:244-51
Blaes O. 2013. *Space Sci. Rev.* (arXiv:1304.4879)
Blaes OM, Arras P, Fragile PC. 2006. *Ap. J.* 369:1235-52
Blandford RD, Begelman MC. 1999. *MNRAS* 303:L1-L5
Blandford RD, Begelman MC. 2004. *MNRAS* 349:66-86
Blandford RD, Payne DG. 1982. *MNRAS* 199:883-903
Blandford RD, Znajek RL. 1977. *MNRAS* 179:433-56
Bondi H. 1952. *MNRAS* 112:195-204
Böttcher M, Liang EP. 1999. *Ap. J. Lett.* 511:L37-40
Bower GC, Falcke H, Herrnstein RM, et al. 2004. *Science* 304:704-8
Bower GC, Wright MCH, Falcke H, Backer DC. 2003. *Ap. J.* 588:331-7
Brandenburg A, Nordlund A, Stein RF, Torkelsson U. 1995. *Ap. J.* 446:741-54
Broderick AE, Fish VL, Doeleman SS, Loeb A. 2011a. *Ap. J.* 735:110
Broderick AE, Fish VL, Doeleman SS, Loeb A. 2011b. *Ap. J.* 738:38
Broderick AE, Loeb A, Narayan R. 2009. *Ap. J.* 701:1357-66
Broderick AE, Narayan R. 2006. *Ap. J. Lett.* 638:L21-4
Brüggen M, Kaiser CR. 2002. *Nature* 418:301-3
Bu DF, Yuan F, Stone JM. 2011. *MNRAS* 413:2808-14
Bu DF, Yuan F, Wu M, Cuadra J. 2013. *MNRAS* 434:1691-701
Burkert A, Schartmann M, Alig C, et al. 2012. *Ap. J.* 750:58
Bursa M, Abramowicz MA, Karas V, Kluźniak W. 2004. *Ap. J. Lett.* 617:L45-L48
Cabanac C, Fender RP, Dunn RJH, Körding EG. 2009. *MNRAS* 396:1415-40
Cao X. 2011. *Ap. J.* 737:94
Chan CK, Liu S, Fryer CL, et al. 2009. *Ap. J.* 701:521-34
Chan CK, Psaltis D, Özel F. 2013. *Ap. J.* 777:13
Chaty S, Haswell CA, Malzac J, et al. 2003. *MNRAS* 346:689-703
Chen K, Halpern JP. 1989. *Ap. J.* 344:115-24
Chen X, Abramowicz MA, Lasota JP, Narayan R, Yi I. 1995. *Ap. J. Lett.* 443:L61-64
Chen X, Abramowicz MA, Lasota JP. 1997. *Ap. J.* 476:61-69
Chen X, Taam RE. 1993. *Ap. J.* 412:254-66
Chiaberge M, Gilli R, Macchetto FD, Sparks WB. 2006. *Ap. J.* 651:728-34
Chiang CY, Done C, Still M, Godet O. 2010. *MNRAS* 403:1102-12
Chiang J, Blaes O. 2003. *Ap. J.* 586:97-111
Churazov E, Forman W, Jones C, Böhringer H. 2000. *Astron. Astrophys.* 356:788-94
Churazov E, Sazonov S, Sunyaev R, et al. 2005. *MNRAS* 363:L91-5
Churazov E, Sunyaev R, Forman W, Böhringer H. 2002. *MNRAS* 332:729-34
Ciotti L, Ostriker JP. 1997. *Ap. J. Lett.* 487:L105-8
Ciotti L, Ostriker JP. 2001. *Ap. J.* 551:131-52
Ciotti L, Ostriker JP. 2007. *Ap. J.* 665:1038-56
Ciotti L, Ostriker JP, Proga D. 2009. *Ap. J.* 699:89-104
Ciotti L, Ostriker JP, Proga D. 2010. *Ap. J.* 717:708-23
Contopoulos J, Lovelace RVE. 1994. *Ap. J.* 429:139-52
Corbel S, Fender RP, Tzioumis AK, et al. 2000. *Astron. Astrophys.* 359:251-68

Corbel S, Koerding E, Kaaret P. 2008. *MNRAS* 389:1697-702
Corbel S, Nowak MA, Fender RP, Tzioumis AK, Markoff S. 2003. *Astron. Astrophys.* 400:1007-12
Cowie LL, Ostriker JP, Stark AA. 1978. *Ap. J.* 226:1041-62
Cowie LL, Songaila A, Hu E, Cohen JG. 1996. *Astron. J.* 112:839-64
Cowling TG. 1933. *MNRAS* 94:39-48
Cox TJ, Jonsson P, Primack JR, Somerville RS. 2006. *MNRAS* 373:1013-38
Crenshaw DM, Kraemer SB. 2012. *Ap. J* 753:75
Croton DJ, Springel V, White SD, et al. 2006. *MNRAS* 365:11-28
Crumley P, Kumar P. 2013. *MNRAS* 436:1955-60
Cuadra J, Nayakshin S, Martins F. 2008. *MNRAS* 383:458-66
Cui W, Zhang SN, Chen W, Morgan EH. 1999. *Ap. J. Lett.* 512:L43-46
D'Angelo C, Giannios D, Dullemond C, Spruit H. 2008. *Astron. Astrophys.* 488:441-50
Davis SW, Stone JM, Pessah ME. 2010. *Ap. J.* 713:52-65
de Gasperin F, Merloni A, Sell P, et al. 2011. *MMRAS* 415:2910-19
De Villiers JP, Hawley JF. 2002. *Ap. J.* 577:866-79
De Villiers JP, Hawley JF. 2003a. *Ap. J.* 589:458-80
De Villiers JP, Hawley JF. 2003b. *Ap. J.* 592:1060-77
De Villiers JP, Hawley JF, Krolik JH. 2003. *Ap. J.* 599:1238-53
De Villiers JP, Hawley JF, Krolik JH, Hirose S. 2005. *Ap. J.* 620:878-88
Debuhr J, Quataert E, Ma CP, Hopkins P. 2010, *MNRAS*, 406, L55-9
Dexter J, Agol E, Fragile PC, McKinney JC. 2010. *Ap. J.* 717:1092-104
Dexter J, Fragile PC. 2011. *Ap. J.* 730:36
Dexter J, Fragile PC. 2013. *MNRAS* 432:2252-72
Di Matteo T, Allen SW, Fabian AC, Wilson AS, Young AJ. 2003. *Ap. J.* 582:133-40
Di Matteo T, Johnstone RM, Allen SW, Fabian AC. 2001. *Ap. J. Lett.* 550:L19-23
Di Matteo T, Springel V, Hernquist L. 2005. *Nature* 433:604-7
Di Matteo T, Quataert E, Allen SW, Narayan R, Fabian AC. 2000. *MNRAS* 311:507-21
Di Salvo T, Done C, Zycki PT, Burderi L, Robba NR. 2001. *Ap. J.* 547:1024-33
Diaz Trigo M, Miller-Jones JCA, Migliari S, Broderick JW, Tzioumis T. 2013. *Nature* in press (arXiv:1311.5080)
Dibi S, Drappeau S, Fragile PC, Markoff S, Dexter J. 2012. *MNRAS* 426:1928-39
Ding J, Yuan F, Liang E. 2010. *Ap. J.* 708:1545-50
Dodds-Eden K, Porquet D, Trap G, et al. 2009. *Ap. J.* 698:676-92
Dodds-Eden K, Sharma P, Quataert E, et al. 2010. *Ap. J.* 725:450-65
Doeleman SS, Agol E, Backer D, et al. 2010. Astro2010: Science White Paper 68. arXiv:0906.3899
Doeleman SS, Fish VL, Schenck DE, et al. 2012. *Science* 338:355-8
Doeleman SS, Weintroub J, Rogers AEE, et al. 2008. *Nature* 455:78-80
Dolence JC, Gammie CF, Shiokawa H, Noble SC. 2012. *Ap. J.* 746:L10
Done C, Diaz Trigo M. 2010. *MNRAS* 407:2287-96
Done C, Gierliński M. 2006. *MNRAS* 367:659-68
Done C, Gierliński M, Kubota A. 2007. *Astron. Astrophys. Rev.* 15:1-66
Dubus G, Hameury JM, Lasota JP. 2001. *Astron. Astrophys.* 373:251-71
Dyda S, Lovelace RVE, Ustyugova GV, et al. 2013. *MNRAS* 432:127-37
Eckart A, Baganoff FK, Morris M, et al. 2004. *Astron. Astrophys.* 427:1-11
Eckart A, Baganoff FK, Schödel R, et al. 2006. *Astron. Astrophys.* 450:535-55

Eracleous M, Hwang JA, Flohic, HMLG. 2010. *Ap. J. Suppl.* 187:135-48
Esin AA. 1999. *Ap. J.* 517:381-95
Esin AA, McClintock JE, Narayan R. 1997. *Ap. J.* 489:865-89 (erratum: 500:523)
Esin AA, McClintock JE, Drake JJ, et al. 2001. *Ap. J.* 555:483-8
Esin AA, Narayan R, Cui W, Grove JE, Zhang SN. 1998. *Ap. J.* 505:854-68
Fabbiano G, Elvis M, Markoff S, et al. 2003. *Ap. J.* 588:175-85
Fabian AC. 2012. *Annu. Rev. Astron. Astrophys.* 50:455-89
Fabian AC, Canizares CR. 1988. *Nature* 333:829-31
Fabian AC, Rees MJ. 1995. *MNRAS* 277:L55-8
Fabrika S. 2004. *Astrophy. and Space Phys. Rev.* 12:1-152
Falcke H, Körding E, Markoff S. 2004. *Astron. Astrophys.* 414:895-903
Falcke H, Markoff S. 2000. *Astron. Astrophys.* 362:113-8
Falcke H, Melia F. 1997. *Ap. J.* 479:740-51
Falcke H, Nagar NM, Wilson AS, Ulvestad JS. 2000. *Ap. J.* 542:197-200
Fanidakis N, Baugh CM, Benson AJ, et al. 2012. *MNRAS* 419:2797-820
Fender RP. 2001. *MNRAS* 322:31-42
Fender RP. 2006. In *Compact stellar X-ray sources.* Edited by W Lewin & M van der Klis. Cambridge Astrophysics Series, 39:381-419
Fender RP, Belloni TM, Gallo E. 2004. *MNRAS* 355:1105-18
Fender RP, Gallo E, Jonker PG. 2003. *MNRAS* 343:L99-103
Fender RP, Gallo E, Russell D. 2010. *MNRAS* 406:1425-34
Fender R, Stirling AM, Spencer RE, et al. 2006. *MNRAS* 369:603-7
Ferrarese L, Merritt D. 2000. *Ap. J. Lett.* 539:L9-12
Fish VL, Broderick AE, Doeleman SS, Loeb A. 2009. *Ap. J. Lett.* 692:L14-L18
Fish VL, Doeleman SS, Beaudoin C, et al. 2011. *Ap. J. Lett.* 727:L36
Fragile PC. 2009. *Ap. J. Lett.* 706:L246-50
Fragile PC, Anninos P. 2005. *Ap. J.* 623:347-61
Fragile PC, Blaes OM, Anninos P, Salmonson JD. 2007. *Ap. J.* 668:417-29
Fragile PC, Lindner CC, Anninos P, Salmonson JD. 2009. *Ap. J.* 691:482-94
Fragile PC, Meier DL. 2009. *Ap. J.* 693:771-83
Frank J, King A, Raine DJ. 2002. *Accretion Power in Astrophysics*, Cambridge, UK: Cambridge University Press
Fromang S, Papaloizou J. 2007. *Astron. Astrophys.* 476:1113-22
Fromang S, Papaloizou J, Lesur G, Heinemann T. 2007. *Astron. Astrophys.* 476:1123-32
Gallo E, Fender RP, Miller-Jones JCA, et al. 2006. *MNRAS* 370:1351-60
Gallo E, Fender RP, Pooley GG. 2003. *MNRAS* 344:60-72
Gammie CF, McKinney JC, Tóth G. 2003. *Ap. J.* 589:444-57
Gammie CF, Narayan R, Blandford R. 1999. *Ap. J.* 516:177-86
Gammie CF, Popham R. 1998. *Ap. J.* 498:313-26
Gammie CF, Shapiro SL, McKinney JC. 2004. *Ap. J.* 602:312-9
Garcia MR, McClintock JE, Narayan R, et al. 2001. *Ap. J. Lett.* 553:L47-50
Gardner E, Done C. 2013. *MNRAS* 434:3454-62
Gaspari M, Brighenti F, Temi P. 2012. *MNRAS* 424:190-209
Gaspari M, Ruszkowski M, Peng Oh S. 2013. *MNRAS* 432:3401-22
Gebhardt K, Bender R, Bower G, et al. 2000. *Ap. J. Lett.* 539:L13-6
Genzel R, Eisenhauer F, Gillessen S. 2010. *Rev. Mod. Phys.* 82:3121-95
Genzel R, Schödel R, Ott T, et al. 2003. *Nature* 425:934-7
Ghez AM, Duchene G, Matthews K, et al. 2003. *Ap. J. Lett.* 586:L127-31
Ghez AM, Salim S, Weinberg NN, et al. 2008. *Ap. J.* 689:1044-62

Ghez AM, Wright SA, Mattews K, et al. 2004. *Ap. J. Lett.* 601:L159-62
Giannios D, Spruit HC. 2004. *Astron. Astrophys.* 427:251-61
Gierliński M, Done C, Page K. 2008. *MNRAS* 388:753-60
Gierliński M, Newton J. 2006. *MNRAS* 370:837-44
Gilfanov M, Churazov E, Revnivtsev M. 1999. *Astron. Astrophys.* 352:182-8
Gillessen S, Eisenhauer F, Quataert E, et al. 2006. *Ap. J. Lett.* 640:L163-6
Gillessen S, Eisenhauer F, Fritz TK, et al. 2009a. *Ap. J. Lett.* 707:L114-7
Gillessen S, Eisenhauer F, Trippe S, et al. 2009b. *Ap. J.* 692:1075-109
Gillessen S, Genzel R, Fritz TK, et al. 2012. *Nature* 481:51-4
Gillessen S, Genzel R, Fritz TK, et al. 2013. *Ap. J.* 774:44
Goldston JE, Quataert E, Igumenshchev IV. 2005. *Ap. J.* 621:785-92
Goodson AP, Bohm KH, Winglee RM. 1999. *Ap. J.* 524:142-58
Goodson AP, Winglee RM. 1999. *Ap. J.* 524:159-68
Gu WM, Lu JF. 2000. *Ap. J.* 540:L33-6
Guan X, Gammie CF, Simon JB, Hohnson BM. 2009. *Ap. J.* 694:1010-18
Guilet J, Ogilvie GI. 2012. *MNRAS* 424:2097-117
Guilet J, Ogilvie GI. 2013. *MNRAS* 430:822-35
Guo F, Mathews WG. 2012. *Ap. J.* 756:181
Gültekin K, Cackett EM, Miller JM, et al. 2009. *Ap. J.* 706:404-16
Haardt F, Maraschi L. 1993. *Ap. J.* 413:507-17
Hada K, Doi A, Kino M, et al. 2011. *Nature* 477:185-7
Hameury JM, Lasota JP, McClintock JE, Narayan R. 1997. *Ap. J.* 489:234-43
Hartnoll SA, Blackman EG. 2001. *MNRAS* 324:257-66
Hawley JF. 2000. *Ap. J.* 528:462-79
Hawley JF, Balbus SA. 1991. *Ap. J.* 376:223-33
Hawley JF, Balbus SA. 1996. in Physics of Accretion Disks, eds. S. Kato et al. New York: Gordon & Breach
Hawley JF, Balbus SA. 2002. *Ap. J.* 573:738-48
Hawley JF, Balbus S, Stone JM. 2001. *Ap. J.* 554:L49-L52
Hawley JF, Gammie CF, Balbus SA. 1995. *Ap. J.* 440:742
Hawley JF, Gammie CF, Balbus SA. 1996. *Ap. J.* 464:690
Hawley JF, Guan X, Krolik JH. 2011. *Ap. J.* 738:84
Hawley JF, Krolik JH. 2001. *Ap. J.* 548:348-67
Hawley JF, Krolik JH. 2002. *Ap. J.* 566:164-80
Hawley JF, Krolik JH. 2006. *Ap. J.* 641:103-16
Hawley JF, Richers SA, Guan X, Krolik JH. 2013. *Ap. J.* 722:102
Hayashi MR, Shibata K, Matsumoto R. 1996. *Ap. J. Lett.* 468:L37-40
Heinz S. 2004. *MNRAS* 355:835-44
Heinz S, Brüggen M, Young A, Levesque E. 2006. *MNRAS* 373:L65-9
Heinz S, Sunyaev RA. 2003. *MNRAS* 343:L59-64
Heyvaerts J, Norman C. 1989. *Ap. J.* 347:1055-81
Hirose S, Krolik JH, Blaes O. 2009. *Ap. J.* 691:16-31
Hirose S, Krolik JH, De Villiers JP, Hawley JH. 2004. *Ap. J.* 606:1083-97
Hirotani K, Okamoto I. 1998. *Ap. J.* 497:563
Ho LC. 1999. *Ap. J.* 516:672-82
Ho LC. 2002. *Ap. J.* 564:120-32
Ho LC. 2008. *Annu. Rev. Astron. Astrophys.* 46:475-539
Ho LC. 2009. *Ap. J.* 699:626-37
Ho LC, Terashima Y, Ulvestad JS. 2003. *Ap. J.* 589:783-9
Honma F. 1996. *Publ. Astron. Soc. Jap.* 48:77-87

Hoshino M. 2012. *Phys. Rev. Lett.* 108:135003
Hoshino M. 2013. *Ap. J.* 773:118
Hopkins PF, Hernquist L, Cox TJ, et al. 2006. *Ap. J.S.* 163:1-49
Huang L, Cai M, Shen ZQ, Yuan F. 2007. *MNRAS* 379:833-40
Ichimaru S. 1977. *Ap. J.* 214:840-55
Igumenshchev IV. 2002. *Ap. J. Lett.* 577:L31-L34
Igumenshchev IV. 2006. *Ap. J.* 649:361-72
Igumenshchev IV. 2008. *Ap. J.* 677:317-26
Igumenshchev IV, Aramowicz MA. 1999. *Ap. J. Lett.* 537:L27
Igumenshchev IV, Aramowicz MA. 2000. *Ap. J. Supp.* 130:463-84
Igumenshchev IV, Aramowicz MA, Narayan R. 2000. *Ap. J. Lett.* 537:L27-30
Igumenshchev IV, Chen XM, Abramowicz M. 1996. *MNRAS* 278:236-250
Igumenshchev IV, Narayan R. 2002. *Ap. J.* 566:137-47
Igumenshchev IV, Narayan R, Abramowicz, MA. 2003. *Ap. J.* 592:1042-59
Ingram A, Done C, Fragile PC. 2009. *MNRAS* 397:L101-05
Ingram A, Done C. 2011. *MNRAS* 415:2323-35
Inogamov NA, Sunyaev RA. 2010. *Astron. Lett.* 36:835-47
Janiuk A, Sznajder M, Mościbrodzka M, Proga D. 2009. *Ap. J.* 705:1503-21
Jaroszynski M, Kurpiewski A. 1997. *Astron. Astrophys.* 326:419-26
Jiang YF, Stone JM, Davis SW. 2013. *Ap. J.* 778:65
Jiao CL, Wu XB. 2011. *Ap. J.* 733:112
Johnson BM, Quataert E. 2007. *Ap. J.* 660:1273-81
Kalemci E, Dincer T, Tomsick JA, et al. 2013. *Ap. J.* 779:95
Kato S, Abramowicz MA, Chen X. 1996. *Publ. Astron. Soc. Jap.* 48:67-75
Kato S, Fukue J, Mineshige S. 2008. *Black-Hole Accretion Disks - Towards a New Paradigm* (Kyoto, Japan: Kyoto Univ. Press)
Kato S, Yamasaki T, Abramowicz MA, Chen X. 1997. *Publ. Astron. Soc. Jap.* 49:221-5
Kato Y, Hayashi MR, Matsumoto R. 2004a. *Ap. J.* 600:338-42
Kato Y, Mineshige S, Shibata K. 2004b. *Ap. J.* 605:307-20
Kato Y, Umemura M, Ohsuga K. 2009. *MNRAS* 400:1742-8
Katz J. 1977. *Ap. J.* 215:265-75
Kawamuro T, Ueda Y, Tazaki F, Terashima Y. 2013. *Ap. J.* 770:157
King A. 2003. *Ap. J. Lett.* 596:L27-9
King A. 2005. *Ap. J. Lett.* 635:L121-3
King AR. 2010. *MNRAS* 402:1516-22
Krolik JH, Hawley JF, Hirose S. 2005. *Ap. J.* 622:1008-23
Koide S. 2003. *Phys. Rev. D* 67:104010
Koide S, Shibata K, Kudoh T. 1999. *Ap. J.* 522:727-52
Koide S, Meier DL, Shibata K, Kudoh T. 2000. *Ap. J.* 536:668-74
Kolehmainen M, Done C, Diaz Trigo M. 2013. *MNRAS* submitted (arXiv:1310.1219)
Komissarov SS. 1999. *MNRAS* 303:343-66
Komissarov SS. 2001. *MNRAS* 326:L41-4
Komissarov S, Barkov MV, Vlahakis N, Konigl A. 2007. *MNRAS* 380:51-70
Komissarov SS, McKinney JC. 2007. *MNRAS* 377:L49-L53
Koratkar A, Blaes O. 1999. *PASJ* 755:1-30
Körding E, Falcke H, Corbel S. 2006. *Astron. Astrophys.* 456:439-50
Kormendy J, Ho LC. 2013. *Annu. Rev. Astron. Astrophys.* 51:511-653
Kriek M, van Dokkum PG, Franx M, et al. 2007. *Ap. J.* 669:776-90
Krolik JH, Hawley JF, Hirose S. 2005. *Ap. J.* 622:1008-23

Kudoh T, Matsumoto R, Shibata K 1998. *Ap. J.* 508:186-99
Kudoh T, Matsumoto R, Shibata K 2002. *PASJ* 54:267-74
Kusunose M, Mineshige S. 1996. *Ap. J.* 468:330-37
Kuwabara T, Shibata K, Kudoh T, Matsumoto R. 2000. *Publ. Astron. Soc. Jap.* 52:1109-24
Lasota JP. 1999. *Phys. Rep.* 311, 247-58
Lasota LP, Abramowicz MA, Chen X, et al. 1996a. *Ap. J.* 462:142-6
Lasota, JP, Gourgoulhon E, Abramowicz M, Tchekhovskoy A, Narayan R. 2014. *Phys. Rev. D*, in press (arXiv:1310.7499)
Lasota JP, Narayan R, Yi I. 1996b. *Astron. Astrophys.* 314:813-20
Lehe R, Parrish IJ, Quataert E. 2009. *Ap. J.* 707:404-19
Li J, Ostriker J, Sunyaev R. 2013a. *Ap. J.* 767:105
Li Z, Morris MR, Baganoff FK. 2013b. *Ap. J.* 779:154
Li Z, Wu XB, Wang R. 2008. *Ap. J.* 688:826-36
Li ZY, Chiueh T, Begelman MC. 1992. *Ap. J.* 394:459-71
Liang EPT, Price RH. 1977. *Ap. J.* 218:247-52
Lightman AP, Eardley DM. 1974. *Ap. J.* 187:L1-4
Liu BF, Done C, Taam RE. 2011. *Ap. J.* 726:10
Liu BF, Meyer F, Meyer-Hofmeister E. 2005. *Astron. Astrophys.* 442:555-62
Liu BF, Taam RE, Meyer-Hofmeister E, Meyer F. 2007. *Ap. J.* 671:695-705
Liu BF, Yuan W, Meyer F, Meyer-Hofmeister E. 1999. *Ap. J.* 527:L17-20
Liu C, Yuan F, Ostriker JP, Gan Z, Yang X. 2013. *MNRAS* 434:1721-35
Liu H, Wu Q. 2013. *Ap. J.* 764:17
Livio M, Ogilvie GI, Pringle JE. 1999. *Ap. J.* 512:100-04
Lu JF, Lin YQ, Gu WM 2004. *Ap. J. Lett.* 602:L37
Lodato G, Pringle JE. 2006. *MNRAS* 368:1196-1208
Loewenstein M, Mushotzky RF, Angelini L, Arnaud KA, Quataert E. 2001. *Ap. J. Lett.* 555:L21-4
Lovelace RVE. 1976. *Nature* 262:649-52
Lovelace RVE, Mehanian CM, Mobarry CM, Sulkanen ME. 1986. *Ap. J. Suppl.* 62:1-37
Lynden-Bell D, Pringle JE. 1974. *MNRAS* 168:603-37
Lynden-Bell D. 2003. *MNRAS* 341:1360-72
MacDonald D, Thorne KS. 1982. *MNRAS* 198:345-82
Machida M, Hayashi MR, Matsumoto R. 2000. *Ap. J. Lett.* 532:L67-70
Machida M, Matsumoto R. 2003. *Ap. J.* 585:429-42
Machida M, Matsumoto R, Mineshige S. 2001. *Publ. Astron. Soc. Jap.* 53:L1-L4
Machida M, Nakamura KE, Matsumoto R. 2004. *Publ. Astron. Soc. Jap.* 56:671-9
Machida M, Nakamura KE, Matsumoto R. 2006. *Publ. Astron. Soc. Jap.* 58:193-202
Magorrian J, Tremaine S, Richstone D, et al. 1998. *Astron. J.* 115:2285-305
Mahadevan R. 1997. *Ap. J.* 477:585-601
Mahadevan R. 1998. *Nature* 394:651-3
Mahadevan R. 1999. *MNRAS* 304:501-11
Mahadevan R, Narayan R, Krolik J. 1997. *Ap. J.* 486:268-75
Mahadevan R, Quataert E. 1997. *Ap. J.* 490:605-18
Malzac J, Belmont R, Fabian AC. 2009. *MNRAS* 400:1512-20
Malzac J, Beloborodov AM, Poutanen J. 2001. *MNRAS* 326:417-27
Malzac, J, Merloni, A, Fabian, AC. 2004. *MNRAS* 351:253-64
Manmoto T. 2000. *Ap. J.* 534:734-46

Manmoto T, Kato S. 2000. *Ap. J.* 538:295-306
Manmoto T, Kato S, Nakamura KE, Narayan R. 2000. *Ap. J.* 529:127-37
Manmoto T, Mineshige S, Kusunose M. 1997. *Ap. J.* 489:791-803
Manmoto T, Takeuchi M, Mineshige S, Matsumoto R, Negoro H. 1996. *Ap. J. Lett.* 464:L135-8
Maoz D. 2007. *MNRAS* 377:1696-710
Maraschi L, Tavecchio F. 2003. *Ap. J.* 593:667-75
Markoff S, Bower GC, Falcke H. 2007. *MNRAS* 379:1519-32
Markoff S, Falcke H, Fender R. 1999. *Astron. Astrophys.* 372:L25-28
Markoff S, Falcke H, Yuan F, Biermann P. 2001. *Astron. Astrophys.* 379:L13-16
Markoff S, Nowak M, Corbel S, Fender R. et al. 2003. *Astron. Astrophys.* 397:645
Markoff S, Nowak MA, Wilms J. 2005. *Ap. J.* 635:1203-16
Marrone DP, Moran JM, Zhao JH, Rao R. 2006. *Ap. J.* 640:308-18
Marrone DP, Moran JM, Zhao JH, Rao R. 2007. *Ap. J. Lett.* 654:L57-L60
Marsch E. 2012. *Space Sci. Rev.* 172:23-39
Massi M, Poletto G. 2011. *Memorie della Societa Astronomica Italiana* 82:145
Matsumoto R, Tajima T. 1995. *Ap. J.* 445:767-79
Matsumoto R, Shibata K. 1997. in IAU Colloq. 163, Accretion Phenomena and Related Outflows, ed. D. Wickramsinghe, G. Bicknell & L. Ferrario, (ASP Conf. Ser. 121; San Francisco: ASP), 443
Mayer M, Pringle JE. 2007. *MNRAS* 376:435-56
McClintock JE, Remillard RA. 2006. In *Compact stellar X-ray sources.* Edited by W Lewin & M van der Klis. Cambridge Astrophysics Series, 39:157-213
McClintock JE, Narayan R, Davis SW, et al. 2011. *Classical and Quantum Gravity* 28:114009
McClintock JE, Narayan R, Garcia MR, et al. 2003. *Ap. J.* 593:435-51
McClintock JE, Narayan R, Steiner JF. 2013. *Space Sci. Rev.*, in press (arXiv:1303.1583)
McKinney JC. 2005. *Ap. J. Lett.* 630:L5-L8
McKinney JC. 2006. *MNRAS* 368:1561-82
McKinney JC, Blandford RD. 2009. *MNRAS* 394:L126-30
McKinney JC, Gammie CF. 2004. *Ap. J.* 611:977-95
McKinney JC, Tchekhovskoy A, Blandford RD. 2012. *MNRAS* 423:3083-117
McKinney JC, Tchekhovskoy A, Blandford RD. 2013. *Science* 339:49-52
McNamara BR, Kazemzadeh F, Rafferty DA, et al. 2009. *Ap. J.* 698:594-605
Medvedev MV. 2000. *Ap. J.* 541:811-20
Meier DL. 2005. *Ap. Space. Sci.* 300:55-65
Melia F. 1992. *Ap. J. Lett.* 387:L25-8
Melia F, Liu S, Coker R. 2001. *Ap. J.* 553:146-57
Menou K, Esin AA, Narayan R, et al. 1999a. *Ap. J.* 520:276-91
Menou K, Hameury JM, Lasota JP, Narayan R. 2000. *MNRAS* 314:498-510
Menou K, Narayan R, Lasota JP. 1999b. *Ap. J.* 513:811-26
Merloni A, Fabian AC. 2002. *MNRAS* 332:165-75
Merloni A, Heinz S, Di Matteo T. 2003. *MNRAS* 345:1057-76
Meyer F, Meyer-Hofmeister E. 1994. *Astron. Astrophys.* 288:175-82
Meyer F, Liu BF, Meyer-Hofmeister E. 2007. *Astron. Astrophys.* 463:1-9
Meyer F, Liu BF, Meyer-Hofmeister E. 2000. *Astron. Astrophys.* 361:175-88
Meyer L, Ghez AM, Schödel R, et al. 2012. *Sci.* 338:84-87
Meyer-Hofmeister E, Liu BF, Meyer F. 2005. *Astron. Astrophys.* 432:181-7
Meyer-Hofmeister E, Liu BF, Meyer F. 2009. *Astron. Astrophys.* 508:329-37
Miller JM, Homan J, Steeghs D, et al. 2006. *Ap. J.* 653:525-35

Mineshige S, Kawaguchi T, Takeuchi M, Hayashida K. 2000. *Publ. Astron. Soc. Jap.* 52:499-508
Morganti R, Fogasy J, Paragi Z, Oosterloo T, Orienti M. 2013. *Science* 341:1082-5
Mościbrodzka M, Proga D, Czerny B, Siemiginowska A. 2007. *Astron. Astrophys.* 474:1-13
Mościbrodzka M, Gammie CF, Dolence JC, Shiokawa H. 2011. *Ap. J.* 735:9
Mościbrodzka M, Gammie CF, Dolence JC, Shiokawa H, Leung PK. 2009. *Ap. J.* 706:497-507
Mościbrodzka M, Shiokawa H, Gammie CF, Dolence JC. 2012. *Ap. J. Lett.* 752:L1
Nagar NM, Falcke H, Wilson AS, Ho LC. 2000. *Ap. J.* 542:186-96
Nakamura KE. 1998. *Publ. Astron. Soc. Jap.* 50:L11-L14
Nakamura KE, Kusunose M, Matsumoto R, Kato S. 1997. *Publ. Astron. Soc. Jap.* 49:503-12
Nakamura KE, Matsumoto R, Kusunose, M, Kato S. 1996. *Publ. Astron. Soc. Jap.* 48:761-69
Narayan R. 1996. *Ap. J.* 462:136-41
Narayan R, Barret D, McClintock JE. 1997a. *Ap. J.* 482:448-64
Narayan R, Fabian A. 2011. *MNRAS* 415:3721-30
Narayan R, Garcia MR, McClintock JE. 1997b, *Ap. J. Lett.* 478:L79
Narayan R, Igumenshchev IV, Abramowicz MA. 2000. *Ap. J.* 539:798-808
Narayan R, Igumenshchev IV, Abramowicz MA. 2003. *Publ. Astron. Soc. Jap.* 55:L69-72
Narayan R, Kato S, Honma F. 1997c. *Ap. J.* 476:49-60
Narayan R, Mahadevan R, Grindlay JE, Popham RG, Gammie C. 1998a. *Ap. J.* 492:554-68
Narayan R, Mahadevan R, Quataert E. 1998b. in Theory of Black Hole Accretion Disks, ed. M. A. Abramowicz, G. Bjornsson, & J. E. Pringle (Cambridge Univ. Press) p148
Narayan R, McClintock JE. 2005. *Ap. J.* 623:1017-25
Narayan R, McClintock JE. 2008. *New Astro. Rev.* 51:733-51
Narayan R, McClintock JE. 2012. *MNRAS* 419:L69-73
Narayan R, McClintock JE, Yi I. 1996. *Ap. J.* 457:821-33
Narayan R, Medvedev MV. 2001. *Ap. J.* 562:L129-32
Narayan R, Özel F, Sironi L. 2012a. *Ap. J. Lett.* 757:L20
Narayan R, Quataert E, Igumenshchev IV, Abramowicz MA. 2002. *Ap. J.* 577:295-301
Narayan R, Raymond J. 1999. *Ap. J. Lett.* 515:L69-72
Narayan R, Sädowski A, Penna RF, Kulkarni AK. 2012b. *MNRAS* 426:3241-59
Narayan R, Yi I. 1994. *Ap. J. Lett.* 428:L13-6
Narayan R, Yi I. 1995a. *Ap. J.* 444:231-243
Narayan R, Yi I. 1995b. *Ap. J.* 452:710-735
Narayan R, Yi I, Mahadevan R. 1995. *Nature* 374:623-5
Nemmen RS, Storchi-Bergmann T, Eracleous M. 2014. *MNRAS* in press (arXiv:1312.1982)
Nemmen RS, Storchi-Bergmann T, Yuan F, et al. 2006. *Ap. J.* 643:652-9
Nipoti C, Blundell KM, Binney J. 2005. *MNRAS* 361:633-7
Noble SC, Krolik JH, Hawley JF. 2010. *Ap. J.* 711:959-73
Noble SC, Leung PK, Gammie CF, Book LG. 2007. *Class. Quantum Grav.* 24:S259-74
Novak GS, Ostriker JP, Ciotti L. 2011. *Ap. J.* 737:26
Novikov ID, Thorne KS. 1973. *Black holes (Les astres occlus)* 343-450

Oda H, Machida M, Nakamura KE, Matsumoto R. 2010. *Ap. J.* 712:639-52
Ogilvie GI. 1999. *MNRAS* 306:L9-13
Ohsuga K, Mineshige S. 2011. *Ap. J.* 736:2
Ohsuga K, Mineshige S, Mori M, Kato Y. 2009. *Publ. Astron. Soc. Jap.* 61:L7-11
Ohsuga K, Mori M, Nakamoto T, Mineshige S. 2005. *Ap. J.* 628:368-81
Omma H, Binney J, Bryan G, Slyz A. 2004. *MNRAS* 348:1105-19
Ostriker E. 1997. *Ap. J.* 486:291-306
Ostriker JP, Choi E, Ciotti L, Novak GS, Proga D. 2010. *Ap. J.* 722:642-52
Özel F, Psaltis D, Narayan R. 2000. *Ap. J.* 541:234-49
Paczyński B, Wiita PJ. 1980. *Astron. Astrophys.* 88:23-31
Pang B, Pen UL, Matzner CD, Green SR, Liebendörfer M. 2011. *MNRAS* 415:1228-39
Papaloizou JCB, Lin DNC. 1995. *Ap. J.* 438:841-51
Park M, Ostriker JP. 2001. *Ap. J.* 549:100-17
Park M, Ostriker JP. 2007. *Ap. J.* 655:88-97
Parrish IJ, Stone JM. 2007. *Ap. J.* 664:135-48
Pedlar A, Ghataure HS, Davies RD, et al., 1990. *MNRAS* 246:477-489
Peitz J, Appl S. 1997. *MNRAS* 286:681-95
Pellegrini S, Baldi A, Fabbiano G, Kim DM. 2003. *Ap. J.* 597:175-85
Pellegrini S, Siemiginowska A, Fabbiano G, et al. 2007. *Ap. J.* 667:749-59
Pen UL, Matzner CD, Wong S. 2003. *Ap. J. Lett.* 596:L207-L210
Penna RF, McKinney JC, Narayan R, et al. 2010. *MNRAS* 408:752-82
Penna RF, Narayan R, Sadowsli A. 2013a. *MNRAS*, 436:3741-58
Penna RF, Sadowski A, Kulkarni AK, Narayan R. 2013b. *MNRAS* 428:2255-74
Penrose R. 1969. *Rivista del Nuovo Cimento, Numero Speziale I* 252
Perna R, Raymond J, Narayan R. 2000. *Ap. J.* 541:898-907
Pessah ME, Chan CK, Psaltis D. 2007. *Ap. J. Lett.* 668:L51-4
Peterson JR, Paerels FBS, Kaastra JS, et al. 2001. *Astron. Astrophys.* 365:L104-9
Phifer K, Do T, Meyer L, et al. 2013. *Ap. J. Lett.* 773:L13
Phinney ES. 1983. in Astrophysical Jets, eds. A Ferrari, AG Pacholczyk. *Ap. Sp. Sci. Library* 103:201-12
Piran T. 1978. *Ap. J.* 221:652-60
Pizzolato F, Soker N. 2005. *ApJ* 632:821-30
Plant DS, Fender RP, Ponti G, Munoz-Darias T, Coriat M. 2013. *MNRAS* submitted (arXiv:1309.4781)
Plotkin RM, Markoff S, Kelly BC, Körding E, Anderson SF. 2012. *MNRAS* 419:267-86
Popham R, Gammie CF. 1998. *Ap. J.* 504:419-30
Poutanen J, Krolik JH, Ryde F. 1997. *MNRAS* 292:L21-5
Poutanen J, Lipunova G, Fabrika S, Butkevich AG, Abolmasov P. 2007. *MNRAS* 377:1187-94
Poutanen J, Veledina A. 2014. *Space Sci. Rev.* in press (arXiv:1312.2761)
Poutanen J, Vurm I. 2009. *Ap. J. Lett.* 690:L97-100
Press WH, Teukolsky SA, Vetterling WT, Flannery BP. 1992. *Numerical Recipes in FORTRAN. The Art of Scientific Computing*, Cambridge, UK: Cambridge University Press
Press WH, Teukolsky SA, Vetterling WT, Flannery BP. 2002. *Numerical Recipes in C++: The Art of Scientific Computing*, William H. Press
Pringle JE. 1981. *Annu. Rev. Astron. Astrophys.* 19:137-162
Proga D. 2007. *Ap. J.* 661:693-701

Proga D, Begelman MC. 2003. *Ap. J.* 582:69-81
Proga D, Ostriker JP, Kurosawa R. 2008. *Ap. J.* 676:101-12
Ptak A, Terashima Y, Ho LC, Quataert E. 2004. *Ap. J.* 606:173-84
Pudritz RE, Norman CA. 1983. *Ap. J.* 274:677-97
Punsly B, Coroniti FV. 1989. *Phys. Rev. D.* 40:3834-57
Qiao E, Liu BF. 2013. *Ap. J.* 764:2
Quataert E. 1998. *Ap. J.* 500:978-91
Quataert E. 2001. In *Probing the Physics of Active Galactic Nuclei*, ed. BM Peterson, RW Pogge, RS Polidan, p. 71. San Francisco: ASP
Quataert E. 2002. *Ap. J.* 575:855-9
Quataert E. 2004. *Ap. J.* 613:322-5
Quataert E, Di Matteo T, Narayan R, Ho LC. 1999. *Ap. J. Lett.* 525:L89-92
Quataert E, Dorland W, Hammett GW. 2002. *Ap. J.* 577:524-33
Quataert E, Gruzinov A. 1999. *Ap. J.* 520:248-255
Quataert E, Gruzinov A. 2000. *Ap. J.* 539:809-814
Quataert E, Narayan R. 1999a. *Ap. J.* 516:399-410
Quataert E, Narayan R. 1999b. *Ap. J.* 520:298-315
Rafferty DA, McNamara BR, Nulsen PEJ, Wise MW. 2006. *Ap. J.* 652:216-31
Rakowski CE. 2005. *Advances in Space Research* 35:1017-26
Ramadevi MC, Seetha S. 2007. *MNRAS* 378:182-8
Rees MJ, Begelman MC, Blandford RD, Phinney ES. 1982. *Nature* 295:17-21
Reis RC, Fabian AC, Miller JM. 2010. *MNRAS* 402:836-54
Reis RC, Fabian AC, Ross RR, et al. 2008. *MNRAS* 387:1489-98
Remillard RA, McClintock JE. 2006. *Annu. Rev. Astron. Astrophys.* 44:49-92
Reynolds CS. 2013. *Space Sci. Rev.* in press (arXiv:1302.3260)
Reynolds CS, Di Matteo T, Fabian AC, Hwang U, Canizares CR. 1996. *MNRAS* 283:L111-6
Reynolds CS, Fabian AC. 2008. *Ap. J.* 675:1048-56
Rezzolla L, Yoshida S, Maccarone TJ, Zanotti O. 2003. *MNRAS* 344:L37-41
Riquelme MA, Quataert E, Sharma P, Spitkovsky A. 2012. *Ap. J.* 755:50
Romanova MM, Ustyugova GV, Koldoba AV, Chechetkin VM, Lovelace RVE. 1998. *Ap. J.* 500:703-13
Różańska A, Czerny B. 2000. *Astron. Astrophys.* 360:1170-86
Rothstein DM, Lovelace RVE. 2008. *Ap. J.* 677:1221-32
Ruffini R, Wilson JR. 1975. *Phys. Rev. D* 12, 2959-62
Russell DM, Gallo E, Fender RP. 2013a. *MNRAS* 431:405-14
Russell HR, McNamara BR, Edge AC, et al. 2013b. *MNRAS* 432:530-53
Ruszkowski M, Begelman MC. 2002. *Ap. J.* 581:223-8
Rykoff E, Miller JM, Steeghs D, Torres MAP. 2007. *Ap. J.* 666:1129-39
Sadowski A, Narayan R, Penna R, Zhu Y. 2013a. *MNRAS*, 436:3856-74
Sadowski A, Sironi L, Abarca D, et al. 2013b. *MNRAS* 432:478-91
Saitoh TR, Makino J, Asaki Y, et al. 2013. *PASJ* in press. arXiv:1212.0349
Sazonov SY, Ostriker JP, Ciotti L, Sunyaev RA. 2005. *MNRAS* 358:168-80
Sazonov S, Sunyaev R, Revnivtsev M. 2012. *MNRAS* 420:388-404
Schartmann M, Burkert A, Alig C, et al. 2012. *Ap. J.* 755:155
Scheuer PAG, Feiler R. 1996. *MNRAS* 282:291-4
Schechter P. 1976. *Ap. J.* 203:297-306
Schnittman JD, Krolik JH, Noblem SC. 2013. *Ap. J.* 769:156
Schödel R, Morris MR, Muzic K, et al. 2011. *Astron. Astrophys.* 532:83
Schödel R, Ott T, Genzel R, et al. 2002. *Nature* 419:694

Shafee R, McKinney JC, Narayan R, et al. 2008.*Ap. J. Lett.* 687:L25-8
Shakura NI, Sunyaev RA. 1973. *Astron. Astrophys.* 24:337
Shapiro SL, Lightman AP, Eardley DM. 1976. *Ap. J.* 204:187-99
Sharma P, Hammett GW, Quataert E, Stone JM. 2006. *Ap. J.* 637:952-67
Sharma P, Quataert E, Hammett GW, Stone JM. 2007a. *Ap. J.* 667:714-23
Sharma P, Quataert E, Stone JM. 2007b. *Ap. J.* 671:1696-1707
Sharma P, Quataert E, Stone JM. 2008. *MNRAS* 389:1815-27
Shen ZQ, Lo KY, Liang MC, Ho PTP, Zhao JH. 2005. *Nature* 438:62-4
Shcherbakov RV. 2013. *Ap. J.* submitted. arXiv:1309.2282
Shcherbakov RV, Baganoff FK. 2010. *Ap. J.* 716:504-9
Shcherbakov RV, McKinney JC. 2013. *Ap. J. Lett.* 774:L22
Shcherbakov RV, Penna RF, McKinney JC. 2012. *Ap. J.* 755:133
Shibata K, Uchida Y. 1985. *Publ. Astron. Soc. Jap.* 37:31-46
Shibata K, Uchida Y. 1986. *Publ. Astron. Soc. Jap.* 38:631-60
Shiokawa H, Dolence JC, Gammie CF, Noble SC. 2012. *Ap. J.* 744:187
Silk J. 2013. *Ap. J.* 772:112
Somerville RS, Hopkins PF, Cox TJ, Robertson BE, Hernquist L. 2008. *MNRAS* 391:481-506
Sorathia KA, Reynolds CS, Armitage PJ. 2010. *Ap. J.* 712:1241-7
Sorathia KA, Reynolds CS, Stone, JM, Beckwith K. 2012. *Ap. J.* 749:189
Spruit HC, Deufel B. 2002. *Astron. Astrophys.* 387:918-30
Spruit HC, Matsuda T, Inoue M, Sawada K. 1987. *MNRAS* 229:517-27
Spruit HC, Uzdensky DA. 2005. *Ap. J.* 629:960-8
Springel V, Di Matteo T, Hernquist L. 2005. *MNRAS* 361:776-94
Steiner JF, McClintock JE, Narayan R. 2013. *Ap. J.* 762:104
Stern BE, Poutanen J, Svensson R, Sikora M, Begelman MC. 1995. *Ap. J. Lett.* 449:L13-6
Stone JM, Gardiner TA, Teuben P, Hawley JF, Simon JB. 2008. *Ap. J.* 178:137-77
Stone JM, Hawley JF, Gammie CF, Balbus SA. 1996. *Ap. J.* 463:656-73
Stone JM, Norman ML. 1992a. *Ap. JS* 80:753-90
Stone JM, Norman ML. 1992b. *Ap. JS* 80:791-818
Stone JM, Pringle JE. 2001. *MNRAS* 322:461-72
Stone JM, Pringle JE, Begelman MC. 1999. *MNRAS* 310:1002-16
Storchi-Bergmann T, Eracleous M, Ruiz MT, et al. 1997. *Ap. J.* 489:87-93
Su M, Slatyer TR, Finkbeiner DP. 2010. *Ap. J.* 724:1044-82
Taam RE, Liu B, Yuan W, Qiao E. 2012. *Ap. J.* 759:65
Tanaka T, Menou K. 2006. *Ap. J.* 649:345-360
Tchekhovskoy A, McKinney JC. 2012. *MNRAS* 423:L55-9
Tchekhovskoy A, McKinney JC, Narayan R. 2012. *JPhCS* 372:012040
Tchekhovskoy A, Metzger BD, Giannios D, Kelley LZ. 2013. *MNRAS* in press (arXiv:1301.1982)
Tchekhovskoy A, Narayan R, McKinney JC. 2010. *Ap. J.* 711:50-63
Tchekhovskoy A, Narayan R, McKinney JC. 2011. *MNRAS* 418:L79-83
Thorne KS, Price RH, MacDonald DA. 1986. Black holes: The membrane paradigm. Yale Univ. Press
Tomsick JA, Yamaoka K, Corbel S. 2009. *Ap. J. Lett.* 707:L87-91
Trap G, Goldwurm A, Dodds-Eden K, et al. 2011. *Astron. Astrophys.* 528:140
van der Laan H. 1966. *Nature* 211:1131-3
van Velzen S, Falcke H. 2013. *Astron. Astrophys.* 557:L7-10
Veledina A, Poutanen J, Ingram A. 2013. *Ap. J.* 773:165

Vernaleo JC, Reynolds C. 2006. *Ap. J.* 645:83-94
Vlahakis N, Konigl A. 2003. *Ap. J.* 596:1080-103
Wang QD, Nowak MA, Markoff SB, et al. 2013. *Science* 341:981-3
Wang R, Wu XB, Kong MZ. 2006. *Ap. J.* 645:890-9
Watarai K, Mizuno T, Mineshige S. 2001. *Ap. J. Lett.* 549:L77-88
Wilson AS, Yang Y. 2002. *Ap. J.* 568:133-40
Wrobel JM, Terashima Y, Ho L. 2008. *Ap. J.* 675:1041-7
Wu Q, Yuan F, Cao X. 2007. *Ap. J.* 669:96-105
Wu XB. 1997. *MNRAS* 292:113-9
Wu XB, Li Q. 1996. *Ap. J.* 469:776-83
Wyithe JSB, Loeb A. 2003. *Ap. J.* 595:614-23
Xie FG, Yuan F. 2008. *Ap. J.* 681:499-505
Xie FG, Yuan F. 2012. *MNRAS* 427:1580-6
Xu G, Chen X. 1997. *Ap. J.* 489:L29-32
Xu YD, Cao XW. 2009. *Res. Astron. Astrophys.* 9:401-8
Xu YD, Narayan R, Quataert E, Yuan F, Baganoff FK. 2006. *Ap. J.* 640:319-26
Xue L, Wang JC. 2005. *Ap. J.* 623:372-82
Younes G, Porquet D, Sabra B, Reeves JN. 2011. *Astron. Astrophys.* 530:149
Younes G, Porquet D, Sabra B, Reeves JN, Grosso N. 2012. *Astron. Astrophys.* 539:104
Yu W, Yan Z. 2009. *Ap. J.* 701:1940-57
Yu Z, Yuan F, Ho LC. 2011. *Ap. J.* 726:87
Yuan F. 1999. *Ap. J. Lett.* 521:L55-58
Yuan F. 2001. *MNRAS* 324:119-27
Yuan F. 2003. *Ap. J. Lett.* 594:L99-102
Yuan F, Bu D. 2010. *MNRAS* 408:1051-60
Yuan F, Bu D, Wu M. 2012a. *Ap. J.* 761:130
Yuan F, Cui W. 2005. *Ap. J.* 629:408-13
Yuan F, Cui W, Narayan R. 2005. *Ap. J.* 620:905-14
Yuan F, Li M. 2011. *Ap. J.* 737:23
Yuan F, Lin J, Wu K, Ho LC. 2009a. *MNRAS* 395:2183-8
Yuan F, Markoff S, Falcke H. 2002a. *Astron. Astrophys.* 383:854-63
Yuan F, Markoff S, Falcke H, Biermann PL. 2002b. *Astron. Astrophys.* 391:139-48
Yuan F, Narayan R. 2004. *Ap. J.* 612:724-28
Yuan F, Quataert E, Narayan R. 2003, *Ap. J.* 598:301-12
Yuan F, Quataert E, Narayan R. 2004, *Ap. J.* 606:894-99
Yuan F, Taam RE, Xue R, Cui W. 2006. *Ap. J.* 636:46-55
Yuan F, Wu M, Bu D. 2012b. *Ap. J.* 761:129
Yuan F, Xie F, Ostriker JP. 2009b. *Ap. J.* 691:98-104
Yuan F, Yu Z, Ho L. 2009c. *Ap. J.* 703:1034-43
Yuan F, Zdziarski A. 2004. *MNRAS* 354:953-60
Yuan F, Zdziarski A, Xue Y, Wu XB. 2007. *Ap. J.* 659:541-48
Yusef-Zadeh F, Roberts D, Wardle M, Heinke CO, Bower GC. 2006. *Ap. J.* 650:189-94
Yusef-Zadeh F, Bushouse H, Wardle M, et al. 2009. *Ap. J.* 706:348-75
Yusef-Zadeh F, Wardle M. 2013. *Ap. J. Lett.* 770:L21
Zdziarski AA, Lubiński P, Gilfanov M, Revnivtsev M. 2003. *MNRAS* 342:355-72
Zdziarski AA, Lubiński P, Sikora M. 2012. *MNRAS* 423:663-75
Zdziarski AA, Gierliński M. 2004. *Prog. Theor. Phys. Supp.* 155:99-119
Zdziarski AA, Poutanen J, Mikolajewska J, et al. 1998. *MNRAS* 301:435-50

Zhang SN. 2013. *Frontiers of Phys.* Eds. Bing Zhang & Péter Mészáros (arXiv:1302.5485)
Zubovas K, King AR, Nayakshin S. 2011. *MNRAS* 415:L21-L25